SBIR 11.04-0236C

NASA Contractor Report 187205

HIGH TEMPERATURE OXIDATION-RESISTANT THRUSTER MATERIALS, PHASE II

Robert H. Tuffias, G.J. Melden, and John T. Harding
Ultramet
12173 Montague Street
Pacoima, CA 91331

March 1991

Final Report for Period May 1987 - August 1990

Prepared for
Lewis Research Center
under contract NAS3-25203

NATIONAL AERONAUTICS AND SPACE ADMINISTRATION
LEWIS RESEARCH CENTER
CLEVELAND, OH 44135

TABLE OF CONTENTS

LIST OF FIGURES

LIST OF FIGURES (cont.)

LIST OF TABLES

1. INTRODUCTION

This is the final technical report submitted by Ultramet, Pacoima, CA 91331 to NASA Lewis Research Center, Cleveland, OH 44135 under SBIR Phase II contract NAS3-25203. The period of this contract was from 22 May 1987 to 17 August 1990. The principal investigator was Dr. John T. Harding, supported by Dr. Robert H. Tuffias as senior scientist and by G.J. Melden as project engineer. The NASA Lewis project manager was John M. Kazaroff.

In 1986, Ultramet completed an SBIR Phase I feasibility study with results that were of substantial significance to the storable propellant rocket community. Ultramet demonstrated a materials system, iridium/rhenium (Ir/Re), and fabrication process for thrust chambers that promised a performance increase of 20 seconds in specific impulse. This increase was accomplished by enabling operation at 2200°C (4000°F), a 900°C (1600°F) increase over the previous state of the art, for an indeterminate amount of time (later determined to be tens of hours). This achievement, a quantum leap in the development of high temperature materials and processes for storable propellant rocket engines, will never be equaled since no materials exist that can provide another 900°C increase in operating temperature for tens of hours.

A follow-on Phase II technology development contract, the subject of this report, was awarded in 1987 with two main goals:

- Refine this technology for use by the propulsion community.
- Expand the technology to develop better oxidation-protective materials for both rhenium and niobium chambers.

While the results demonstrated initially in Phase I and continued in Phase II of this program were spectacular in terms of technological advancement, the opportunity for application required the serendipitous synergy of a number of seemingly unrelated events. One such happening occurred in late 1987, concerning NASA's planned Comet Rendezvous Asteroid Flyby (CRAF) mission. As originally defined, the CRAF propulsion system incorporated a 100-lb_f (445-N) disilicide-coated niobium alloy thrust chamber, which at the time was considered the state of the art. However, the number and weight of experiments on the spacecraft had subsequently increased such that the performance of this engine would no longer be sufficient for the payload requirements. NASA analysis projected that the incorporation of Ultramet's iridium/rhenium technology would permit a reduction in spacecraft wet mass of some 600 kg (1320 lb_m) that could then be utilized by the experimental payload.

To that time, Ultramet had never fabricated Ir/Re chambers larger than the 5-lb_f (22-N) size. A 100-lb_f chamber is substantially larger: five times larger in its major diameter and 3½ times longer. Because of the importance of the CRAF mission and the potential positive impact of Ultramet's technology, NASA chose to redirect this project to support CRAF objectives.

Despite technological difficulties in scaling up to the larger size, two 100-lb_f chambers were built and tested. One unit amassed over six hours of test time and confirmed the results of previous tests. Although performance was better than anticipated, a number of processing problems were discovered. A major portion of the Phase II effort was spent addressing and solving these problems.

Because of the unusual sequence of events involved in the performance of this technology development project, a chronological presentation of the effort is not possible. The developments are described instead as stand-alone efforts, in an attempt to provide clarity without detracting from the significance of each accomplishment.

Finally, while the accomplishments made in this program have been considered a great leap forward in the field of chemical rockets, not only Ultramet personnel were involved in making it a success. Ultramet would like to thank all the NASA Lewis Research Center personnel associated with the project for their continued patience, encouragement, understanding, and support throughout the course of the effort. Special thanks go to John M. Kazaroff, the NASA project manager, whose contribution was enormous.

2. BACKGROUND

2.1 Material Selection

Operating temperature, lifetime, and chemical compatibility constraints limit the performance of thrusters for applications such as space station, space platform, spacecraft, and satellite on-board auxiliary propulsion. Alleviating these material-imposed constraints would permit a wider range of potential propellants, greater cycle life capability, and increased specific impulse, resulting in improved mission performance.

To illustrate, state-of-the-art low-thrust liquid rocket engines employ extensive fuel film cooling to suppress the maximum temperature to 1300°C (2370°F). This temperature limit is imposed by the disilicide coating that protects the refractory metal (niobium) nozzle from oxidation. Fuel film cooling flows of up to 30% result in a 4% loss in operating efficiency for these engines. The availability of a 2200°C (4000°F) oxidation-resistant material having a high thermal cycle life capability would allow this cooling loss to be eliminated. A 4% increase in the apogee engine performance of a propulsion system for a typical one-tonne (metric ton) satellite would result in significant savings. These savings could be realized by offloading 4% of the propellant, or 40 kg (88 lb_m), producing a corresponding increase in payload. Alternately, the satellite life could be increased by 4%.

Candidate materials and fabrication processes must be identified that are compatible with radiatively cooled thrusters utilizing nitrogen tetroxide/monomethyl hydrazine (NTO/MMH), oxygen/hydrogen (O_2/H_2), and other state-of-the-art oxidizing propellants at temperatures of at least 2200°C and able to withstand at least 10,000 temperature cycles. This environment requires the development of materials or material combinations, and the process(es) for their fabrication, that will retain sufficient strength at that temperature, will be resistant to oxidation, and will not react with the combustion products.

Candidate materials for use in this environment are severely limited because of strength and corrosion requirements. No single material exists that has sufficient strength at 2200°C and will not catastrophically oxidize at that temperature. The solution to this problem, then, requires a base structural material that does have sufficient strength coupled with an oxidation- and corrosion-protective coating (surface).

Ceramics can be immediately eliminated as base structural materials because their fabrication is not sufficiently advanced with regard to strength, reliability, and thermal shock considerations, although they may be useful as coatings. This assessment is based on a minimum acceptable strength of 70 MPa (10 ksi) with thrust chamber pressures up to 3.5 MPa (500 psi), chamber diameters up to 30 mm (1.18 in), and a wall thickness of 1 mm (0.040 in).

Figure 1 shows the effect of temperature on the tensile strength of refractory materials [1]. Strength considerations at 2200°C eliminate all the listed materials except rhenium, W-1ThO_2, and possibly Mo-50Re. Carbon/carbon composites, meanwhile, typically exhibit a tensile strength of 275 MPa (40 ksi) at room temperature, actually rising to over 300 MPa (44 ksi) at 2200°C. However, their anisotropic thermophysical properties cause severe coating

compatibility problems on thermal cycling. Similar problems exist with fiber-reinforced ceramics.

Elemental rhenium has many properties that make it an attractive candidate for structural operation in the 1500-2500°C (2730-4530°F) temperature range. Rhenium has a high melting temperature of 3180°C (5756°F) and retains substantial strength at high temperatures, with 100-MPa (14-ksi) ultimate strength and 55-MPa (8-ksi) yield strength at 1800°C (3270°F). With proper heat treatment, rhenium is ductile at room temperature and is machinable. Rhenium shells of 100% density can be reliably fabricated by chemical vapor deposition (CVD) at a fraction of the cost of a similar carbon/carbon structure, and Ultramet had considerable experience in fabricating rhenium thrusters by CVD beginning in the late 1970s [2-6]. These factors determined the choice of rhenium as the base structural material.

In the case of the rhenium thrusters fabricated previously by Ultramet, employing a variety of propellants, it had been necessary to operate in a fuel-rich mode to avoid rapid oxidation of the rhenium. All the candidate refractory structural materials, including rhenium, oxidize severely above 500°C (930°F) and thus must be protected with oxidation-resistant coatings for operation in the optimal thruster environment (i.e., oxidizer-rich mode producing highly oxidizing conditions). Candidate oxidation-resistant coatings for use at 2200°C and above fall into two categories:

1. Intermetallic compounds that form compact crystalline oxide layers (e.g. hafnium oxide and zirconium oxide). The results of other work indicated that HfO_2 and ZrO_2 cannot be used alone as oxidation-resistant coatings. Although they are compatible with oxygen (i.e., resistant to oxidation), they are also porous with respect to oxygen. In addition, these brittle ceramics are unable to withstand more than a few temperature cycles without cracking, making them unsuitable since the cracked surface provides a path for oxygen to attack the substrate.

2. The noble or platinum group metals (i.e., platinum, rhodium, ruthenium, and iridium) and their alloys, which react slowly with oxygen to form volatile oxides. With operation above the melting temperature of the coating being impossible, platinum and rhodium are eliminated for the 2200°C environment with their respective melting temperatures of 1772 and 1965°C (3222 and 3569°F). That leaves iridium and ruthenium, with respective melting points of 2410 and 2250°C (4370 and 4082°F).

Iridium has the highest melting temperature of the platinum group metals and is the most oxidation-resistant of all metals at 2200°C. Figure 2 shows iridium to be more oxidation-resistant than ruthenium up to at least 1400°C (2550°F) [7]. Iridium is compatible with rhenium and can be deposited with rhenium by CVD, producing coatings that have previously demonstrated greater oxidation protection at higher temperatures, under both continuous and cyclic temperature exposure in air, than any other material. Oxidation data for iridium up to 2200°C are shown in Figure 3 [8]. The recession rate appears to be very rapid at 2200°C, but this is irrelevant for liquid rocket thruster applications in space, where the oxidizing conditions appear to be far less severe than those encountered in flowing air.

Additionally, strategies exist for reducing the amount of oxidizer that comes in contact with the iridium. One such method is to overcoat the iridium coating with HfO_2 or ZrO_2. While these surfaces have been found to crack under repeated temperature cycles [9,10], they still would act as a barrier to both the ingress of oxidizer and the egress of oxidation products, and either material would reduce the rate of oxidation. Another strategy is to utilize alloys of iridium with rhodium or platinum. Work elsewhere has shown that, with arc-melted specimens, the addition of 30% rhodium or platinum greatly reduces the oxidation rate as compared to that of unalloyed iridium, though reducing the melting point to about 2200°C [11].

While both carbon/carbon and rhenium are viable base materials, the likelihood based on current technology of depositing a successful coating able to withstand a large number of temperature cycles is much greater with rhenium than with carbon/carbon. Coating failure during thermal cycling is usually the result of a mismatch between the thermal expansion coefficients (CTEs) of the substrate and the coating. Rhenium and iridium have nearly identical expansion coefficients (6.7 and 6.5 ppm/°C, respectively). Carbon/carbon, however, has a highly anisotropic expansion coefficient, and substantial additional research would be needed to overcome the high thermal stresses caused by this anisotropy.

The iridium/rhenium (Ir/Re) material system, then, is the most likely candidate to have maximum life in an oxidizing and corrosive environment at 2200°C and 10,000 or more temperature cycles.

2.2 Chemical Vapor Deposition (CVD)

Chemical vapor deposition has been used to produce coatings for more than a century, but only recently has this technique left the laboratory and become a production tool. CVD is a method of plating that relies on the chemical reaction of a vapor at a surface to form solid structural deposits. Since this is done on an atom-by-atom basis, impurity levels are typically less than 0.1% and densities are greater than 99.9%. The CVD process utilizes a gaseous precursor compound of the element to be deposited, which is flowed over a heated substrate, resulting in thermal decomposition or reduction of the gaseous compound and subsequent deposition of the desired material onto the substrate. The first layer forms at nucleation sites; after the substrate is fully coated, growth continues on the crystal faces of the deposit.

Successful CVD, producing dense, adherent coatings, depends on experimentally determining the optimal deposition parameters. These include the gaseous precursor compound of the material to be deposited, the substrate temperature, the concentration, pressure, and flow rate of the gas(es), and geometry within the reaction chamber. For the coating to have good integrity and adhesion to the substrate, the substrate must either have a similar CTE to that of the deposited material, or form a strong chemical or metallurgical bond with it. The thinner the coating, the less similar the expansion coefficients need be. Where coating and substrate form no intermetallic bond and have widely differing CTEs, a good bond may often be achieved by utilizing a thin interlayer of a third material.

The essential requirements of a CVD facility are that the substrate be maintained at the correct temperature and that the plating gases be supplied in the correct ratio and at the correct pressure. The substrate is typically heated

inductively, resistively, or radiatively in a hot wall furnace. The composition of the plating gases is determined by the type of reaction to be used; these include decomposition and reduction. Some of the plating gases are commercially available; in other cases, they are generated in situ from volatile liquids or solids. The same material may be deposited using different compounds and different reactions at different temperatures, with each producing good coatings but different structures. Compounds and alloys can be deposited by simultaneous codeposition of the appropriate elements.

Figure 4 shows a schematic of a typical CVD apparatus for the deposition of rhenium, which is accomplished by the thermal decomposition of rhenium pentachloride ($ReCl_5$). The process reactant, $ReCl_5$, is formed by chlorinating very pure rhenium metal in situ. Chlorine gas is fed into a chamber containing rhenium metal. The rhenium is heated resistively to 500°C (930°F) for chlorination, reacting with the chlorine to form gaseous $ReCl_5$. The $ReCl_5$ gas thus formed is then flowed into the reaction chamber. A vacuum in the chamber pulls the rhenium-bearing $ReCl_5$ past the substrate, which has been inductively heated to a temperature sufficient to cause the thermal decomposition of the $ReCl_5$ at 1200°C (2190°F). At the hot substrate surface, the $ReCl_5$ decomposes, with rhenium metal depositing on the substrate and chlorine gas forming and being exhausted from the system. The rhenium deposit can be made to any desired thickness, and nearly any substrate configuration can be coated. The rhenium may be used as a coating, in which case the substrate would be the actual part to be coated, or by making the rhenium sufficiently thick and removing the substrate, a free-standing shape may be obtained.

The halide process described above, characterized by the in situ generation of the plating compound, has proved unsuccessful in the case of the platinum group metals. This is because the volatilization and decomposition temperatures of the platinum group halides are too close to permit their efficient use [12]. The procedure developed at Ultramet for depositing platinum group metals utilizes organometallics, specifically acetylacetonate and its fluorine-substituted complexes, as precursor compounds [13,14]. As their synthesis is a complex process, Ultramet obtains these compounds commercially. They are solid (powders) and have appreciable volatility and stability at 200°C (390°F). The gaseous process reactant is formed by vaporization of the solid, which occurs via sublimation. In the case of iridium, the plating compound is iridium acetylacetonate, $Ir(CH_3COCHCOCH_3)_3$, commonly referred to as Ir ac-ac. The rate of formation of the iridium deposit is typically 3-20 μm/hr (0.00012-0.0008 in/hr). Efficiency, the fraction of the iridium used that is ultimately deposited on the part, is high, over 70% in the case of iridium ac-ac. A schematic of the CVD apparatus for iridium deposition is shown in Figure 5.

2.3 Inside-Out Fabrication Technique

The "inside-out" fabrication technique combined with CVD has many advantages. The inner surface of a thrust chamber is the critical surface, but machining outer surfaces is much easier than machining inner surfaces. Since CVD exactly replicates the surface upon which the coating is deposited, the critical inner surface may be produced by depositing onto the outside of a mandrel whose outer surface replicates the desired inner surface of the part being fabricated. And whereas inspection of inner surfaces is difficult, depositing on the outside of a mandrel allows each surface to be easily examined. Figure 6 is a flow chart

of the inside-out fabrication technique for Ir/Re thrust chambers. Iridium is first deposited onto a mandrel, forming the inner oxidation-resistant surface of the chamber that will be exposed to the hot combustion environment. Rhenium is then deposited onto the iridium, forming the outer structural element of the chamber. Finally, the mandrel is removed by chemical means, leaving a free-standing Ir/Re chamber.

2.4 Phase I Results

The principal objective of Phase I was to demonstrate the feasibility of fabricating a rocket thruster able to withstand cyclic firing in an oxidizing environment at 2200°C. This goal was accomplished by means of novel coating technology, specifically the use of chemical vapor deposition to form a structural rhenium shell overcoated with iridium for oxidation protection [15].

A 5-lb_f Re/Ir/HfO_2 thruster was produced entirely by CVD, using the inside-to-outside fabrication technique described above: that is, the thruster was built up from its inside surface to its outside surface. A 25-μm (0.001-in) deposit of HfO_2 was first made on an expendable molybdenum mandrel conforming to the desired inner surface of the thruster. A 40-μm (0.0015-in) layer of iridium was then deposited on the hafnia, followed by the 1-mm (0.040-in) rhenium structure, which in turn was coated with 40 μm of iridium. Finally, the molybdenum mandrel was chemically removed, leaving a free-standing thruster. The deposition of HfO_2 by CVD was a development in itself, particularly with regard to achieving a uniform coating on the 85-mm (3.35-in) long part.

Although the testing of the Phase I thruster had been planned to be a part of Phase II, Aerojet TechSystems (Sacramento, CA) began hot-firing tests at its own expense. This decision derived from excellent results obtained earlier from iridium/rhenium chambers fabricated previously by Ultramet [16-18]. Only a limited amount of data was obtained, but after five cycles, including over 20 minutes at temperatures between 1840 and 2200°C (3340-4000°F), there was only a 0.02% loss of mass from the thruster, apparently due to spalling of HfO_2. Most importantly, no cracks or pinholes were found in the iridium coating. The oxidizer/fuel combination was NTO/MMH at optimal proportions. Under these same conditions, an uncoated rhenium nozzle loses 50 μm (0.002 in) of rhenium per minute. Preliminary data obtained in Phase I showed that the overcoating of hafnia on iridium lowered the oxidation rate of the latter (in air) by a factor of 20 or more.

3. EXPERIMENTAL APPROACH

The overall objective of this Phase II program was to advance the state of the art in materials and processes for the fabrication of chemical rocket thrust chambers.

Uncooled high-performance liquid rocket thrust chambers have frequently used niobium alloys as the structural material, a logical choice compared with the alternatives. The temperature limit of niobium alloys while maintaining good thermomechanical performance is approximately 200°C (360°F) higher than that of the best superalloys. Adequate oxidation resistance has been provided by disilicide coatings, which are considered reasonably trustworthy based on some twenty years of development.

Current niobium alloys are also the result of sustained development. They have dramatically better high temperature creep-rupture properties, while maintaining acceptable ductility, than either pure niobium or earlier simple alloys such as Nb-1Zr. For example, the creep-rupture stress values at 1370°C (2500°F) for such modern alloys as FS-85 or C-103 are two to three times better than those for Nb-1Zr or pure niobium.

Niobium is the lightest of the refractory metals, making it generally more attractive for structural use than molybdenum, tantalum, tungsten, or rhenium. At temperatures of 1200°C (2190°F) and above, however, its properties are generally inferior to those of other refractory metal alloys. Molybdenum and tungsten alloys are clearly stronger, and enough so at the highest contemplated operating temperatures to make up for their higher densities. Unfortunately, both molybdenum and tungsten tend to embrittle upon recrystallization. In addition, no suitable oxidation protection systems have been available to take advantage of their better high temperature strength.

Tantalum alloys do not have the recrystallization/embrittlement problem, but are likewise limited by the lack of higher temperature oxidation protection. Also, they are not as attractive from a thermomechanical point of view.

Rhenium, however, has excellent high temperature strength and does not embrittle upon recrystallization. It has not generally been considered as a high temperature structural material (e.g. for uncooled liquid rockets) because of its (incorrectly) perceived scarcity with concomitant high cost, and because suitable high temperature oxidation protection systems had not been developed. For these reasons, relatively little investigation of the benefits of rhenium, or refractory metal alloy systems using rhenium as the significant component, had been done prior to Ultramet beginning work with CVD rhenium in the late 1970s.

An overview of the considerations discussed above suggests the following:

- The utility of niobium alloys would be enhanced if higher temperature oxidation protection for such structures were available.
- The utility of niobium alloys would be further and dramatically enhanced if better oxidation protection were available and present thermomechanical limits were extended.

- Pure rhenium, and dilute rhenium alloys, are under-exploited as high temperature structural materials due to the apparent lack of suitable oxidation protection.

- The utility of rhenium could be further extended by an investigation of more sophisticated alloying techniques to enhance high temperature mechanical properties.

- The alloying of rhenium may also be contributory to solving the high temperature oxidation problem.

The noble metal coatings developed by Ultramet in Phase I of this program, and in other work, should extend the oxidation protection of niobium alloys in terms of both reliability and maximum operating temperature. Since the most optimistic maximum operating temperature for current niobium alloys, based on thermomechanical considerations, is about 1650°C (3000°F), any of the platinum group metals, or alloys thereof, should be useful for oxidation protection.

The Phase I data would tend to suggest that the use of iridium as oxidation protection for niobium would actually constitute overkill, since the protection afforded by iridium (2200°C) would exceed the current maximum anticipated temperature capabilities of niobium and its alloys (1650°C). As an alternative, the less scarce, lower melting point noble metals (e.g. platinum) could be applied to the protection of niobium alloys.

Since the improved oxidation protection provided by iridium would appear to exceed the thermostructural capabilities of niobium alloys, two possible methods of system improvement are indicated.

The first method would be to effect a dramatic improvement in the thermomechanical properties of niobium alloys in order to take full advantage of the iridium oxidation protection system. This could be made possible by means of advanced codeposition techniques available at Ultramet. Specifically, a refractory dispersoid could be codeposited in niobium, an approach that is particularly well-suited to the inside-out fabrication method. Although this clearly would be a worthwhile effort, it was considered beyond the scope of the Phase II program, in which work with niobium was limited to developing the best methods of applying an adherent, protective noble metal coating on current advanced niobium alloy structural bodies.

The second approach would be to discard niobium alloys entirely, in favor of a more capable material system. As noted, rhenium is an excellent structural material with regard to thermomechanical properties, and its alleged rarity and expense have been exaggerated. Approximately 13.6 tonnes (30,000 lb_m) of rhenium were produced worldwide in 1985 [19]. This amount represents a relatively small portion of the rhenium content of the molybdenite byproduct of copper ores. In fact, more rhenium was exhausted as Re_2O_7 than was actually recovered for use. Like the noble metals, rhenium is easy to recycle, so that use can be quite conservative.

The majority of work in Phase II was to follow the second approach, concentrating on rhenium base structures protected from oxidation by iridium. In addition to pure rhenium, both dispersoid codeposition and graded deposits could be incorporated. For the latter, chemical vapor deposition is used to continuously

grade a coating from one composition to another. Such grading avoids a discontinuity in composition at which stress accumulates, leading to delamination, spalling, cracking, and the like. In previous work, Ultramet successfully demonstrated a continuously graded SiC to HfO_2 coating with the composition SiC-->HfC-->HfO_2 [20].

The following systems, described with the interior hot gas-exposed surface first to reflect the inside-out fabrication method, offer potential advancement in the state of the art of CVD fabrication and high temperature oxidation protection for liquid rocket thrust chambers:

1. Pure iridium continuously graded to pure rhenium (or Re-20Ir)

2. Pure stoichiometric hafnium carbide (HfC) graded to pure rhenium

3. Stabilized HfO_2 with graded interface to stoichiometric HfC, continuously graded to pure rhenium

4. Stabilized HfO_2 with graded interface to pure iridium, continuously graded to pure rhenium

5. Codeposited, dispersion-strengthened rhenium with HfO_2 dispersoid

6. Systems 1-4 with dispersion-strengthened rhenium substituted for pure rhenium

7. Systems 1-5 with iridium partially alloyed with rhodium

The first of these potential systems (Ir-->Re or Re-20Ir) offers the advantage of an integral body utilizing the demonstrated iridium oxidation protection, eliminating concern about coating delamination while maintaining excellent thermomechanical properties. Tests at Aerojet have shown that an Ir-20Re alloy has virtually the same oxidation resistance as pure iridium but a higher melting point [21].

The second system (HfC-->Re) makes use of the demonstrated high temperature oxidation/erosion resistance of HfC, not as a coating but as an actual integral surface alloy layer in the high-strength rhenium body. The ductility of the rhenium mollifies the brittle behavior of the ultra-refractory HfC ceramic. Actual strengthening of the rhenium body is anticipated in this system.

The third system (HfO_2-->HfC-->Re) is designed to increase the usable lifetime of the second system through the use of a HfO_2 surface layer.

The fourth system (HfO_2-->Ir-->Re) is an extension of the promising work done in Phase I. It is designed to demonstrate the improved performance of stabilized HfO_2 in minimizing the amount of iridium needed for protection. Hafnia melts at 2758°C (4996°F), is not attacked by oxygen, and forms a fair diffusion barrier to oxygen. Because of its brittleness, hafnia tends to crack and spall and hence is not a suitable oxidation-resistant coating by itself. It was observed in Phase I that spalling of HfO_2 is associated with the phase transformation, accompanied by a volume change, that occurs between 1700 and 1800°C (3090-3270°F) [1]. Hafnia, like zirconia, can be stabilized against this transformation by the addition of certain other refractory oxides. Ultramet has incorporated Ta_2O_5

into HfO_2 by means of codeposition by CVD, with no cracking observed during temperature cycling through the phase transition temperature [22]. A stabilized hafnia overcoating would be more effective in extending the life of an iridium coating than the simple hafnia used in Phase I.

The fifth and sixth systems, utilizing dispersion-strengthened rhenium, are designed to increase the high temperature thermomechanical properties of rhenium. It is well known that dispersion-strengthened alloys such as TD nickel and TD tungsten allow the maintenance of good strength at temperatures approaching the melting point of the host metal. As a high-strength, ductile metal with a very high melting point, rhenium is an ideal candidate for such a system. The noble metal-like chemical characteristics of rhenium not only make it ideal for codeposition with a dispersoid, but also ensure the high temperature compatibility of the dispersoid with the host.

The concept of utilizing a refractory oxide dispersoid in rhenium is based on previously demonstrated technology. Powder metallurgy alloys of tungsten, nickel, and copper have been fabricated successfully using thorium oxide as a dispersoid. Additions of 1-2% ThO_2 to tungsten prevent grain growth at high temperatures and effectively maintain high temperature mechanical properties. The effect of small thoria additions to nickel and copper, more ductile host metals, is even greater than it is to tungsten. Excellent mechanical properties are maintained nearly to the melting point of the host metal.

Ultramet would chose hafnia rather than thoria as the dispersoid in rhenium, although either oxide should be acceptable. The most important considerations in choosing the oxide are that it be refractory, have sufficient high temperature thermochemical stability with the host metal and in the anticipated use environment, and have an appropriate thermal expansion coefficient. In the case of the CVD fabrication method, an additional requirement is imposed: a deposition process for the oxide must be available that is compatible with the conditions for the deposition of rhenium.

Of all candidate oxide species, both hafnia and thoria best fulfill the above requirements. Alternately, refractory carbide or refractory nitride species could also be considered, since a number of these are also believed to fulfill the cited requirements, but their codeposition with rhenium would be somewhat more complicated than the oxides.

Of these two oxides, hafnia would be Ultramet's selection for three reasons:

1. Hafnia has an almost perfect CTE match with rhenium, whereas the CTE of thoria is significantly higher.

2. The deposition conditions for hafnia, including stabilized HfO_2, are well known at Ultramet [22]. A project for the deposition of ThO_2, however, demonstrated a number of difficulties [23].

3. Minor, but real additional expense would be incurred in working with ThO_2 because of the industrial hygiene problems involved with this slightly radioactive material.

The deposition of either hafnia or thoria could be effected by any of three processes:

1. Decomposition of the metal alkoxide
2. Decomposition and oxidation of another volatile metallorganic, such as an acetylacetonate
3. Oxidation of a volatile halide

The decomposition of the alkoxide is the most straightforward process, for both hafnia and thoria. Acetylacetonate oxidation is well known, but requires more exacting partial pressure control. A completely inorganic system (e.g. $ReCl_5$ decomposition combined with oxidation of $HfCl_4$, HfI_4, or ThI_4) is similarly possible, but requires even more exacting partial pressure control.

Dispersions should be limited to dilute concentrations of hafnium oxide, i.e. below 5 vol%. A codeposition method of formation has the potential for obtaining a highly uniform dispersion of extremely small particles of the second phase, which is not possible by other methods such as powder metallurgy or casting. Such a structure has the potential of maintaining attractive thermomechanical properties, such as the 2200°C strength of rhenium, to 2480°C (4500°F) or higher. As noted, the successful demonstration of a dispersion-strengthened rhenium alloy would allow its substitution for pure rhenium in any of the other systems.

The final potential material system, the Ir-Rh binary, can be a building block for use in the other systems as well. Rhodium additions to iridium lower the melting point of iridium, but not unduly. At the same time, they actually increase oxidation resistance [11], apparently because of the lower vapor pressure of rhodium oxide. Any performance degradation due to the lower melting point could be countered in the graded or dispersed-phase systems. In addition, the extension of an Ir-Rh binary system to an Ir-Rh-Re ternary would more than eliminate any melting point depression.

The preceding potential material systems all relate to attaining a substantial increase in the operating temperature of thrusters, and realizing the full potential of state-of-the-art propellants: enhanced thrust, increased fuel efficiency, and reduced engine size and weight. The technology that can make this possible is chemical vapor deposition, an innovative method of fabricating refractory materials. Through CVD, oxidation protection becomes an integral part of the material system and fabrication process.

To achieve the stated objective, the Phase II program was divided into three major portions:

1. Process improvement and control
2. Scaleup
3. Advanced material and process development

4. RESULTS AND DISCUSSION

A number of significant achievements resulted from this project:

1. Process defined for reproducibly fabricating 5-lb_f (22-N) Ir/Re thrust chambers exhibiting 15-hour minimum life at ≥2200°C (4000°F).

2. Potential demonstrated for scaleup to 100-lb_f (445-N) chambers.

3. Reactor geometry and process parameters defined to significantly increase iridium deposition rate and coating uniformity for large chamber fabrication; single-layer iridium coating process demonstrated for 100-lb_f size.

4. Fluid bed evaporator developed, required for iridium precursor gas generation in volumes needed for large chamber fabrication.

5. Feasibility demonstrated of using graphite/molybdenum mandrel for large chamber fabrication.

6. Iridium precursor purification process developed to produce high-purity coatings.

7. Improved performance through higher temperature operation demonstrated for niobium chambers using iridium oxidation protection.

8. Extensive additional iridium-related investigations performed.

4.1 Process Definition for 5-lb_f Ir/Re Chambers

The standard chamber for all Ir/Re process development work has been the 5-lb_f Aerojet design shown schematically in Figure 7. In this segment of the project, all of the variables associated with the fabrication process were defined, investigated, and optimized in order to produce consistently reproducible parts. These variables included:

- Reactor design
- Process control using mass flow meters and temperature controllers
- Mandrel surface preparation (for iridium deposition)
- Iridium precursor purity through incoming quality control, processing, and reprocessing
- Precursor bed structure
- Precursor sublimation temperature and carrier gas interaction
- Precursor evaporation rate vs. time and temperature
- Carrier gas purity, pressure, flow rate, and temperature
- Iridium surface preparation (for rhenium deposition)
- Re/Ir diffusion vs. deposition temperature and time

Based on the results of these investigations, a process was defined. A demonstration chamber was fabricated, with photomicrographs of the end rings from the top and bottom of the chamber shown in Figure 8.

This process was applied to the fabrication of two 5-lb_f Ir/Re chambers for evaluation by Aerojet under a separate, concurrent NASA Lewis program [24,25]. These chambers were fired with NTO/MMH propellant with excellent results:

- Over eight hours at temperatures between 2040 and 2320°C (3700-4200°F) before failure on chamber #003. Failure was the result of oxidation of the outside surface of the chamber.

- Over 15 hours at temperatures between 1980 and 2260°C (3600-4100°F) without failure on chamber #004. Measurement of the throat inner diameter showed no dimensional change. Total weight loss during testing was less than 1%.

In a follow-on Aerojet program for NASA Lewis, Ultramet fabricated the same Ir/Re chambers but with a 144:1 area ratio nozzle, as shown in Figure 9 [26]. This design was identical to an existing niobium chamber to permit direct comparison. A total of three chambers were fabricated; chamber #3 was deliberately fabricated with two layers of iridium. The test results with NTO/MMH propellant were again excellent, demonstrating:

- Specific impulse 20 seconds higher than that obtained previously with the comparable niobium thruster.

- Reduction in operating temperature by 170-280°C (300-500°F) with the addition of "black" (dendritic) rhenium to the outer surface of the chamber.

- More than 100,000 starts, verifying pulsing capability (see Table I).

Figure 10, a NASA Lewis viewgraph, summarizes these results.

4.2 Scaleup Potential for 100-lb_f Ir/Re Chambers

In late 1987, Ultramet subcontracted to Aerojet under a NASA Jet Propulsion Laboratory (JPL) program to fabricate two 100-lb_f Ir/Re chambers to the design shown schematically in Figure 11. The purpose of this program was technology demonstration with applicability to the CRAF mission [27]. Incorporation of the previously demonstrated 5-lb_f Ir/Re chamber technology would permit a reduction in spacecraft wet mass of 600 kg (1320 lb_m), which would have enabled the addition of three more experiments.

The initial reactor design for the 100-lb_f chambers was based on a linearly geometric scaleup of the 5-lb_f system. The surface area (area to be coated) of the 100-lb_f mandrel was 20 times greater than that of the 5-lb_f mandrel. Due to size constraints, it was not possible to increase the surface area of the precursor bed by a factor of 20 as required by the scaleup; however, by layering the bed, its surface area was increased by a factor of ten. The bed and mandrel temperatures were the same as for the 5-lb_f chambers, but flow rates were increased to compensate for the enlarged reactor geometry.

The first iridium deposition run on chamber #1 revealed that the simplified reactor scaling theory was not adequate to produce the same iridium deposition

rate and distribution on the 100-lb_f chamber as was produced on the 5-lb_f chambers. While typical iridium deposition rates on the 5-lb_f units were 12 μm/hr (0.0005 in/hr), the 100-lb_f deposition rate was on the order of 1 μm/hr (0.00004 in/hr). In addition, the iridium distribution was poor, with little being deposited in the throat and even less on the exhaust cone.

Since time constraints prevented a process investigation, it was decided to make a number of successive runs to attain the necessary iridium thickness. This meant, of course, that the iridium would be deposited in layers. This method had been tried only once previously, on one 5-lb_f chamber that had never been test-fired.

Layering required a number of new procedures, the effects of which had not previously been investigated. These included:

- Iridium surface preparation between runs
- Precursor bed rework between runs
- Reactor rework between runs
- Post-process treatment between runs
- Gas flow rates and pressures
- Temperature distribution

A number of spontaneous, on-the-spot decisions were made concerning these new procedures, and variations attempted, during the course of the layering work.

Three 100-lb_f molybdenum mandrels were coated with iridium. Five iridium runs were made on unit #1, while four runs were made on unit #3. In addition to the low deposition rate, significant blistering and spalling were encountered during a number of runs, as shown in Figure 12, although never during the initial run.

No problems were encountered in the rhenium deposition, but the quality of the iridium coatings, based on visual observation, was not nearly as good as on the 5-lb_f chambers.

Units #1 and #3 were completed and delivered to Aerojet. These 100-lb_f chambers were tested by Aerojet with the following results [28]:

- A durability experiment demonstrated five hours of burn time without failure.
- One chamber demonstrated 3,381 seconds and 30 starts.
- The other chamber demonstrated over 15,000 seconds and 33 starts.
- Local blistering was encountered early in the testing on both chambers.
- Testing was terminated due to funding limitations.

While the quality of the iridium coatings was less than optimal in this initial scaleup effort, the testing proved that it was more than sufficient to fulfill the required function. Although scaleup was demonstrated, more work clearly was required on scaleup process development.

An extensive investigation was then instituted to more thoroughly characterize the process required to produce high-quality iridium coatings on 100-lb_f chambers [29]. This effort included:

- Investigation of scaling phenomena to define reactor geometry and process parameters in order to increase deposition rate and coating uniformity for large chambers, to permit the deposition of 50-μm (0.002-in) iridium coatings in one continuous run.
- Development of a means for increasing the production of iridium ac-ac vapor in the precursor bed.
- Investigation of contamination sources and corrective action, with assistance from Aerojet and NASA-JPL.

4.3 Process Parameter and Reactor Geometry Definition for Large Chamber Fabrication

4.3.1 Process Parameters

The influence of deposition parameters, specifically hydrogen pressure, hydrogen flow rate, and annular gap, on the iridium deposition rate under roughly full-scale 100-lb_f conditions was examined.

Four cylindrical stacked 3-in (76.2-mm) diameter by 2-in (50.8-mm) thick stainless steel rings were coated with iridium in the 140-mm (5.51-in) diameter reaction chamber used in coating 100-lb_f thrusters, and also in a 90-mm (3.54-in) diameter chamber. The hydrogen pressure was varied while the hydrogen volumetric flow (and hence Ir ac-ac mass flow) was kept fixed.

At a pressure of 1 atm in the 140-mm chamber, the deposition rate was highest on the bottom ring, contrary to usual conditions. Reducing the pressure to 0.5 atm doubled the deposition rate on the top ring, and resulted in all rings plating at about the same rate. Reducing reaction chamber diameter to 90 mm greatly increased the deposition rate on the top ring without a corresponding effect on the lower ring, resulting in a large taper. This was most likely due to the depletion of reactant gas.

4.3.2 Reactor Geometry

Since 100-lb_f chamber experiments typically cost \$10-20,000 each, an innovative method was required to minimize the expense of investigating the effects of reactor geometry on iridium deposition on these chambers. Material costs alone for 100-lb_f chambers include \$5000 for the molybdenum mandrel and \$4000 for the iridium ac-ac precursor, which permits the deposition of approximately 50 μm (0.002 in) of iridium on the mandrel. Due to the size and weight of the mandrel, the deposited iridium must be 25-50 μm (0.001-0.002 in) thick in order to obtain meaningful measurements. Metallurgical analysis then requires sectioning the mandrel, effectively making it non-reusable.

By using a segmented molybdenum mandrel with removable and replaceable molybdenum insert rings, as shown schematically in Figure 13, the experimental costs were significantly reduced. The advantages of this device are:

1. The small size of the insert rings permits short runs (low iridium usage) for accurate analysis.
2. The replaceable insert rings cost several hundred dollars, while an entirely new molybdenum mandrel costs $5000.
3. The replaceable insert rings permit investigation of annealing and surface treatment without requiring an entirely new mandrel.

Due to the complex nature of the process(es) occurring within the reactor, design does not readily lend itself to analytical methods. Reactor design is largely empirical and to a large extent based on experience. A significant number of iterations were performed using the segmented molybdenum mandrel. Iridium deposition rate and distribution were measured while keeping the flow conditions and temperature constant.

A conformal reaction chamber was substituted for the cylindrical reaction chambers previously used for iridium deposition on the 100-lb_f thrusters, in order to eliminate the complex convective gas flow effects. A reaction chamber conforming to the shape of the 100-lb_f thruster mandrel was fabricated of pyrex. Flow visualization techniques were used to observe the gas flow patterns along the mandrel. It was found that the plating gas flowed at a more uniform speed along the mandrel and was free of convective vortices. Contoured chambers have been used for all subsequent iridium deposition on 100-lb_f mandrels. Figure 14 shows a schematic of the 90-mm (3.54-in) conforming chamber with mandrel in place.

The final reactor design for 100-lb_f chambers resulted in an increase in deposition rate from approximately 1-2 μm/hr (0.00004-0.00008 in/hr) to 6-8 μm/hr (0.0002-0.0003 in/hr) and significantly improved the coating distribution along the mandrel.

4.4 Fluid Bed Evaporator for Large Chamber Fabrication

To maintain the iridium ac-ac flow per unit mandrel area for a 100-lb_f chamber at the level used for 5-lb_f chambers, the sublimation rate of the solid precursor must be increased by a factor of 20. Despite the much larger evaporator incorporating a four-tiered bed used for the Aerojet/NASA-JPL 100-lb_f chamber fabrication, the in situ decomposition of Ir ac-ac imposes a practical limit on the sublimation rate increase of about six times with a single stationary bed evaporator. Multiple stationary beds or a fluidized bed are needed to remove this limitation.

As noted, the precursor for the iridium deposit, Ir ac-ac, is a solid compound that must sublime to form the plating gas. The compound, in the form of small crystals, is spread on a horizontal section of the evaporator, where it is heated and sublimed in the carrier gas stream. When coating larger parts, the supply of precursor gas is ultimately limited by the size of the exposed surface area of the precursor crystals. Even the use of stacked tiers of horizontal bed surface becomes inadequate. A related problem is that the very long times required for coating large parts results in appreciable decomposition of the expensive iridium precursor compound in the evaporator bed.

A solution to all of these problems may be achieved by the use of a fluidized bed evaporator. This concept was initially evaluated using the simplified fluid bed

evaporator shown in Figure 15. Iridium ac-ac crystals are fed into the apparatus, which consists of silica sand particles that are fluidized by the carrier gas stream. The bed, comprised of the silica sand and the precursor compound, is maintained at the desired temperature (Ir ac-ac sublimation temperature) by a nichrome heater.

An important characteristic of a fluid bed is that it is nearly isothermal. The precursor crystals promptly attain the temperature of the bed, and since the entire surface area of each crystal is exposed to the carrier gas, they evaporate quickly. Decomposition is thus minimized because exposure to high evaporation temperatures occurs only briefly before sublimation. Consequently, the mass transport of the plating compound is controlled by the solid feed rate, which is far more reliable than attempting to saturate the carrier gas, as must be done with a stationary bed.

A series of experiments was conducted to characterize the operation of the fluid bed evaporator and to define the laws that relate feed rate, carrier gas flow and pressure, bed temperature, and Ir ac-ac vapor production. Samples were coated and their quality related to these characteristics.

With this accomplished, a "production" fluid bed evaporator was designed and fabricated. The chamber design is shown schematically in Figure 16, and a photograph of the entire apparatus is shown in Figure 17. This apparatus is comprised of five sections: preheater, fluid bed evaporator, diverter, disentrainment volume, and particle filter. Two auxiliary devices support the evaporator in its function: the oven, which maintains the desired bed temperature, and the solid delivery system, which feeds Ir ac-ac into the bed at a constant rate. Accumulation of Ir ac-ac in the bed is prevented by maintaining a sufficient carrier gas flow to keep the resultant gas mixture at 90% saturation.

In this reactor, the carrier gas flow is introduced at the bottom of the fluid bed. An electric preheater ensures that the temperature of the gas stream is adjusted to the operating temperature of the bed, thereby minimizing thermal variations within the evaporator. The fluid bed proper consists primarily of silica stand, screened to 140-180 mesh. The bulk of the bed must be composed of a material other than Ir ac-ac, which has a tendency to agglomerate as the temperature approaches its melting point of 265°C (510°F). Silica provides an acceptable medium for fluidization, prevents agglomeration, and minimizes the resident mass of Ir ac-ac contained in the bed. Crystalline Ir ac-ac is introduced directly into the fluid bed, where turbulence ensures rapid mixing and prompt evaporation. A diverter, located above the bed, then performs a rough separation of the gas mixture and energetic silica particles. It also redirects the gas flow and helps to quickly establish a uniform flow profile in the disentrainment volume, where additional separation occurs as the flow velocity is reduced. As a final precaution against particulate contamination of the iridium deposit, the flow is directed through a particle filter to remove any remaining solids.

This device was tested with the segmented molybdenum mandrel and the redesigned reactor, with the result that iridium deposition rates of 15 μm/hr (0.0006 in/hr) could be sustained indefinitely and without appreciable loss of precursor due to decomposition. Iridium coating thickness was measured at 50-75 μm (0.002-0.003 in) over the entire surface of the mandrel.

4.5 Graphite/Molybdenum Mandrel for Large Chamber Fabrication

As chamber sizes become larger, cost and difficulty of handling (i.e., weight) make molybdenum a poor choice as a mandrel material. Powder metallurgy molybdenum bar stock, from 2-6 inches (50.8-152.4 mm) in diameter, costs approximately $\$26/lb_m$ ($\approx\$11.80/kg$) and has a specific gravity of 10.2. For the Aerojet/NASA-JPL 100-lb_f chambers, molybdenum mandrels were fabricated from 4-in (101.6-mm) diameter by 10-in (254-mm) long bars, weighing approximately 46 lb_m (20.9 kg) and costing approximately $1200. An 8-in (203.2-mm) diameter, 10-in long bar would weigh 184 lb_m (83.5 kg) and cost nearly $5000. Machining molybdenum is also difficult and costly; cost estimates for machining a JPL-type mandrel were about $4000. Production costs could be substantially reduced even for small units if a less costly alternative were available.

The characteristics necessary for a thrust chamber mandrel material are:

1. Good CTE match with iridium
2. Minimal interaction with iridium
3. Ability to withstand 1300°C (2370°F) rhenium deposition temperature
4. Good machinability
5. Stability and ability to hold tight tolerances
6. Ability to be removed without damage to the iridium or rhenium

In the past, Ultramet has used graphite mandrels for large rhenium structures [2]. Graphite is available with a wide variety of expansion coefficients, is easy to machine, and potentially meets all of the criteria for a successful mandrel material. One of the potential difficulties is removing the mandrel. In the past, Ultramet had removed the mandrel by machining it away, but this would be a risky procedure with the iridium coating on the inside of the chamber.

Experimental tubes were fabricated to test graphite as a mandrel material for Ir/Re structures. Several 0.5-in (12.7-mm) diameter POCO graphite mandrels, whose thermal expansion matches that of iridium very closely over the 20-1200°C (70-2190°F) temperature range, were coated with 25 μm (0.001 in) of iridium followed by 0.5 mm (0.02 in) of rhenium. Using a mask to protect the rhenium, the graphite was electrolytically dissolved out to leave free-standing rhenium tubes coated internally with iridium. The tubes were sound, with no evidence of attack of the rhenium or debonding of the iridium. Metallography revealed porosity in the iridium at the iridium/graphite interface, as shown in Figure 18. Since these graphites are made of fine, $\approx$1-μm (0.00004-in) graphite powder, it is hypothesized that the porosity resulted from trapped gases that were released during iridium deposition.

Another such structure was fabricated using Toyo SIC6 graphite, which has a somewhat lower CTE. The metallographic results, shown in Figure 19, revealed no porosity.

Clearly, graphite is a potential mandrel material for Ir/Re thrust chambers. A further refinement would be to overcoat the surface with a thin layer of CVD molybdenum, which can be deposited using chloride or fluoride precursors. Feasibility experiments were performed using the chloride ($MoCl_5$). It was concluded that overcoating with molybdenum is feasible, but that additional work is required on surface finishing after the molybdenum is deposited.

4.6 Iridium Contamination and Purification

In this study, Ultramet was assisted by JPL in analyzing the iridium precursor and suggesting precursor processing improvements, and by JPL and Aerojet in analyzing samples of deposited iridium.

4.6.1 Iridium Precursor

Iridium acetylacetonate (Ir ac-ac), the precursor compound for iridium deposition, is obtained commercially as a solid, in either powder or crystal form. Extensive communication with the manufacturer was unsuccessful with regard to their certifying, measuring, or guaranteeing contamination control of the Ir ac-ac. Apparently, the manufacturer altered its procedure when Ultramet's orders started reaching several troy ounces; recrystallization of the product was omitted because it greatly reduced the yield. Thin layer chromatography (TLC) yielded evidence of slight contamination. Infrared spectroscopy showed no clear difference between various processed Ir ac-ac samples. Ultramet then contacted another manufacturer whose material was of higher purity and more reproducible.

At the same time, Ultramet developed a proprietary purification procedure through which all as-received Ir ac-ac is subjected in an attempt to provide both improved purity and reproducibility. JPL analyzed samples from before and after the institution of this purification procedure and concluded that the purity of the Ultramet-processed material was significantly higher than the as-received material.

To date, no quality assurance procedure has been developed to guarantee the quality of the Ir ac-ac used in the iridium deposition process. The real test appears to be in the CVD process itself, which has shown Ultramet's proprietary purification procedure to be a reliable guarantee of purity.

4.6.2 Deposited Iridium

Iridium flakes that peeled from the skirt of Aerojet/NASA-JPL 100-lb_f unit #3 after the fourth iridium deposition were examined. About 100 cm^2 (15.5 in^2) of iridium spalled from the molybdenum mandrel following the fourth iridium deposit. Several of these flakes were furnished to Aerojet and JPL for examination. Ultramet mounted several flakes for metallographic analysis and hardness testing. The flakes exhibited multilayering, which ordinarily suggests periodic contamination. However, no contamination was evident in energy-dispersive X-ray spectroscopy (EDX) performed by Aerojet. Knoop 100-g hardness averaged 502, which is high compared to the Knoop value of 200 for annealed bulk iridium.

JPL performed an analysis of the iridium on the cap that covered unit #3 and spalled iridium flakes from the skirt of the same chamber. Chemical analysis was performed on the surface and at various levels within the surface after the surface was ion etched. Both the inner (next to the molybdenum mandrel) and outer surfaces were analyzed.

The results on a spalled flake from the interior surface showed high concentrations of oxygen and carbon (≈36 and ≈33 at% respectively) on the surface; ≈9 at% nitrogen, ≈7 at% molybdenum, and ≈13 at% iridium. After etching off 1000 Å, concentrations of 31 at% iridium, 60 at% molybdenum, and 9 at% oxygen were measured.

The results on a spalled flake from the exterior surface showed similar results for carbon, nitrogen, and oxygen (≈36, 8, and 30 at% respectively) with 0.4 at% molybdenum and 26 at% iridium. After etching off 1000 Å, the oxygen was reduced to 4 at%, the iridium increased to 96 at%, and no molybdenum was found.

A continuous etch/analysis was performed from the Mo/Ir interface side (interior surface) of a flake to a depth of approximately 20 μm (0.0008 in). The results showed a decrease in molybdenum from more than 50 at% to ≈8 at% at 20 μm, with a concomitant increase in the iridium fraction.

Analysis of the multilayered iridium deposit on the molybdenum cap showed carbon, nitrogen, oxygen, and sodium (all common surface contaminants) in addition to iridium, as well as copper, calcium, silicon, phosphorus, and traces of molybdenum and aluminum on the exterior surface. Most of these elements appear to be surface contaminants, which are greatly reduced by ion etching. The interior surface (Mo-Ir interface) showed the same elements, but the relative amount of phosphorus, calcium, and silicon was significantly less than appeared on the exterior surface. This reduction is likely due to diffusion into the molybdenum substrate. Similar contaminants were found at all interfaces.

The following conclusions were drawn from this analysis:

- Contamination is a surface phenomenon.
- The contaminants are mostly associated with volatiles found in cleaning materials, and could be significantly reduced by proper cleaning procedures.
- Significant molybdenum diffusion/alloying occurs from the Mo-Ir interface, but even though as much as 8 at% molybdenum was found 20 μm into the iridium, no problems occurred during later test-firing.
- All contamination (except molybdenum) in the bulk iridium could be eliminated if the iridium could be deposited in one run (single layer).
- If the iridium could be deposited in one run, the surface contamination would be problematic only if it caused defects at the Mo-Ir interface, which has never been observed (probably because the contaminants diffuse into the molybdenum); or if it prevented bonding/diffusion of the iridium and the rhenium. This also has never been observed, probably due to the fact that the part is cleaned in flowing hydrogen for one hour at 1200-1300°C (2190-2370°F) prior to rhenium deposition, which removes most of the surface contamination.

Based on these conclusions, a detailed cleaning and storage procedure was developed to eliminate surface contamination.

4.7 Iridium/Niobium Chamber Fabrication and Testing

Two promising approaches lend themselves to overcoming the bonding failure typically encountered in the CVD coating of niobium and its alloys. The source

of the problem appears to lie in the extreme reactivity of niobium at elevated temperatures. One solution is to employ a relatively low temperature for deposition, until the niobium surface is completely covered. Experiments at Ultramet have shown that adherent coatings of iridium on niobium can be achieved by starting the iridium CVD process at a temperature 150°C (270°F) lower than normally employed. Buildup of coating thickness is consequently slow, but very adherent. After a few microns of iridium have accumulated, the temperature may be raised in order to more quickly build up the coating to the desired thickness. This approach is appropriate for coating existing niobium parts. The second approach employs an intermediate layer of rhenium or tungsten to prevent interdiffusion of the iridium and niobium. Deposition parameters must be properly established to prevent free chlorine from attacking the niobium.

Under a cooperative agreement, Aerojet supplied Ultramet with a standard 5-lb_f C-103 niobium alloy chamber, which Ultramet would coat with iridium and Aerojet would then test-fire. Experiments were performed to determine the processing parameters associated with depositing iridium onto niobium. The Aerojet-supplied niobium thrust chamber was then coated with iridium on both the interior and exterior surfaces and delivered to Aerojet for hot-fire testing [30].

4.7.1 Iridium Coating

Coating the chamber provided by Aerojet presented unique problems, some of which became evident only after the chamber had been coated. Ultramet normally fabricates the entire thrust chamber in-house, starting with a molybdenum mandrel, coating it with 50 μm (0.002 in) of iridium, followed by 1 mm (0.04 in) of rhenium. In this case, however, Ultramet was presented with an already fabricated niobium alloy chamber. Thus, instead of depositing iridium on the outside of a mandrel, the interior of a narrow and irregular cavity had to be coated. Because the fluid dynamics of the CVD process are very different when the plating gases flow over a mandrel rather than through a cavity, it was very difficult to predict the effects of heat exchange, diffusion, and depletion along the length of the chamber.

Constraints of time, funding, and the lack of a spare chamber on which to practice necessitated the selection of deposition conditions without the benefit of experimentation or adequate instrumentation. In order to minimize risk, it was decided to coat the niobium chamber in three runs, rather than the one run employed previously for 5-lb_f chambers that required no outer coating. The first run was designed to coat the exterior of the chamber; the second run coated the interior of the chamber and the throat; and the third run coated primarily the interior of the skirt, but also added a thin coating to all previously coated areas. Flakes of this thin layer later spalled from the outside of the chamber, leaving undamaged iridium beneath.

Except for the last run, elaborate shielding was employed to keep the plating gases away from regions not intended for coating. Nonetheless, there were obvious regions of overlap. Visual inspection revealed that the coating was flaking off in the overlap regions. Because it appeared that only the second layer was debonding while the initial layer remained intact, Ultramet did not regard this deterioration as a serious problem with regard to oxidation resistance. However, Aerojet was concerned about the debonding and was initially reluctant to test the chamber. Aerojet decided to proceed with testing, but to be very conservative about exposing the chamber to highly oxidizing conditions,

i.e. mixture ratios significantly higher than employed with disilicide coatings. Indeed, the overlapping area of the throat eroded most severely during testing.

Measurement of substrate temperature, a critical deposition parameter, was difficult to obtain without the existence of a mandrel, which when used contains an axially positioned thermocouple. It was not possible to measure the temperature of the part during interior coating with any degree of reliability.

The decision to shield certain regions during coating also led to the inability to rotate the part, which is normally done to ensure symmetrical coverage. The asymmetrical failure of the throat region could well be a consequence of an asymmetrical distribution of coating gases due to slight imperfections in the alignment of the system.

Still another deviation from normal practice arose because the deposition process employs hydrogen; experience had indicated that iridium does not adhere to niobium that has been exposed to hydrogen at the deposition temperature. Niobium reacts with, and is embrittled by, hydrogen most rapidly at the temperature used for optimal iridium deposition. Thus, the standard deposition conditions for iridium could not be used, as it was necessary to avoid hydrogen during the critical initial moments when bonding occurs. In addition, the standard heat treatment after deposition (to promote bonding) was eliminated to avoid contamination from condensed reaction products.

4.7.2 Hot-Firing Tests

The iridium-coated 5-lb_f C-103 niobium thrust chamber was tested by Aerojet in a configuration where the iridium coating directly substituted for the standard Hitemco R512E disilicide coating. Eleven tests were performed, for an accumulated burn time of 4023 seconds, using NTO/MMH propellant at a mixture ratio of 1.5. Five short-performance survey tests at mixture ratios ranging from 1.2 to 2.0 indicated that specific impulse and operating temperature were higher than those expected for a disilicide-coated chamber. The low emissivity of the external iridium coating and the smoothness of the throat and nozzle could account for this significant performance improvement. Despite the fact that this was the first attempt at coating a niobium alloy chamber with iridium, the chamber survived 4023 seconds before the coating delaminated locally. This is about half the lifetime expected under the same conditions for the disilicide coating.

These initial test results were very encouraging. The fact that the tested article was able to operate for over one hour at temperatures in the 1480-1590°C (2700-2900°F) range, in spite of the relatively poor fabrication quality of such an initial attempt, indicates that the iridium liner concept has merit for further investigation as a replacement for the disilicide coating normally used.

As noted, the purpose of the hot-firing tests of the iridium-coated niobium chamber was to demonstrate proof-of-concept, comparing iridium and disilicide coatings on a niobium alloy chamber using firing conditions established for disilicide coatings. Niobium alloys can withstand temperatures up to about 1930°C (3500°F) in low stress environments; however, the life of the disilicide coating degrades rapidly starting at ≈1370-1430°C (2500-2600°F). At 1320°C (2400°F), disilicide coatings have a life in excess of 20 hours; at 1590°C (2900°F), the life is reduced to a few thousand seconds.

Although iridium coatings have been demonstrated to provide oxidation protection to rhenium thrusters at operating temperatures of 2200°C (4000°F) or more without fuel film cooling, this is the first known attempt to hot-fire an iridium-lined niobium alloy chamber. Under normal firing conditions for this chamber, fuel film cooling of the wall is employed, amounting to 30% of the fuel flow. Normal firing conditions include a chamber pressure of 0.79 MPa (115 psi) and a mixture ratio of 1.65. When higher mixture ratios are employed, fuel is cut back in order to keep the chamber pressure fairly close to the nominal value. This strategy is responsible for the decline in specific impulse with increasing mixture ratio, as shown in Figure 20 [30]. As a consequence of the appreciable fuel devoted to wall cooling, the core becomes oxidation-rich at a mixture ratio of 1.2, and beyond the maximum in the relationship between specific impulse and mixture ratio.

It did not seem prudent to expose the iridium-coated niobium chamber to conditions much more severe than disilicide coatings can withstand. Demonstrating improved specific impulse with higher mixture ratios was not possible because of the injector design, which diverts a large fraction of fuel to film cooling.

Based on this experience, the fabrication process for iridium-coated niobium thrust chambers could be improved in several ways:

- Learn how to coat thrusters in one run. This would eliminate the problem of bonding multiple layers of iridium, the need to protect uncoated areas from embrittlement and contaminating reaction products for many hours, and the setups and time required for multiple runs. Experimentation with dummy chambers would be required to achieve a satisfactory coating distribution. A "mute" would be needed in the skirt to ensure proper flow in the divergent region.

- Rotate thruster during coating. This will be facilitated by not having to shield any areas from plating gases.

- Use a two-color optical pyrometer to obtain non-contacting measurements of temperature.

- Use an interlayer to impede the diffusion of niobium into iridium. Niobium diffuses into iridium at firing temperatures, impairing the oxidation resistance of the coating. Ultramet has successfully used CVD tungsten as a thin diffusion barrier between niobium and iridium on test coupons. Tungsten adheres well to both niobium and iridium. Since tungsten can be deposited without the use of hydrogen, this strategy would also eliminate the deposition process compromises designed to avoid embrittlement.

- Fabricate the entire chamber by CVD using the inside-out method. Niobium and its alloys are readily and uniformly deposited by CVD. This method has the potential for reducing overall chamber cost.

In any case, the results of this initial effort were encouraging. It is impressive that a coating was achieved on the first attempt that lasted more than one hour in hot-fire testing, whereas disilicide coatings, which have undergone

a multimillion-dollar development effort over many years, last only two hours under the same conditions.

4.8 Other Iridium-Related Investigations

A number of other iridium-related investigations were performed in order to provide a complete material and process characterization.

4.8.1 Bond Strength

To investigate the bond strength of iridium to molybdenum, and of multiple iridium layers, metallography and pull tests were performed on the iridium coating of the cap that covered Aerojet/NASA-JPL 100-lb_f chamber #3. Pull tests were performed on the cap by means of a Sebastian adhesion tester after each of four iridium depositions. After the mth coating, $(4-m)$ quadrants were sandblasted to bare molybdenum. After four coating runs, the resultant configuration was such that quadrant I had four layers, quadrant II had three layers, quadrant III had two layers, and quadrant IV had one layer.

The adherence between each coating and the bare molybdenum, and between each iridium layer, was determined by performing pull tests on each of the four quadrants after every run. The epoxy, rather than the coating, failed at 5-10 ksi (34.5-68.9 MPa) for each coating and set of coatings until the fourth coating, when quadrants I, III, and IV failed at low pull stress. JPL was supplied samples from each quadrant for metallographic and chemical analysis.

4.8.2 Interaction with Rhenium

An investigation was conducted as to why the outer iridium coating (iridium deposited on rhenium) of Ir/Re thrust chambers so often failed during firing while the inner iridium coating (rhenium deposited on iridium) was generally unaffected, and whether it correlated with the surface preparation of the rhenium prior to iridium deposition. Various techniques of smoothing as-deposited 1-mm (0.04-in) rhenium coatings on 0.5-in (12.7-mm) diameter molybdenum mandrels were employed before overcoating with 20 μm (0.0008 in) of iridium to simulate the outer coating on a thruster. Machining, belt sanding, grinding, peanut grinding, sandblasting, stoning, and combinations thereof were evaluated.

Pinholes occurred in the iridium coating unless the rhenium was removed to the bottom of the "valleys" caused by dendritic growth of the rhenium deposit. As long as enough material was removed to accomplish this smoothing effect by some process, the resulting surface finish caused by the process did not seem to affect coverage or adhesion.

4.8.3 Effect of Heat Treatment

The influence of heat treatment temperature and duration on adhesion and interdiffusion between molybdenum and iridium was investigated. Heat treatment, which is intended to promote bonding, was suspected of degrading bonding.

Twelve 0.5-in (12.7-mm) diameter by 0.5-in long cylindrical molybdenum slugs were prepared, and a flat was ground in each for hardness and adhesion testing. Four of these cylinders at a time were stacked and coated with iridium in a small

reaction chamber. Coating thicknesses from 25 to 80 μm (0.001-0.003 in) were achieved by removing slugs periodically during the plating process. The slugs were heat treated from 0.5 to 16.5 hours at 1000 or 1200°C (1830 or 2190°F).

None of the iridium coatings spalled, and all withstood 10-ksi (68.9-MPa) pull tests with a Sebastian adhesion tester. Metallography revealed that longer, higher temperature heat treatment resulted in thicker diffusion layers, as would be expected, but these showed no evidence of decrepitation.

To investigate the hardness of the iridium coating as a function of heat treatment temperature, one of the twelve 0.5-in molybdenum slugs described above, coated with 75 μm (0.003 in) of iridium, was subjected to heat treatments varying in 100°C (180°F) increments from 1000 to 1500°C (1830-2730°F). The hardness of the coating was measured after each heat treatment.

The onset of iridium recrystallization was observed to occur at 1200°C (2190°F), and significant recrystallization occurred at 1300°C (2370°F) and above. No statistically significant decrease in hardness was seen until the part was heat treated at 1400 and 1500°C (2550 and 2730°F). A 5% and 10% decrease was measured at these temperatures respectively.

4.8.4 Oxidation of Iridium/Rhenium Alloys

The oxidation of Ir/Re alloys is of interest for two reasons:

1. As operating life in thrust chambers increases, iridium and rhenium interdiffuse. This results in an increasing concentration of rhenium in the iridium, and possibly a decrease in the oxidation resistance of the iridium.

2. Ir/Re alloys have the potential to operate at higher temperatures than pure iridium, based on phase diagram considerations.

Under subcontract to Ultramet, the University of Pennsylvania investigated the oxidation of Ir/Re alloys using arc-melted materials. Iridium-10, 20, and 30 at% rhenium alloys were prepared using an arc melter. X-ray diffraction (XRD) analysis showed that the iridium-10 and 20 at% rhenium alloys were solid solutions, while the iridium-30 at% rhenium alloy was a two-phase mixture of iridium and rhenium.

Oxidation tests were carried out at 2300 and 2430°C (4170 and 4410°F) in 0.09 and 0.36 atm of air. Oxidation results for the iridium-10, 20, and 30 at% rhenium alloys are shown in Tables IIA-C, and plotted in Figures 21A (weight loss) and 21B (recession). A non-linear relationship was found to exist between oxidation rate, pressure, and alloy composition. The oxidation rates of these Ir/Re alloys at 2500°C (4530°F) were estimated assuming linear oxidation and an Arrhenius-type relationship between the oxidation rates and the temperature. The estimated oxidation rates at 2500°C are shown in Table IID and Figures 21A-B.

4.8.5 Diffusion Couple Studies

This research effort has focused on developing the iridium deposition process to provide improved oxidation protection for a secondary base metal, rhenium. Due to its high material cost, high density, and inferior structural properties, it

is likely that iridium will see service primarily as a protective coating for less expensive, lighter or stronger materials that are chemically more active than iridium. Iridium coatings on such materials will provide enhanced chemical (oxidation) protection without compromising structural integrity.

High temperature service may result in rapid diffusion at the iridium interface, with unknown consequences. Diffusion may promote adhesion or, alternatively, the formation of voids or brittle interlayers may have deleterious consequences. Three diffusion couples were investigated in this project: iridium-molybdenum, iridium-rhenium, and iridium-niobium.

Iridium-Molybdenum

Molybdenum was investigated for two reasons. First, in comparison to iridium, it is chemically active, forming a volatile oxide at temperatures above 800°C (1470°F). Second, molybdenum is used as a male mandrel for iridium deposition, defining the interior thrust chamber contour. Although iridium deposition is a low temperature process, the iridium remains in contact with the molybdenum throughout the subsequent rhenium deposition, which occurs at temperatures up to 1250°C (2280°F). A substantial amount of molybdenum diffuses into iridium at this temperature.

This investigation focused on the temperatures experienced during processing at Ultramet. It sought to quantitatively assess the temperature/time dependence of diffusion in the Ir-Mo couple. In addition, general observations such as microstructural changes and the chemical reactivity of the diffusion layers were noted.

Ten commercially pure molybdenum specimens, 0.5 inches (12.7 mm) in diameter by 0.5 inches long with flat, were coated with iridium by the standard procedure. Five samples were coated multiple times (2, 4, 4, 5, and 3 times, respectively) to assess the effect of thermal cycling on iridium-to-iridium adhesion. The results of that investigation, as well as more detailed information regarding the substrate geometry, were described above (section 4.8.3). All ten specimens were thermally cycled to the test temperature in argon at ambient pressure. The duration of each cycle was 30 minutes, with some samples being cycled up to 33 times.

The processed samples were sectioned across the diameter to evaluate the extent of diffusion. Electrolytical etching of the iridium layer was necessary to resolve all diffusion layers. Because the layer nearest the molybdenum mandrel was chemically reactive (in comparison with iridium), selective etching was required to resolve all layers simultaneously.

All the heat-treated samples exhibited solid state diffusion. The extent of penetration into the iridium was observed to increase with increasing time and temperature. Selective etching revealed the diffusion layer to be composed of three distinct layers, designated α, β, and γ, with α bordering iridium, γ neighboring molybdenum, and β between them.

The formation of three distinct phases in the diffusion layer may be explained as a consequence of the Mo-Ir phase diagram, shown in Figure 22 [31]. At temperatures below about 1400°C (2550°F), three phases are shown in the diagram: $MoIr_3$, MoIr, and Mo_3Ir. The diffusion layer at the interface should have a composition that spans the phase diagram. Thus, each phase should be represented

in the diffusion layer. As the number of observed layers coincides with the expected number of phases, the assignment of layers may be made simply as α, β, and γ for $MoIr_3$, MoIr, and Mo_3Ir respectively.

Figures 23-25 are photomicrographs that show the diffusion layer(s). Figure 23 is a cross-section of an unetched sample. Two layers are clearly visible, γ and (unresolved) $\alpha+\beta$. Also noteworthy is the exceptional bond quality, and the observation that nine hours of heat treatment at 1200°C (2190°F) did not cause the formation of voids or delamination. Figure 24 is a selectively etched region, which documents the chemical reactivity of γ with the iridium etchant. Figure 25 is a typical view of α and β after 16.5 hours at 1200°C.

The depth of each diffusion layer was measured from the photomicrographs. These measurements are provided in Table III, and graphs of the data are shown in Figures 26 and 27. This data was fit by a simple power expression with respect to time:

$$\lambda = C_1 t^{C_2} \tag{1}$$

where λ is the total diffusion layer thickness and C_1, C_2 are provided in Table IV, derived from a least-squares fit of the data. For the lowest temperatures, insufficient data was available to calculate the power coefficient, but since C_2 was close to the ideal solid mixtures theoretical value of 0.5 at 1200°C, this was chosen to be the value at 1000°C (1830°F).

Two comparative assessments of the diffusion kinetics were made, the first comparing the rate of propagation of the diffusion front at a constant time, and the second at a constant lambda. The former is useful in predicting the diffusion depth after a known time, while the latter predicts the rate of diffusion at comparable concentration gradients:

$$\left(\frac{\partial \lambda}{\partial t}\right)_t = C_1 C_2$$
$$\left(\frac{\partial \lambda}{\partial t}\right)_\lambda = C_1^{\left(1+\frac{1}{C_1}\right)} C_2 \tag{2}$$

Arrhenius plots of this data are shown in Figures 28 and 29. By assuming similar concentration gradients for identical lambda, the diffusion rate models may be combined to obtain

$$D = C_3 e^{-\frac{\Delta E}{RT}} \tag{3}$$

where ΔE = 268 kJ/mol (254 Btu/mol), based on a least-squares fit.

The diffusion of molybdenum in iridium was shown to be insignificant at the temperatures routinely used at Ultramet in processing Ir/Re chambers. The phase diagram indicates that temperatures up to the eutectic limit of 2080°C (3780°F) may be of interest. High temperature diffusion was not addressed by this study, and should be investigated prior to recommending high temperature service of iridium-molybdenum couples.

Iridium-Rhenium

Ir/Re thrusters have demonstrated survival in excess of 15 hours at 2200°C (4000°F). Rapid diffusion is expected at these temperatures. To predict thruster longevity, diffusion information was collected from the witness end rings of a 5-lb_f thrust chamber.

A 5-lb_f Ir/Re thrust chamber was manufactured using standard procedures. Both the small and the large end rings were parted from the chamber proper for analysis. As the rhenium deposition process requires a thermal gradient along the length of the chamber, the two end rings were representative of four hours of diffusion at 1150 and 1225°C (2100 and 2240°F).

Metallographic analysis revealed a single diffusion layer. This is consistent with the Re-Ir phase diagram, shown in Figure 30 [31], which shows the system to have only one mixed-phase region. The interface is continuous and free of defects, as seen in the photomicrograph of a polished cross-section shown in Figure 31. The depth of each diffusion layer was measured from the photomicrograph. A graph of the data is shown in Figure 32. This data was fit by a simple power expression with respect to time, as in equation (1) above, where C_1 = 0.00635 at 1150°C and 0.0148 at 1225°C and C_2 = 0.5 (ideal mixture).

Two comparative assessments of the diffusion kinetics were made, the first comparing the rate of propagation of the diffusion front at a constant time and the second at a constant lambda, as in equation (2) above. Arrhenius plots of this data are shown in Figures 33 and 34. It should be noted that two points are not statistically sufficient to define the response. By assuming similar concentration gradients for identical lambda, the diffusion rate models may be combined as in equation (3) above, with ΔE = 601 kJ/mol (570 Btu/mol) based on a least-squares fit.

These experiments provided guidelines for estimating the extent of iridium diffusion in the iridium-rhenium couple. Unfortunately, the sample population was too small to draw firm conclusions. In addition, the test temperatures of 1150 and 1225°C are far below the expected service temperature of 2200°C. These experiments should be supplemented with additional data, particularly at high temperatures. Nonetheless, metallography confirms the excellence of the bond and the absence of thermally induced flaws at lower temperatures.

Iridium-Niobium

Superior performance for Ir/Re thrusters has been demonstrated in this and previous work, with a substantial improvement over the existing state-of-the-art technology, disilicide-coated niobium, allowing thruster operating temperature to reach 2200°C. For less demanding (lower temperature) applications, niobium may be preferred over rhenium due to its lower density. In addition, many current storable propellant thrusters rely on disilicide-coated niobium technology. A replacement or supplemental coating for use with proven thrusters may reduce the flight qualification criteria.

A study of the diffusion at an iridium-niobium interface was undertaken to assess the temperature and time dependence. In addition, general observations such as microstructural changes, void formation, and delamination of the diffusion layers were sought and recorded.

Two commercially pure niobium specimens, 0.5 inches (12.7 mm) in diameter by 1.5 inches (38.1 mm) long, were coated with approximately 50 μm (0.002 in) of iridium using a modification of the standard coating procedure. This process modification, discussed in more detail above (section 4.7), minimizes hydriding of the niobium surface by introducing it into the plating environment only after the active gas (Ir ac-ac) has been stabilized at the steady state value. Plating of iridium thus commences immediately, and this newly formed iridium envelope protects against hydrogen infiltration. Niobium hydriding is a reversible process, and niobium hydride that does form may be dissociated by following the deposition process with a heat treatment at 900°C (1650°F), which also greatly improves adhesion.

A thin disk was cut from the second niobium cylinder as a sample of the iridium-niobium interface prior to heat treatment. Technically, the diffusion that occurred during iridium deposition at 430°C (810°F) for 120 minutes would represent the extent of heat treatment for this sample. The remaining cylinders were sectioned into two pieces to be used for heat treatment studies at 1320, 1430, 1540, and 1650°C (2400, 2600, 2800, and 3000°F). Each of the four specimens was repeatedly cycled to the test temperature in flowing argon at roughly 5 kPa (0.7 psi) pressure for 30, 30, 60, and 120 minutes. A thin disk was cut from the end of each cylinder between cycles for evaluation, giving samples having a total exposure time of 30, 60, 120, and 240 minutes at each of the test temperatures.

Each of the heat-treated samples exhibited solid state diffusion. When electrolytically etched to reveal the iridium microstructure, the diffusion layer was resolved into four different regions, with trace evidence for a fifth layer in the specimen treated at 1650°C. These layers were designated α, β, γ, and δ, with the α layer neighboring the iridium, followed by the β and γ layers, and then the δ layer next to the niobium substrate. A fifth layer may possibly be sandwiched between β and γ.

The formation of distinct phases in the diffusion layer may be explained as a consequence of the Nb-Ir phase diagram, shown in Figure 35 [31]. For temperatures below 1840°C (3340°F), the eutectic point, five phases are shown in the diagram: $NbIr_3$, σ, α_1, α_2, and Nb_3Ir. The diffusion layer at the iridium-niobium interface would be expected to have a continuum of composition spanning the entire phase diagram, and thus should have layers representing each of the five phases. A tentative assignment would place α, β, γ, and δ with $NbIr_3$, σ, α_2, and Nb_3Ir, respectively. The fifth layer, which is supported by only trace evidence, would be assigned to α_1, which is the "thinnest" layer, and is located in the proper position between β and γ.

These diffusion layers are absent from the sample taken prior to heat treatment. It is not clear if the layer is simply too thin to be visible, or if hydriding has interfered with diffusion activity. Adhesion of the iridium deposit was unacceptably poor for this specimen, and substantial delamination occurred as a result of the machining that was performed to extract the sample. Figure 36 is a photomicrograph of a representative region, which clearly shows debonding.

Figures 37A-D are photomicrographs of four samples that document the progression of the diffusion layer with time. Noteworthy is the expected increase in depth of all the layers, and the formation of voids, particularly between α and β. These may be Kirkendall voids, which form as a result of asymmetric diffusion

rates. At high temperatures, these voids are particularly prominent and seriously compromise the structural integrity of the coating. Figure 38 shows the extent of damage following 240 minutes at 1650°C.

The depth of each diffusion layer was measured from the cross-sectional photomicrograph. These measurements are provided in Table V, and graphs of the data are shown in Figures 39-42. This data was fit by a simple power expression with respect to time, as in equation (1) above, where C_1, C_2 are provided in Table VI, derived from a least-squares fit of the data. For the two lowest temperatures, C_2 is close to the theoretical value of 0.5 for ideal mixtures. At higher temperatures, this relationship may break down as the accumulation of voids acts as a bottleneck, restricting free diffusion.

Two comparative assessments of the diffusion kinetics were made, the first comparing the rate of propagation of the diffusion front at a constant time and the second at a constant lambda, as in equation (2) above. Arrhenius plots of this data are shown in Figures 43 and 44. By assuming similar concentration gradients for identical lambda, the diffusion rate models may be combined as in equation (3) above, with ΔE = 769 kJ/mol (729 Btu/mol) based on a least-squares fit.

In contrast to rhenium, niobium is very mobile in iridium. This diffusion gives rise to voids, which may seriously compromise the structural integrity of the coating. These effects may be mitigated to some extent by the judicious selection of a diffusion barrier, such as a thin layer of rhenium or tungsten, which may attenuate diffusion sufficiently to render feasible the idea of protecting niobium with iridium at temperatures in excess of 1300°C (2370°F). The scope of this study did not permit such an investigation.

5. CONCLUSIONS AND RECOMMENDATIONS

Propellant for orbit insertion and/or attitude control is the largest single item contributing to the mass of most satellites. Not only does this increase the cost of placing the systems into orbit, but generally it is the depletion of this propellant that limits satellite life. Anything that can be done to decrease satellite propellant requirements or make more effective use of the propellant will have a significant beneficial impact on these systems.

The rocket engines in general use on current satellites are either relatively low-performing hydrazine monopropellant thrusters or liquid bipropellant engines employing NTO/MMH. The bipropellant engines deliver performance considerably lower than theoretically possible because of the way the thrust chambers operate. They employ simple disilicide-coated niobium chambers, which have a nominal upper use temperature of 1320°C (2400°F) with approximately ten hours life. To maintain the wall temperature at or below this level, a significant amount of the fuel, typically 30-40% for a 5-lb_f thruster, is used for film cooling of the chamber walls. This results in performance losses on the order of 20 seconds of specific impulse for a 5-lb_f thruster. The use of a chamber material capable of operating at a higher wall temperature would improve engine performance since fuel film cooling could be reduced or eliminated.

In this program, Ultramet demonstrated the materials and process technology that permits the fabrication of thrust chambers able to operate at 2200°C (4000°F) without sacrificing the life associated with disilicide-coated niobium chambers. The performance improvements were verified by actual testing for 15 hours at Aerojet TechSystems. Not only was the technology demonstrated, but the process was defined, characterized, and scaled up, and is ready for application to future systems. Meanwhile, work continues on optimizing the process for large (e.g. 100-lb_f) chambers [32].

The overall objective of this program was to advance the state of the art in materials and processes for the fabrication of chemical rocket thrust chambers. Although the objectives were clearly met and exceeded, improvements can still be made, particularly in two major areas:

1. Performance improvement for niobium alloy chambers. In this project, Ultramet demonstrated the feasibility of coating state-of-the-art niobium alloy chambers with iridium to permit operation at higher temperatures. This work should be continued in the areas of interlayers to prevent diffusion of niobium and iridium, and process development to ensure viable iridium coatings. In addition, other protective coatings should be investigated, such as platinum and iridium aluminide.

2. Performance improvement through higher temperatures, longer life, and lighter weight chambers. A number of potential material and process improvements were discussed previously (section 3) that should be pursued. Thermal/diffusion barriers should lead to higher temperature operation and/or longer life; graded materials should improve thermal shock resistance; and dispersion-strengthened rhenium should lead to lighter weight structures.

REFERENCES

1. I.E. Campbell and E.M. Sherwood, eds., High Temperature Materials and Technology (John Wiley, New York, 1967).

2. M.A. Appel, R.B. Kaplan, and R.H. Tuffias, "Liquid Fluorine/Hydrazine Rhenium Thruster Update," Proc. 1983 JANNAF Propulsion Meeting (Chemical Propulsion Information Agency, Laurel, MD, 1983), 85.

3. R.A. Bjorklund and M.A. Appel, "Very Low Thrust and Low Chamber Pressure GO_2/GH_2 Thruster Technology," Proc. 1984 JANNAF Propulsion Meeting (Chemical Propulsion Information Agency, Laurel, MD, 1984), 29.

4. L.E. Saltz and D.L. Emmons, "High Temperature Augmented Monopropellant Hydrazine Thruster," Proc. 1984 JANNAF Propulsion Meeting (Chemical Propulsion Information Agency, Laurel, MD, 1984), 75.

5. M.A. Appel, L. Schoenman, and D.K. Berkman, "Oxygen/Hydrogen Thrusters for the Space Station Auxiliary Propulsion System," Proc. 1984 JANNAF Propulsion Meeting (Chemical Propulsion Information Agency, Laurel, MD, 1984), 339.

6. J.M. Shoji, I. Kaith, and A.G. Pard, "Solar Thermal Rocket Design and Fabrication," Proc. 1985 JANNAF Propulsion Meeting (Chemical Propulsion Information Agency, Laurel, MD, 1985), 495.

7. C.A. Krier and R.I. Jaffee, "Oxidation of the Platinum Group Metals," J. Less-Common Metals 5 (1963), 411.

8. J.M. Criscione et al., "High Temperature Protective Coatings for Graphite," ML-TDR-64-173, Part III (Air Force Materials Laboratory, Wright-Patterson AFB, OH, 1965).

9. J.T. Harding, R.H. Tuffias, and R.B. Kaplan, "High Temperature Oxidation-Resistant Coatings," AFRPL-TR-84-036 (Air Force Rocket Propulsion Laboratory, Edwards AFB, CA, 1984). [ULT/TR-84-3905]

10. J.T. Harding, R.H. Tuffias, and R.B. Kaplan, "Oxidation-Resistant Coatings for Refractory Metals," Proc. 1985 JANNAF Propulsion Meeting (Chemical Propulsion Information Agency, Laurel, MD, 1985), 181.

11. D.T. Dickson et al., "Very High Temperature Coatings for Tantalum Alloys," AFML-TR-66-317 (Air Force Materials Laboratory, Wright-Patterson AFB, OH, 1966).

12. C.F. Powell, J.H. Oxley, and J.M. Blocher Jr., eds., Vapor Deposition (John Wiley, New York, 1966).

13. J.T. Harding, R.H. Tuffias, and R.B. Kaplan, "Platinum Group Coatings for Refractory Metals," AFRPL-TR-84-035 (Air Force Rocket Propulsion Laboratory, Edwards AFB, CA, 1984). [ULT/TR-84-3904]

14. J.T. Harding, R.B. Kaplan, and R.H. Tuffias, "The Deposition of Platinum Group Metals by CVD," presented at 10th International Precious Metals Institute Technical Conference, Lake Tahoe, NV, 8-12 June 1986.

15. J.T. Harding, R.H. Tuffias, and R.B. Kaplan, "Oxidation Protection of Rhenium Thrusters for 2480 K Cyclic Operation by Means of CVD Coatings," Final Report (ULT/TR-86-4676), Contract NAS3-24868, NASA Lewis Research Center, Cleveland, OH, June 1986.

16. J.T. Harding, R.H. Tuffias, and R.B. Kaplan, "Oxidation Resistance of CVD Coatings, Phase II," AFRPL-TR-86-099 (Air Force Rocket Propulsion Laboratory, Edwards AFB, CA, 1987). [ULT/TR-86-4256]

17. L. Schoenman and P.T. Lansaw, "Oxidation Resistance of CVD Coatings, Appendix," AFRPL-TR-86-099 Supplement (Air Force Rocket Propulsion Laboratory, Edwards AFB, CA, 1987).

18. J.T. Harding, R.H. Tuffias, and R.B. Kaplan, "Oxidation Protection of Refractory Metals to 2400°C," TMS Technical Paper F87-10 (The Metallurgical Society, Warrendale, PA, 1987).

19. J. Blossom (U.S. Bureau of Mines, Washington, DC), communication with author, August 1986.

20. H.O. Pierson, R.H. Tuffias, and R.B. Kaplan, "HfO_2 and ZrO_2 Overcoating of SiC for Extending the Oxidation Protection of Carbon Composites to 3500°F," Final Report (ULT/TR-86-4511), Contract F33615-85-C-5117, Air Force Materials Laboratory, Wright-Patterson AFB, OH, January 1986.

21. L. Schoenman (Aerojet TechSystems, Sacramento, CA), communication with author, August 1986.

22. H.O. Pierson, "Stabilized High Temperature Oxides by CVD," Final Report (ULT/TR-87-4829), Contract N62269-87-C-0204, Naval Air Development Center, Warminster, PA, June 1987.

23. H.O. Pierson, "Thoria Coating for Oxidation Protection," Final Report (ULT/TR-87-4858), Contract DNA001-86-C-0231, Defense Nuclear Agency (DNA), Washington, DC, March 1987; sponsored by Strategic Defense Initiative Organization (SDIO).

24. M.V. Whalen, P.T. Lansaw, and J.R. Wooten, "High-Temperature, Oxidation Resistant Thrusters," Proc. 1987 JANNAF Propulsion Meeting (Chemical Propulsion Information Agency, Laurel, MD, 1987), 413.

25. J.T. Harding, J.M. Kazaroff, and M.A. Appel, "Iridium-Coated Rhenium Thrusters by CVD," NASA TM-101309 (NASA Lewis Research Center, Cleveland, OH, 1988).

26. J.R. Wooten and P.T. Lansaw, "The Enabling Technology for Long-Life, High Performance On-Orbit and Orbit Transfer Propulsion Systems: High Temperature, Oxidation Resistant Thrust Chambers," Proc. 1989 JANNAF Propulsion Meeting (Chemical Propulsion Agency, Laurel, MD, 1989).

27. R. Draper, "Comet Rendezvous Asteroid Flyby: First Mariner Mark II," AAS-86-333 (American Aeronautical Society, 1986).

28. M. Appel, L. Schoenman, J. Franklin, and P.T. Lansaw, "Feasibility Demonstration of A High-Performance 100-lb_f Rocket Engine," Proc. 1989 JANNAF Propulsion Meeting (Chemical Propulsion Agency, Laurel, MD, 1989).

29. R.H. Tuffias, G.J. Melden, J.T. Harding, and R.B. Kaplan, "CVD Fabrication Applied to Advanced 2200°C Chemical Rocket Combustion Chambers," in Surface Modification Technologies IV, T.S. Sudarshan, D.G. Bhat, and M. Jeandin, eds. (The Minerals, Metals, and Materials Society (TMS), Warrendale, PA, 1991), 855.

30. P.T. Lansaw and L. Schoenman, "Hot-Fire Test Report: Iridium-Coated Columbium (C-103) Thrust Chamber," Aerojet TechSystems IR&D Report NLR9EA, June 1989.

31. T.B. Massalski, ed., Binary Alloy Phase Diagrams, Vol. 2 (American Society for Metals, Metals Park, OH, 1986).

32. R.H. Tuffias, G.J. Melden, and J.T. Harding, "CVD Iridium Process Control and Improvement and Chamber Fabrication," work in progress under contract NAS3-25792, NASA Lewis Research Center, Cleveland, OH, July 1989-present.

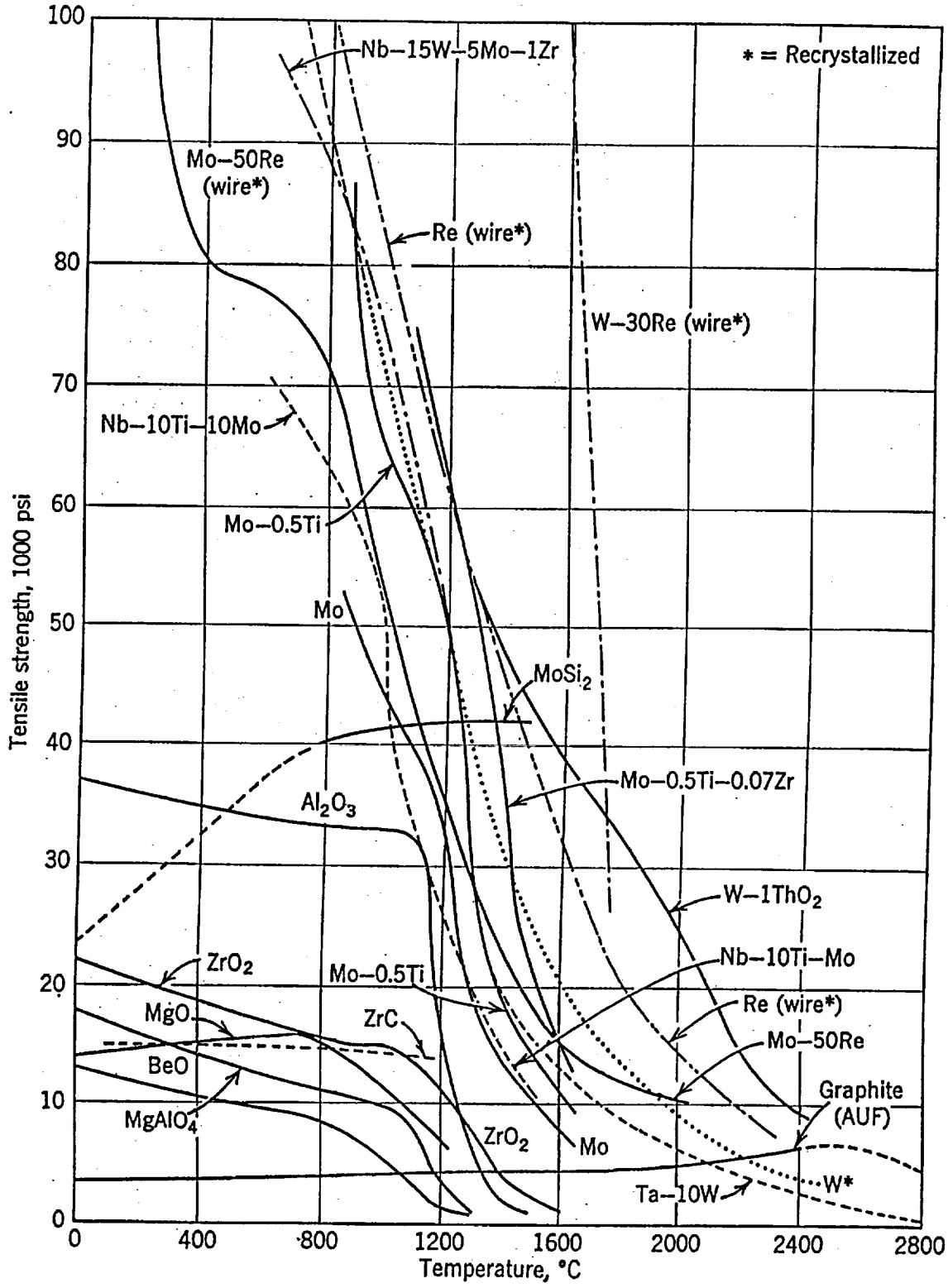

Figure 1. Temperature vs. tensile strength for refractory materials

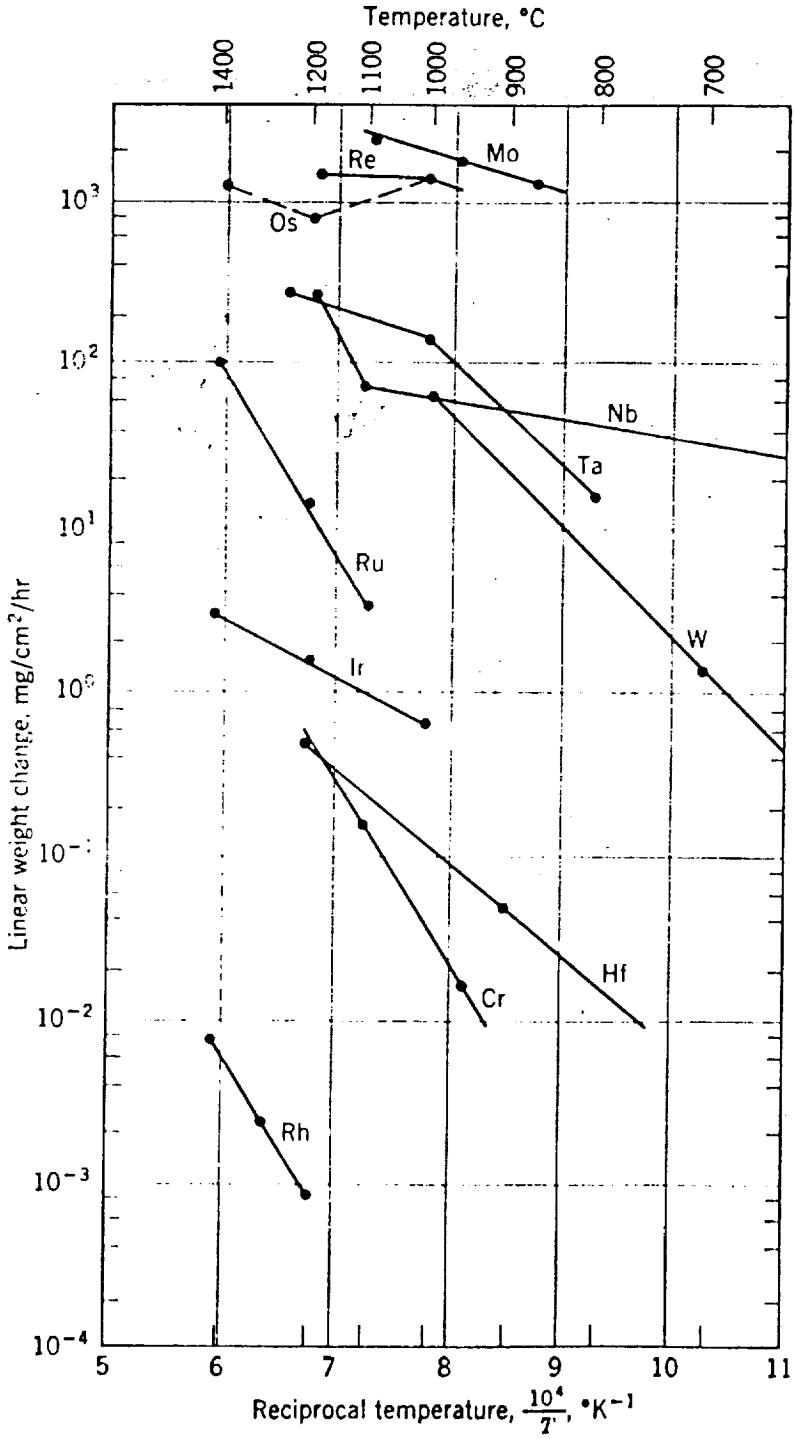

Figure 2. Temperature vs. oxidation rate for refractory metals

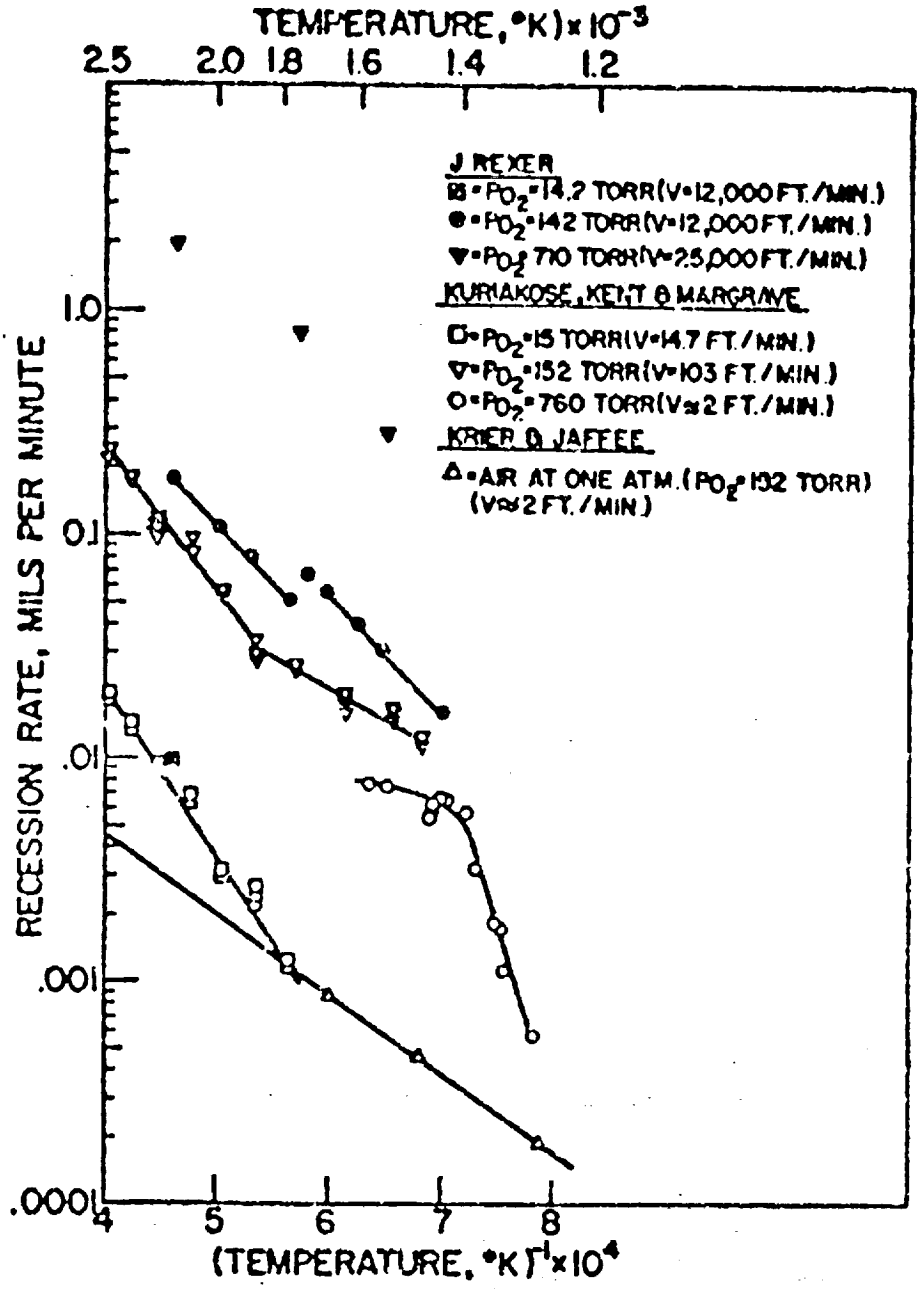

Figure 3. Recession rate vs. reciprocal absolute temperature for iridium

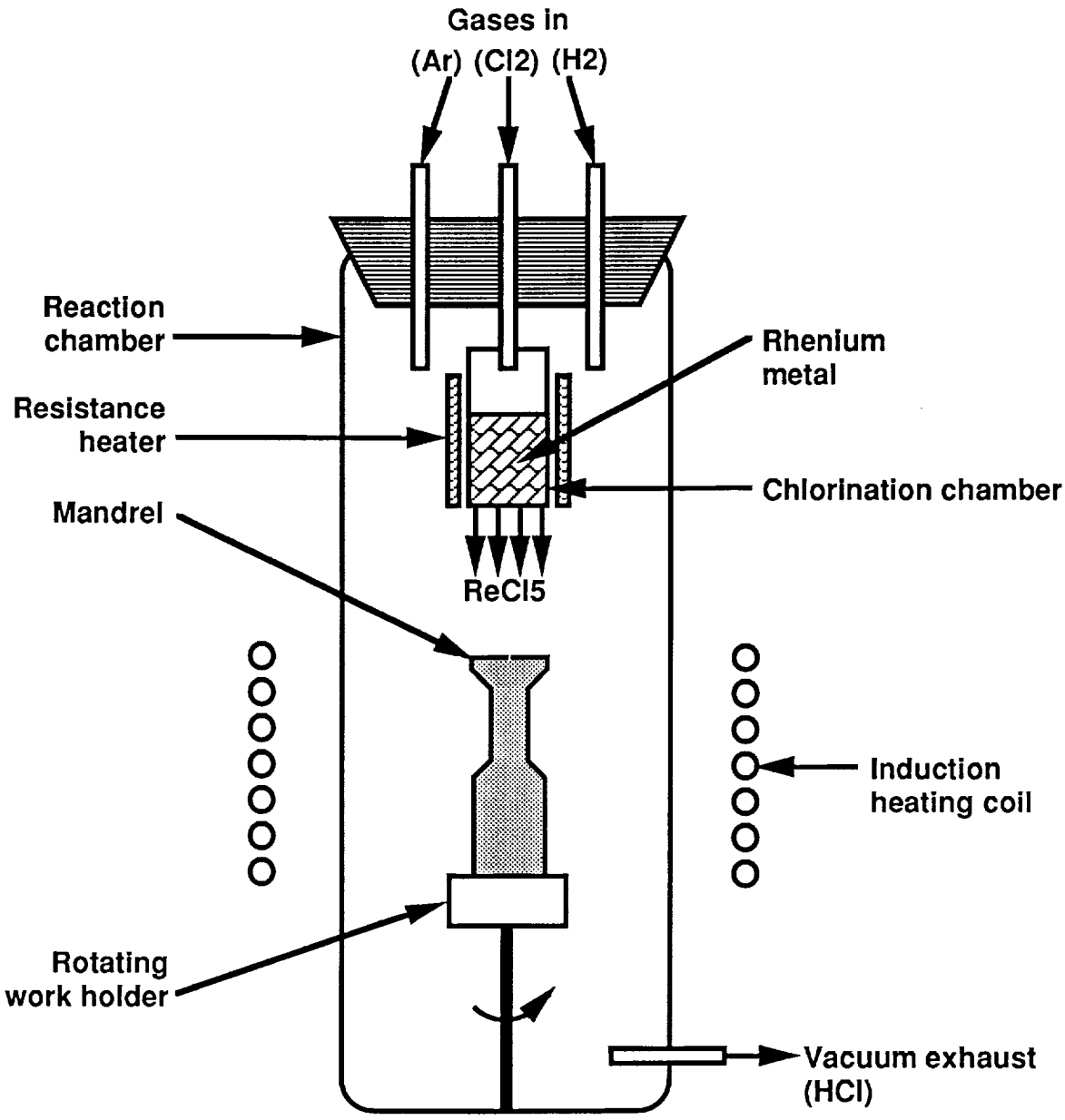

Figure 4. Schematic of CVD apparatus for rhenium deposition

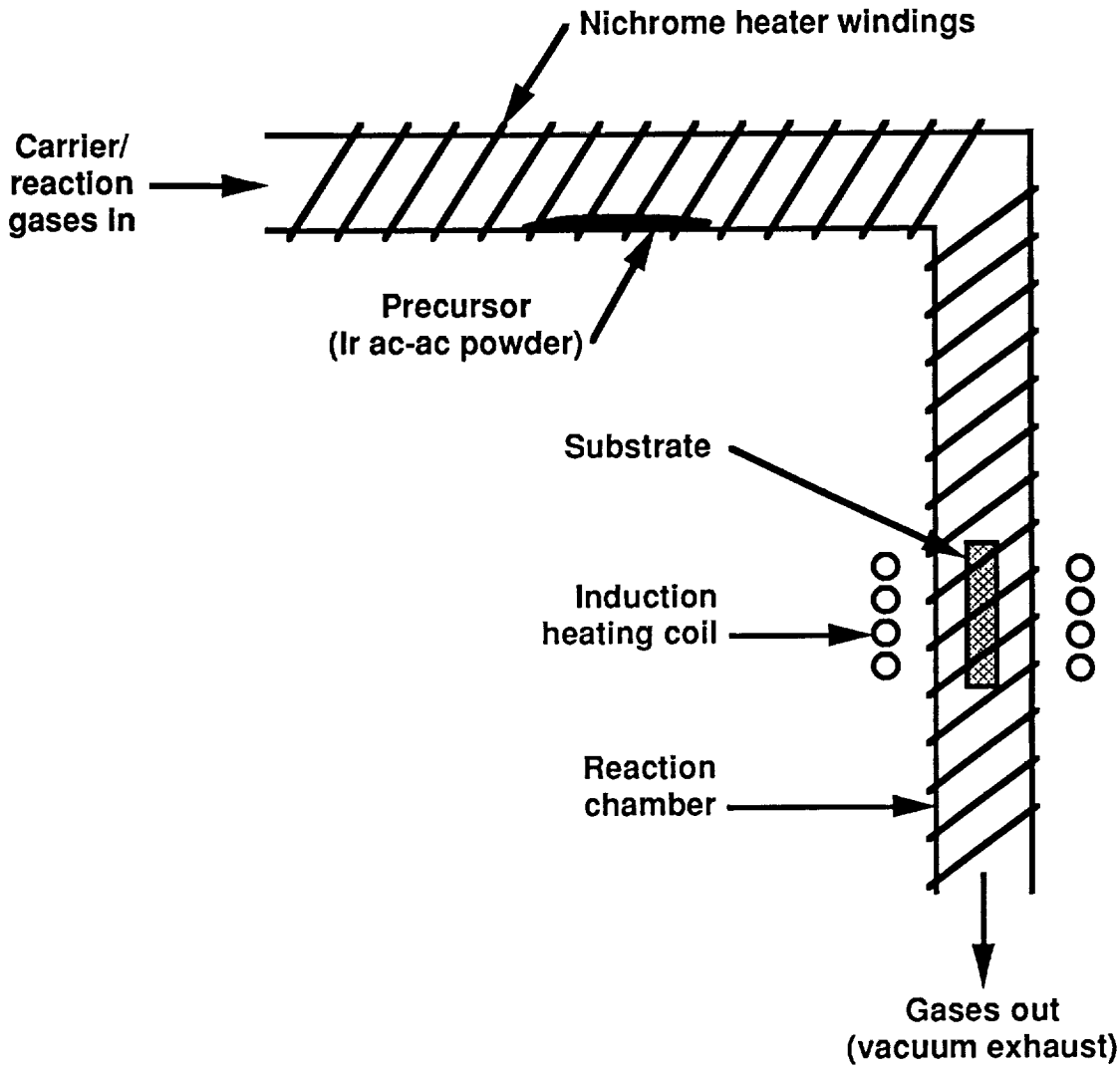

Figure 5. Schematic of CVD apparatus for iridium deposition

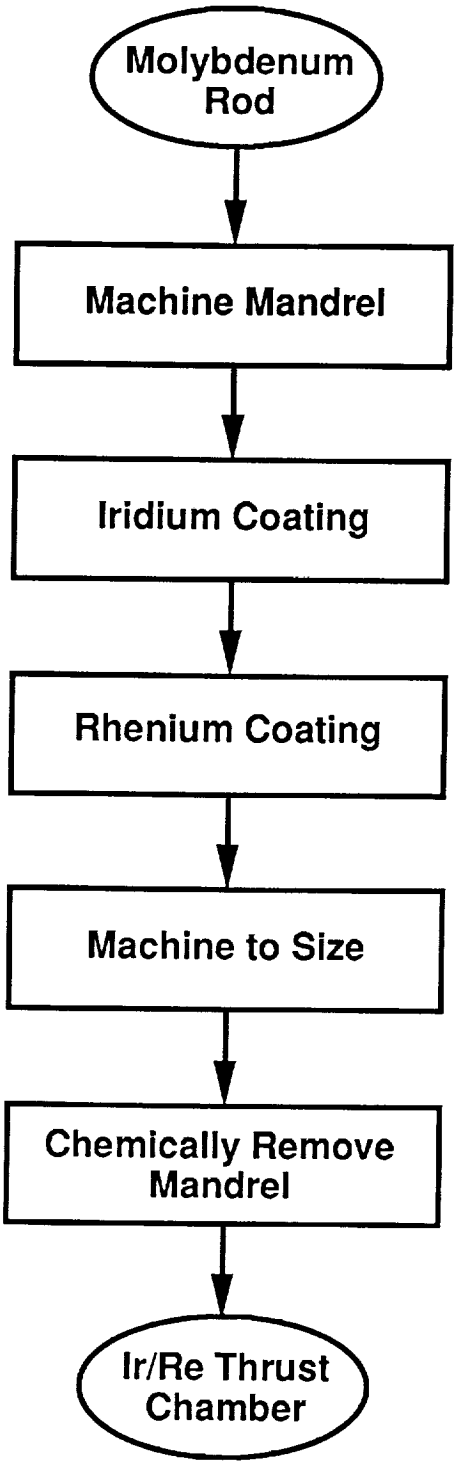

Figure 6. Schematic of inside-out fabrication technique for Ir/Re chambers

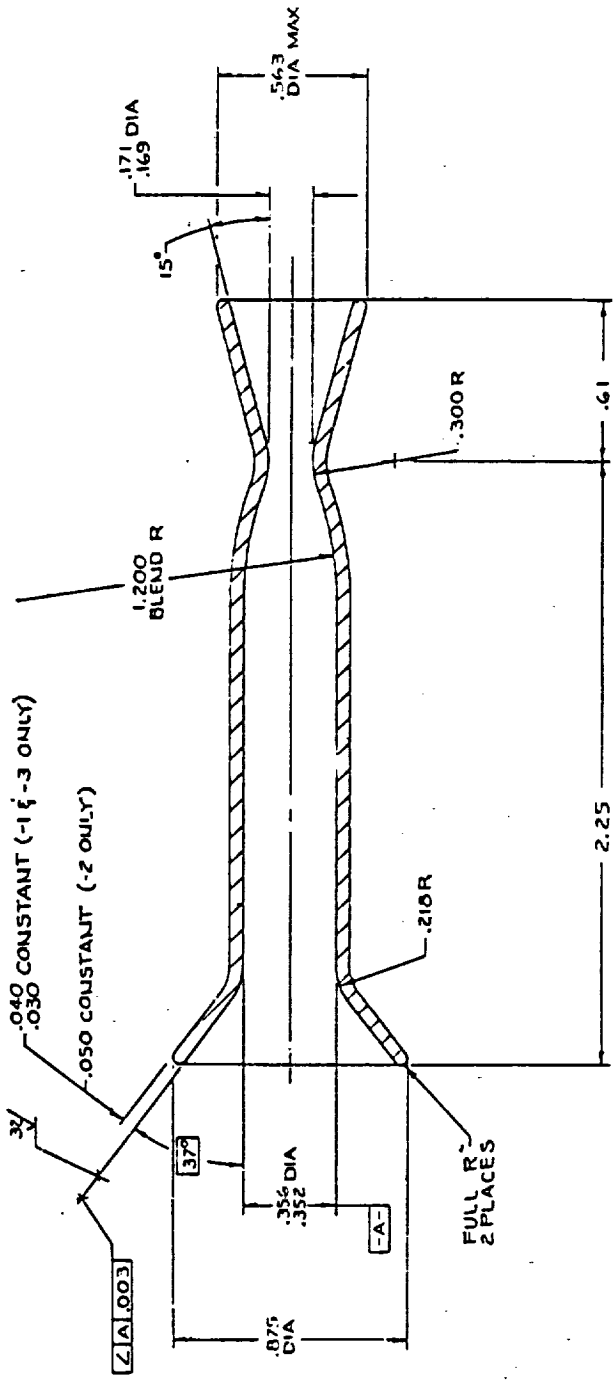

Figure 7. Schematic of Aerojet 5-lb_f chamber design

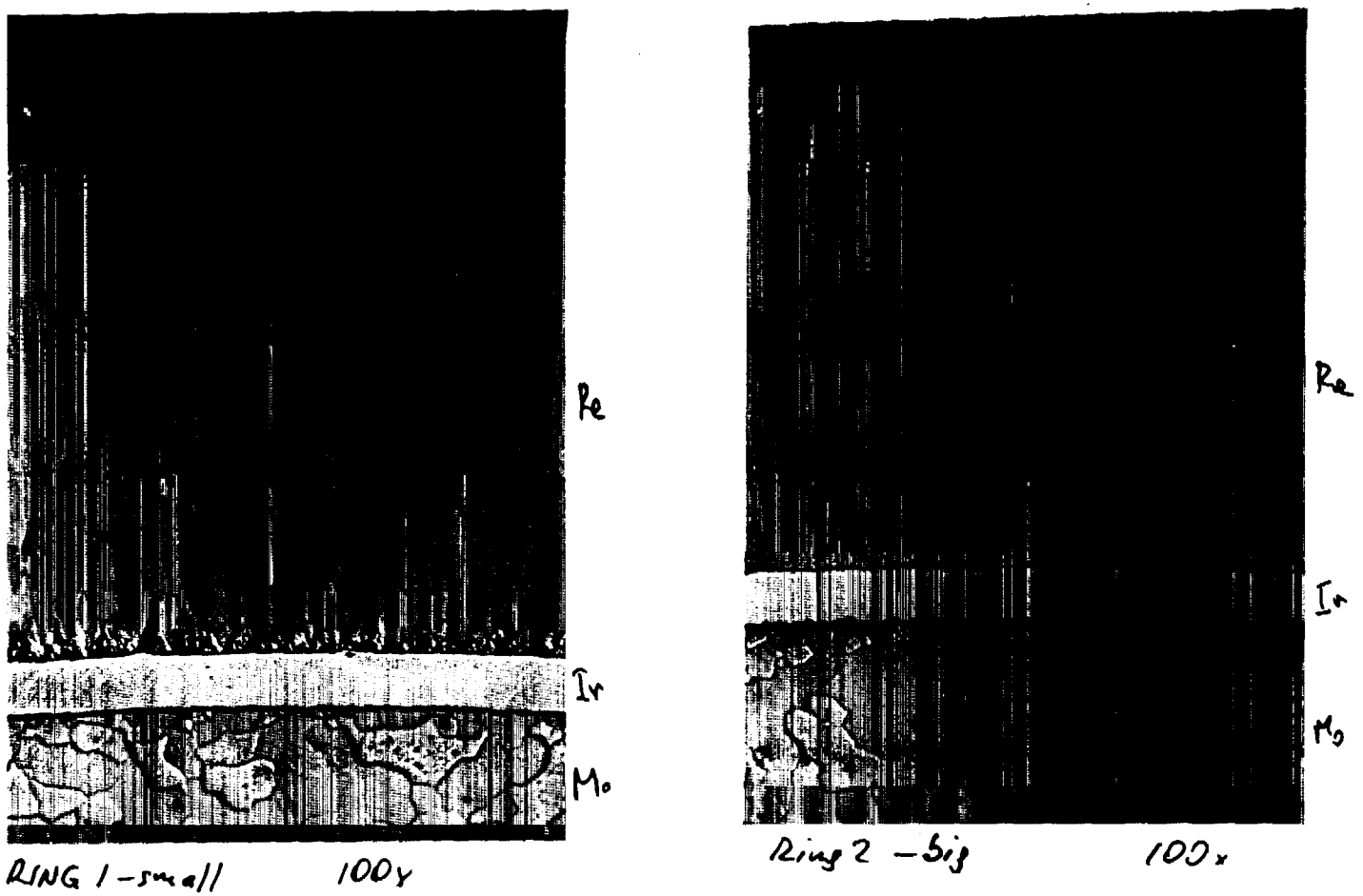

Figure 8. Optical micrographs of top (left) and bottom (right) end rings from 5-lb_f Ir/Re chamber (100x)

Figure 9A. As-deposited 5-lb_f Ir/Re chamber with 144:1 area ratio nozzle

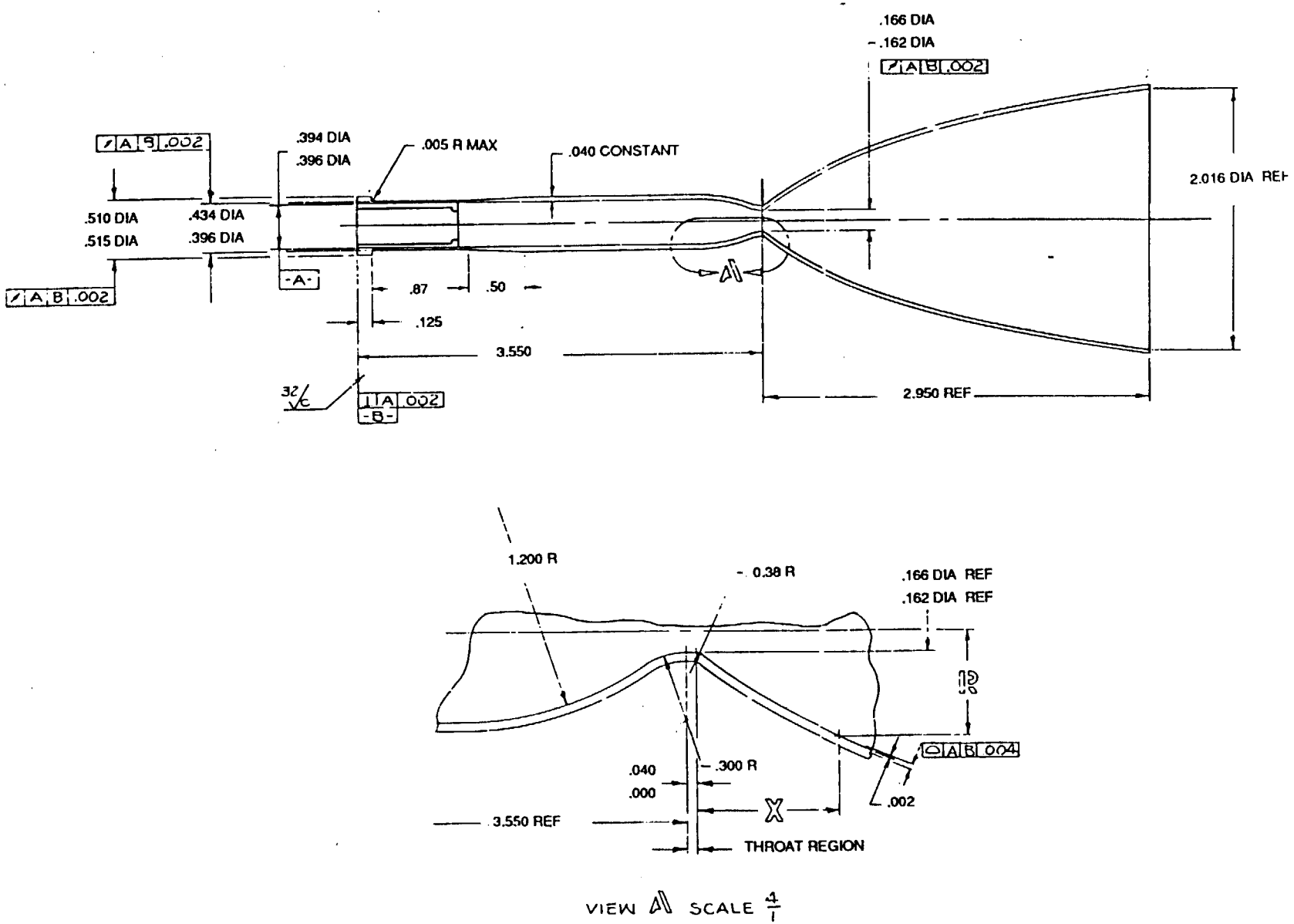

Figure 9B. Schematic of Aerojet 5-lb_f extended skirt chamber design

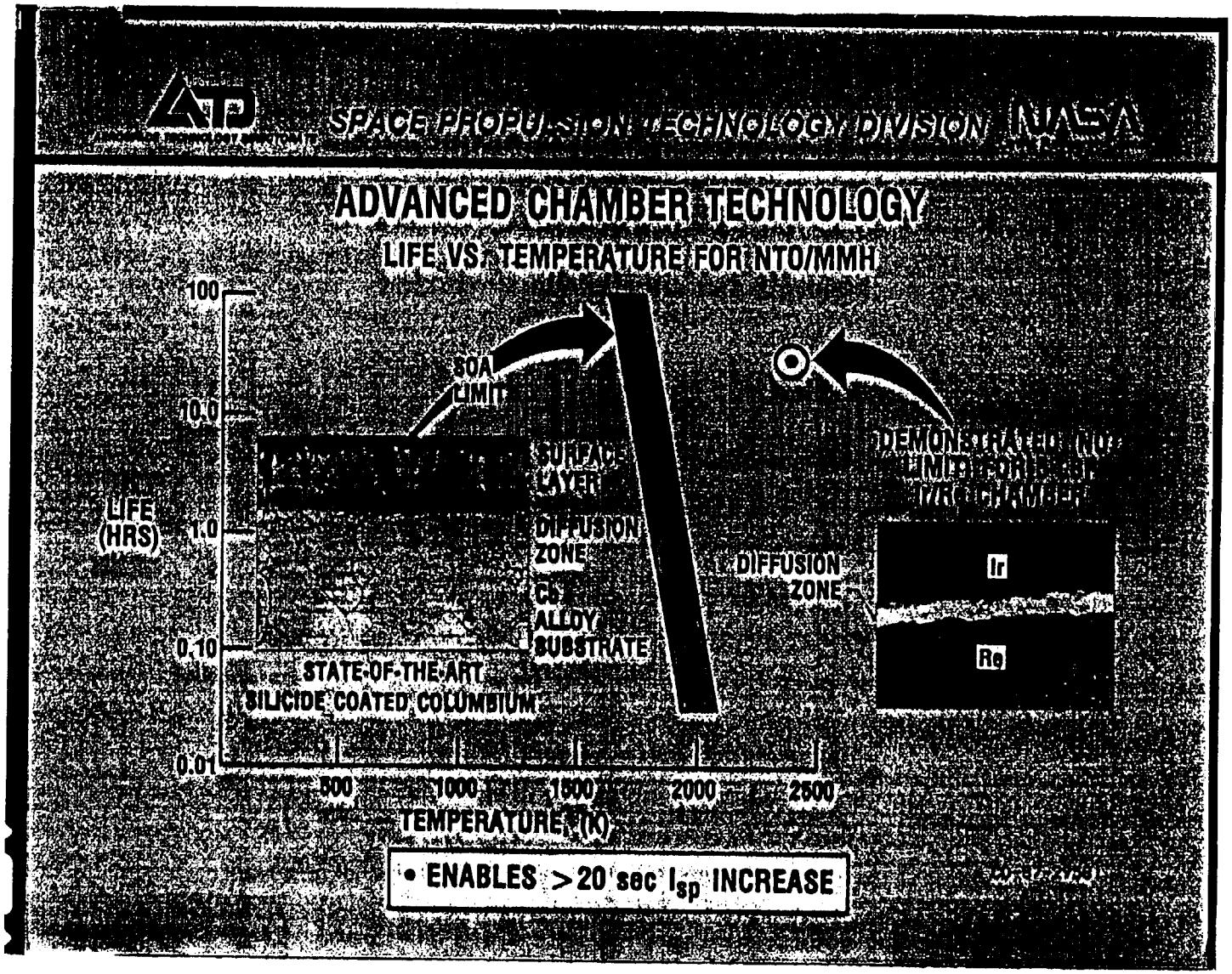

Figure 10. Life vs. temperature in NTO/MMH for 5-lb_f Ir/Re and silicide/niobium chambers

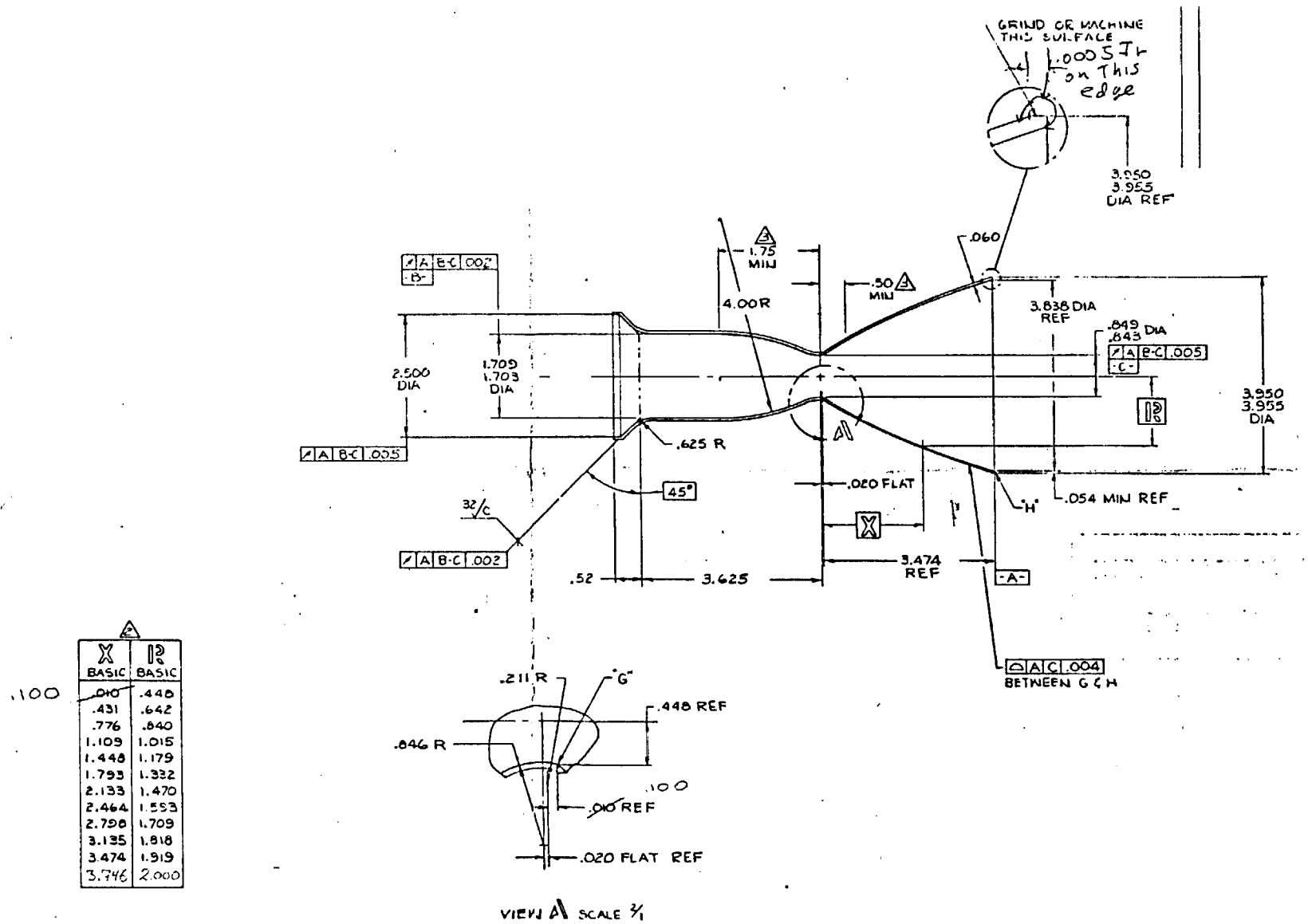

X BASIC	R BASIC
.010	.448
.431	.642
.776	.840
1.109	1.015
1.448	1.179
1.793	1.332
2.133	1.470
2.464	1.553
2.798	1.709
3.135	1.818
3.474	1.919
3.746	2.000

.100

Figure 11. Schematic of Aerojet 100-lb_f chamber design

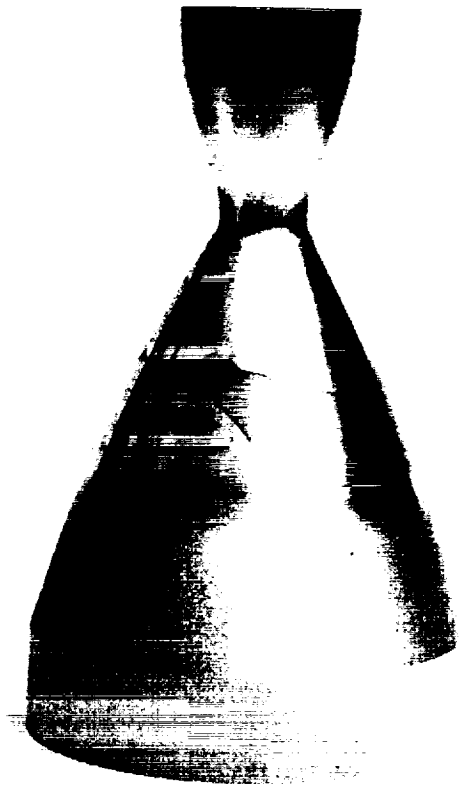

Figure 12. Spalling of iridium coating on 100-lb_f mandrel

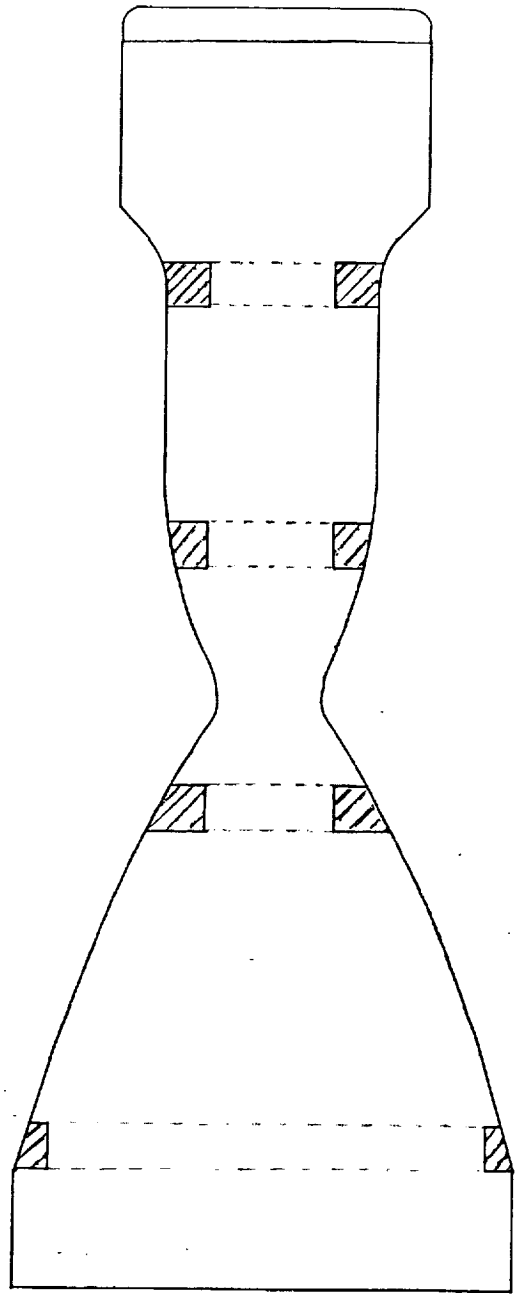

Figure 13. Schematic of segmented molybdenum mandrel with removable, replaceable insert rings

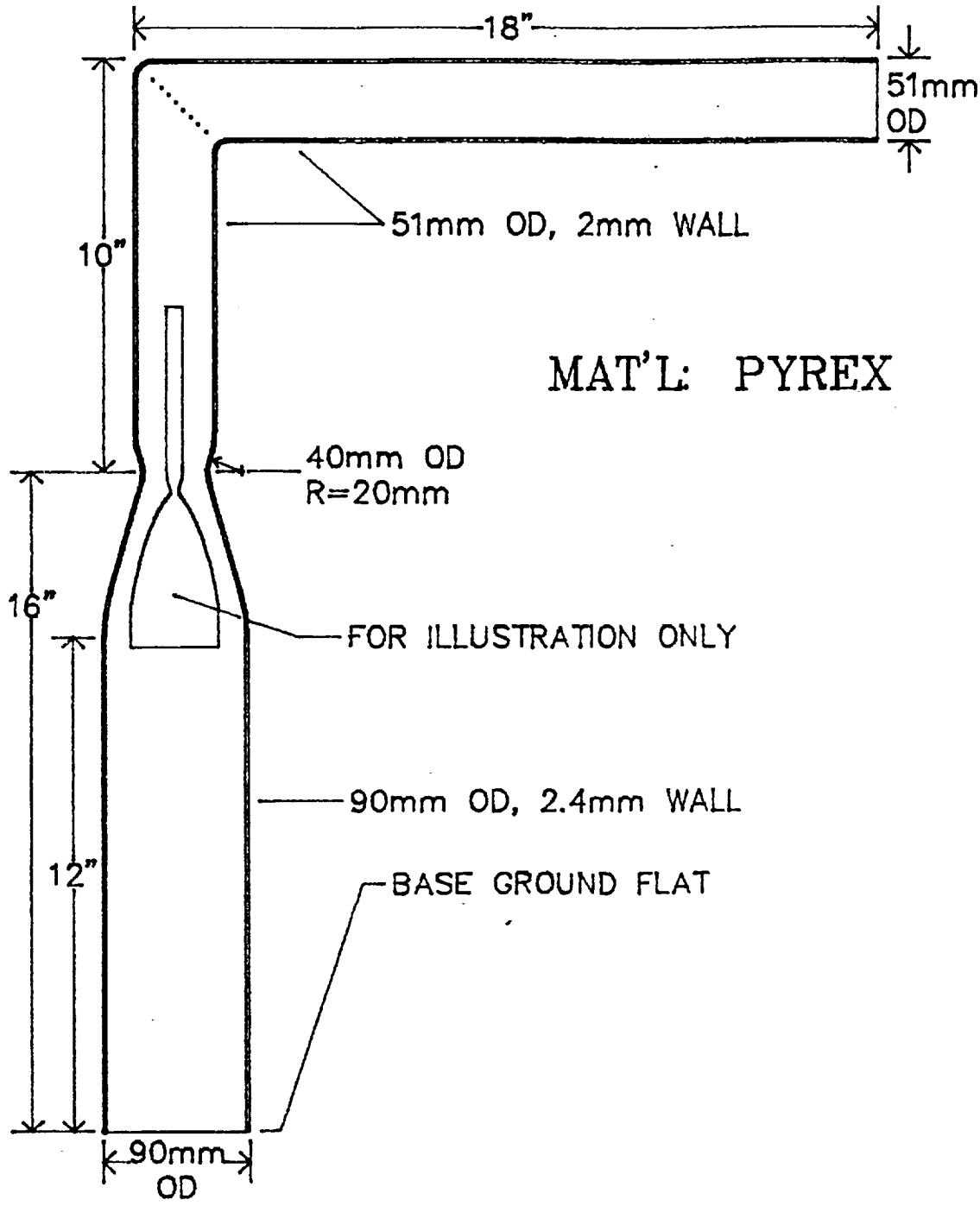

Figure 14. Schematic of conformal reaction chamber with mandrel in place

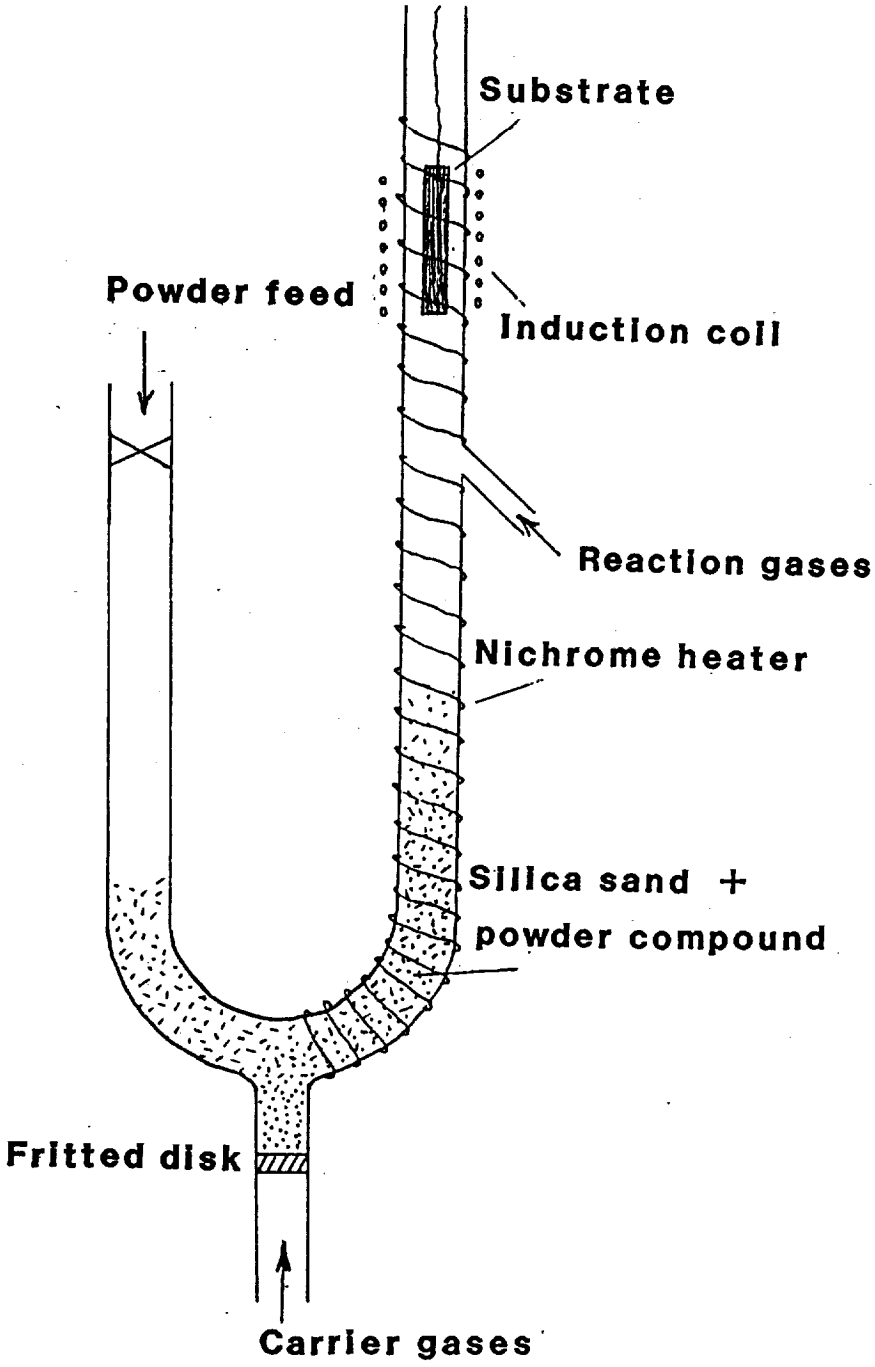

Figure 15. Schematic of initial fluid bed evaporator design

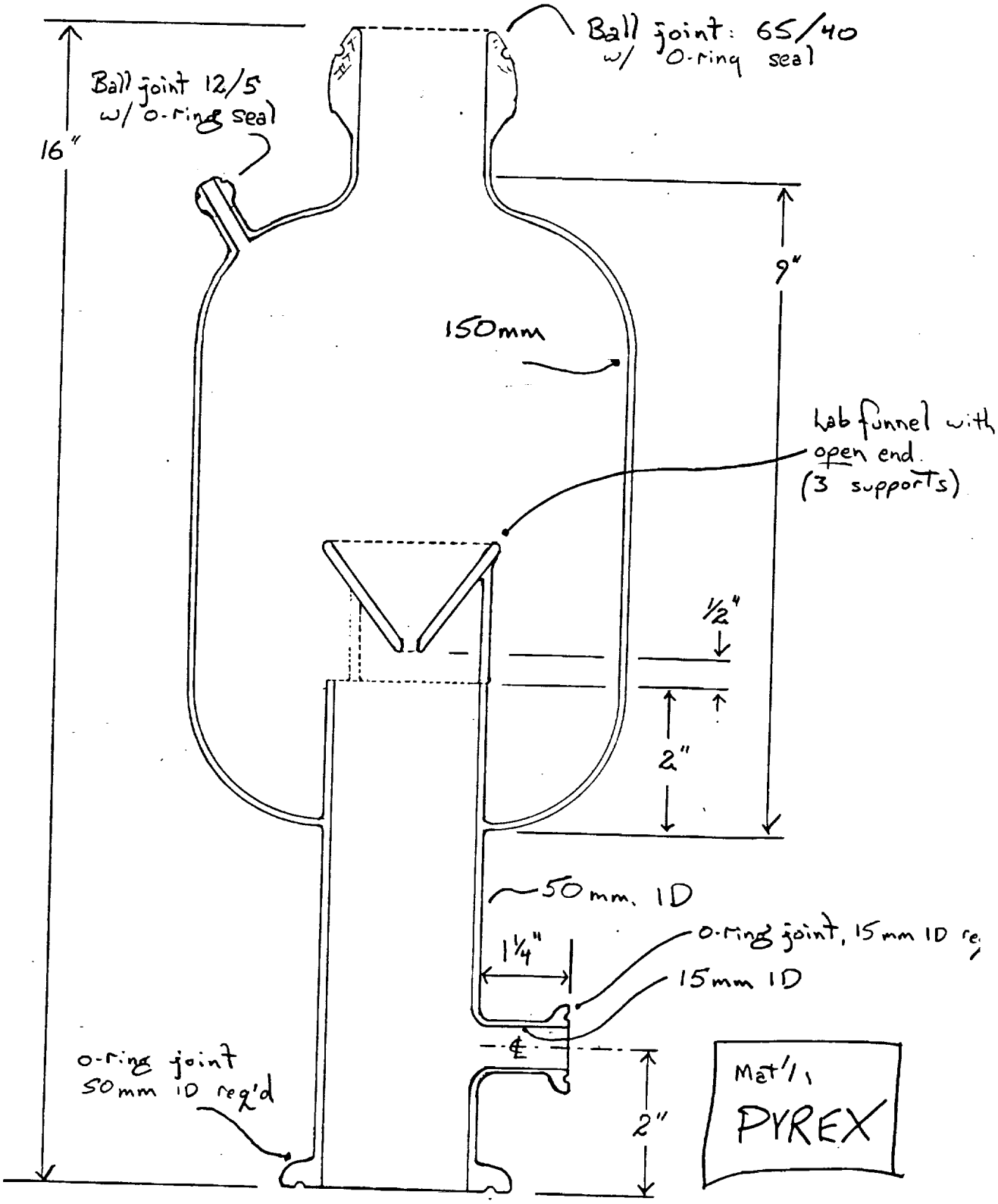

Figure 16. Schematic of final fluid bed evaporator chamber design

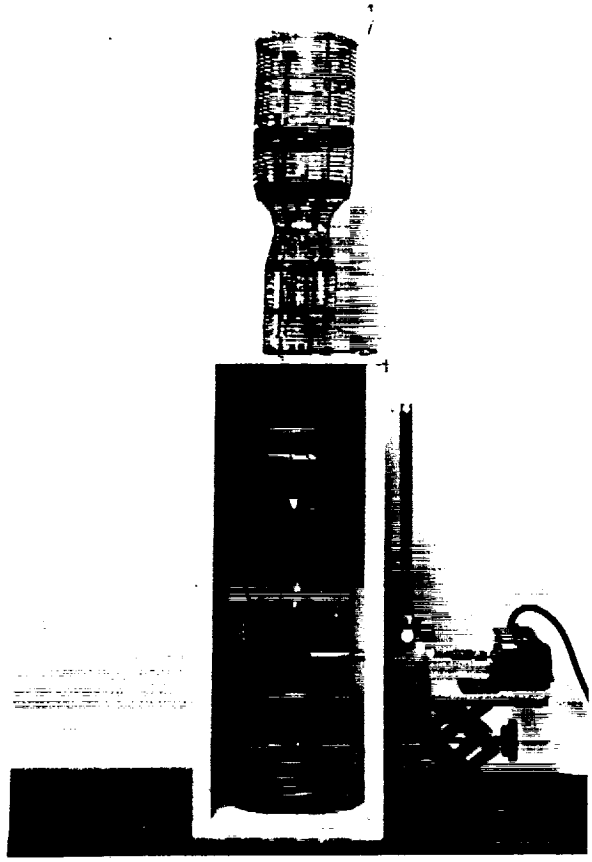

Figure 17. Final fluid bed evaporator apparatus

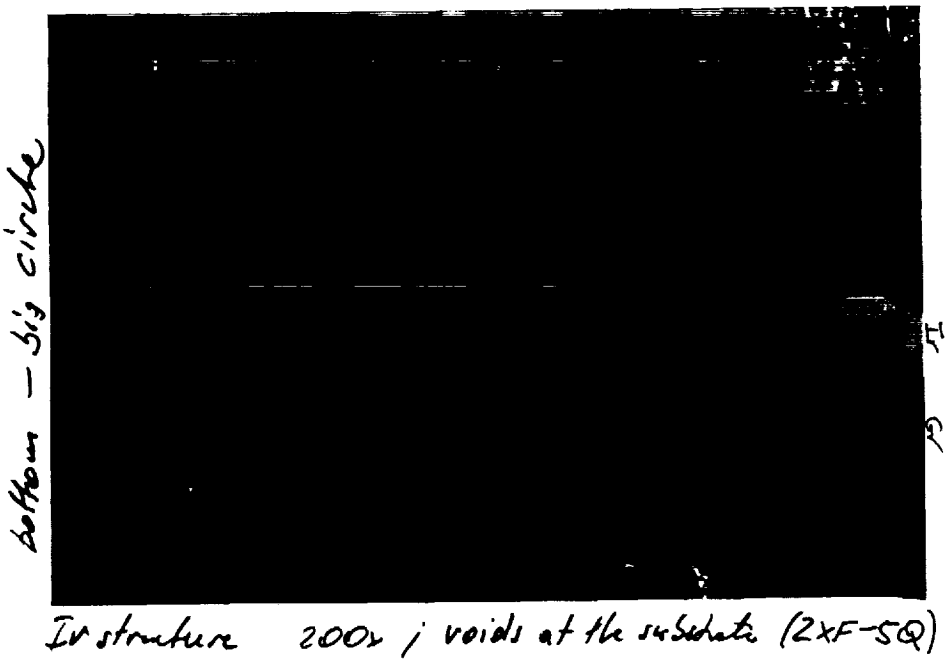

Figure 18. Optical micrograph of iridium/POCO ZXF-5Q graphite interface, showing porosity in iridium (200x)

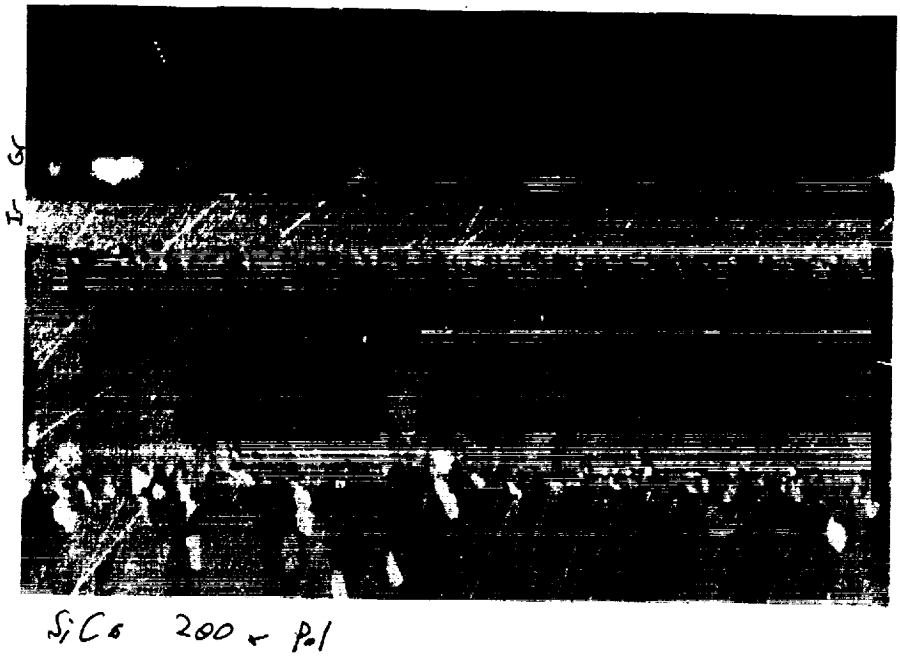

Figure 19. Optical micrograph of iridium/Toyo SIC6 graphite interface, showing no porosity in iridium (200x)

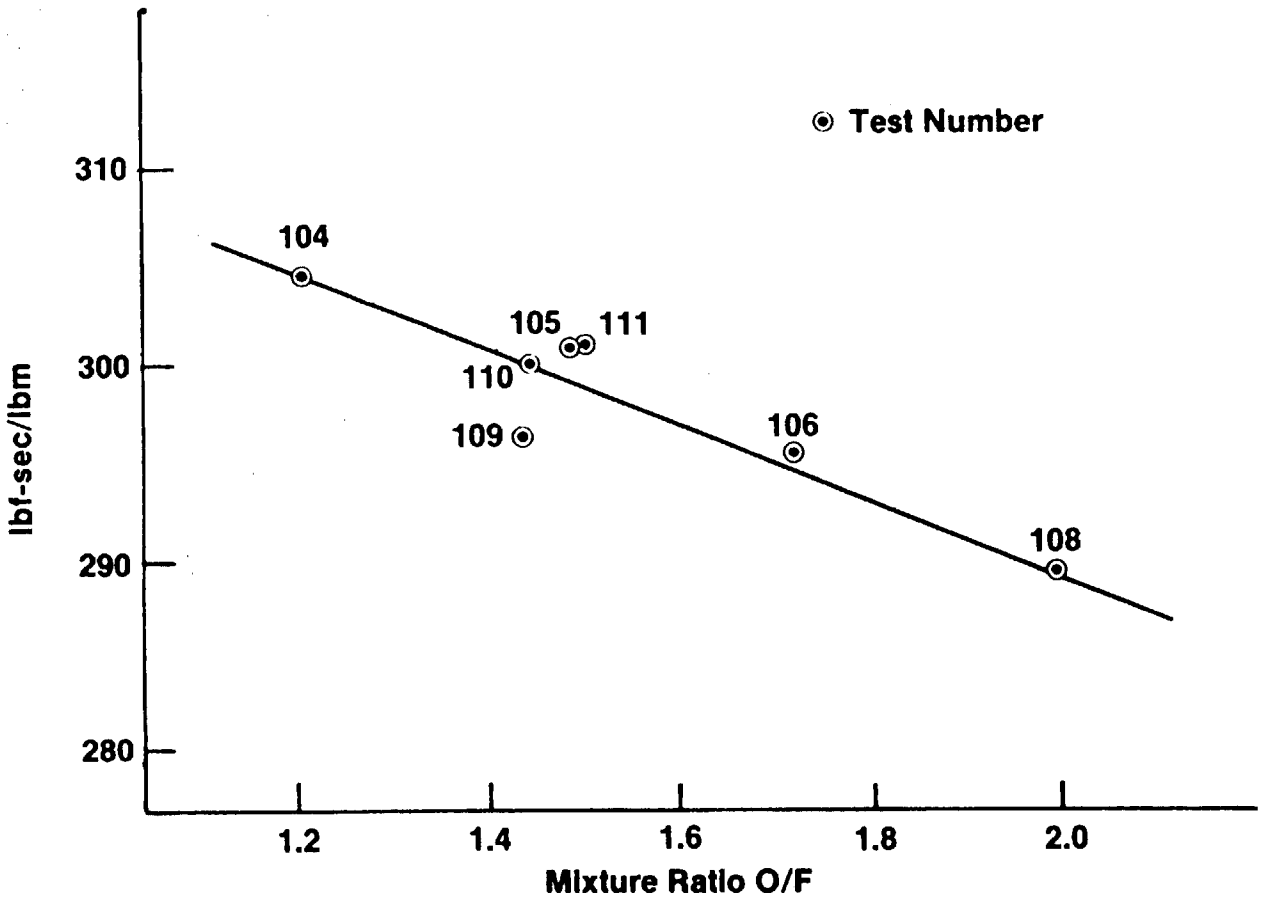

Figure 20. Specific impulse vs. NTO/MMH mixture ratio for 5-lb_f Ir/Nb chamber hot-firing

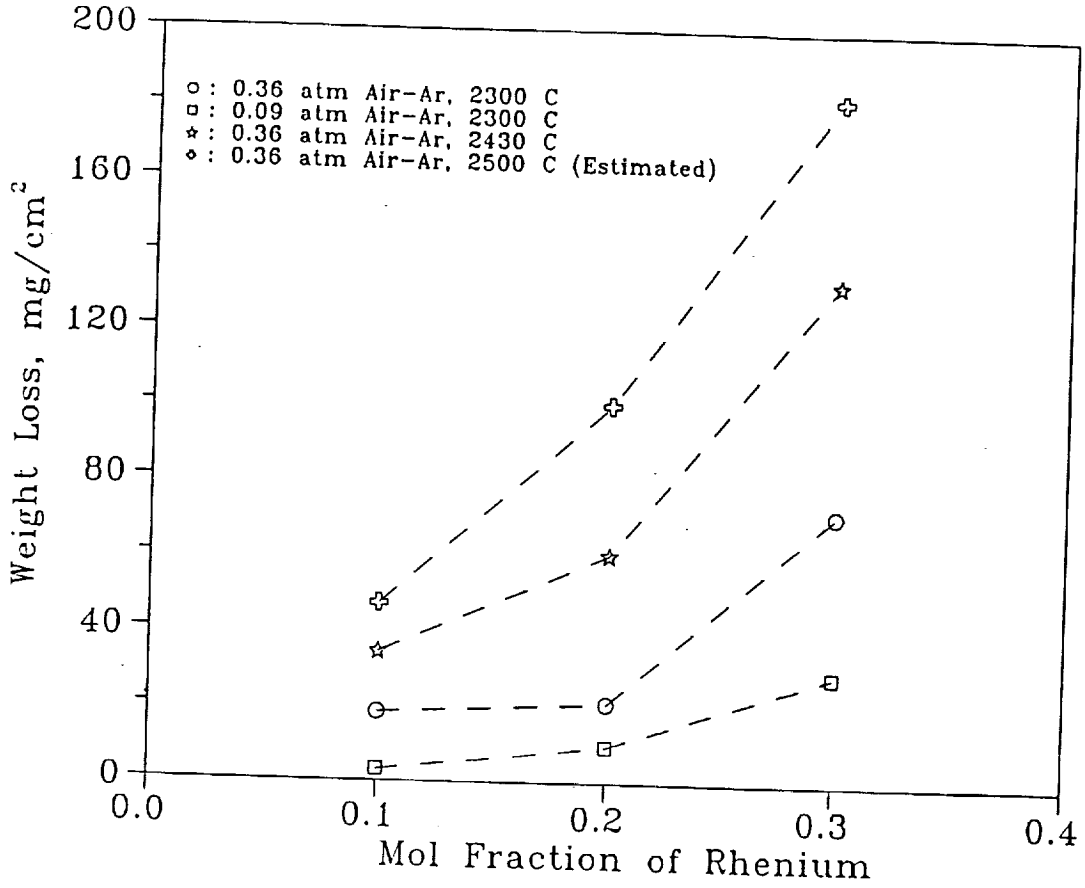

Figure 21A. Weight loss of Ir/Re alloys after oxidation testing for 30 minutes

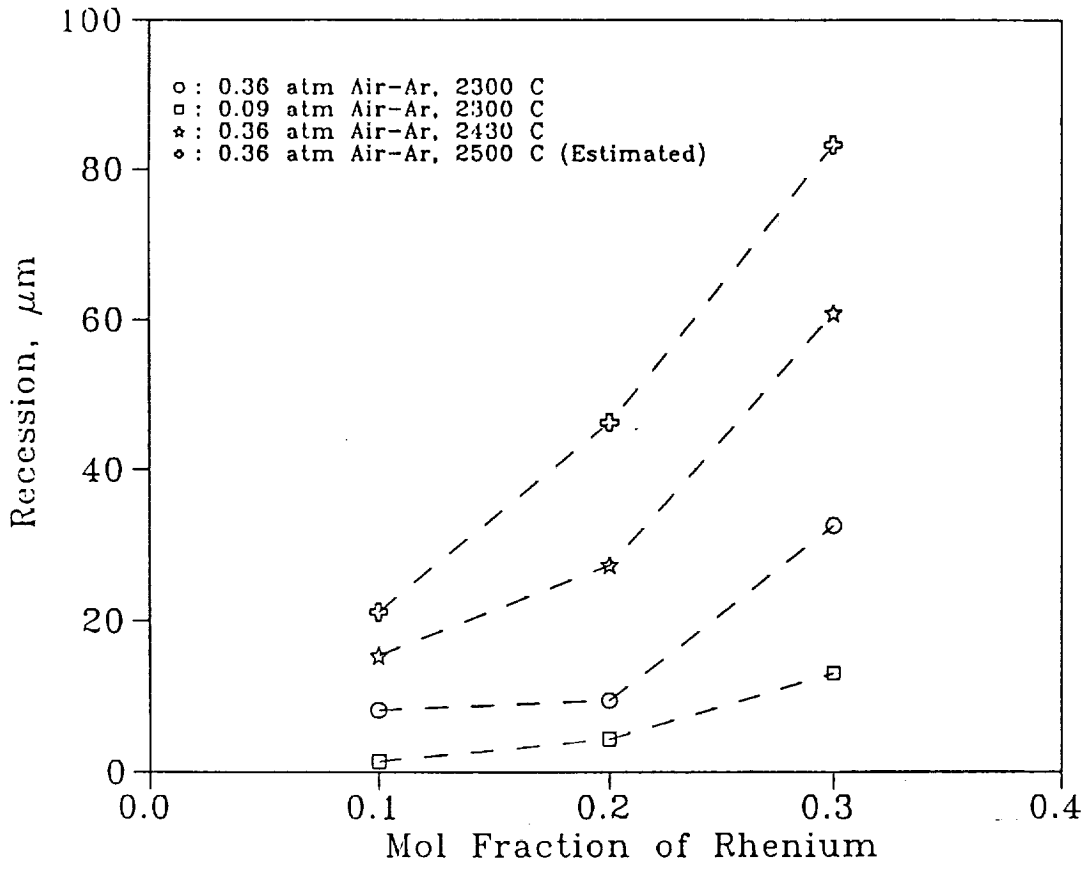

Figure 21B. Recession of Ir/Re alloys after oxidation testing for 30 minutes

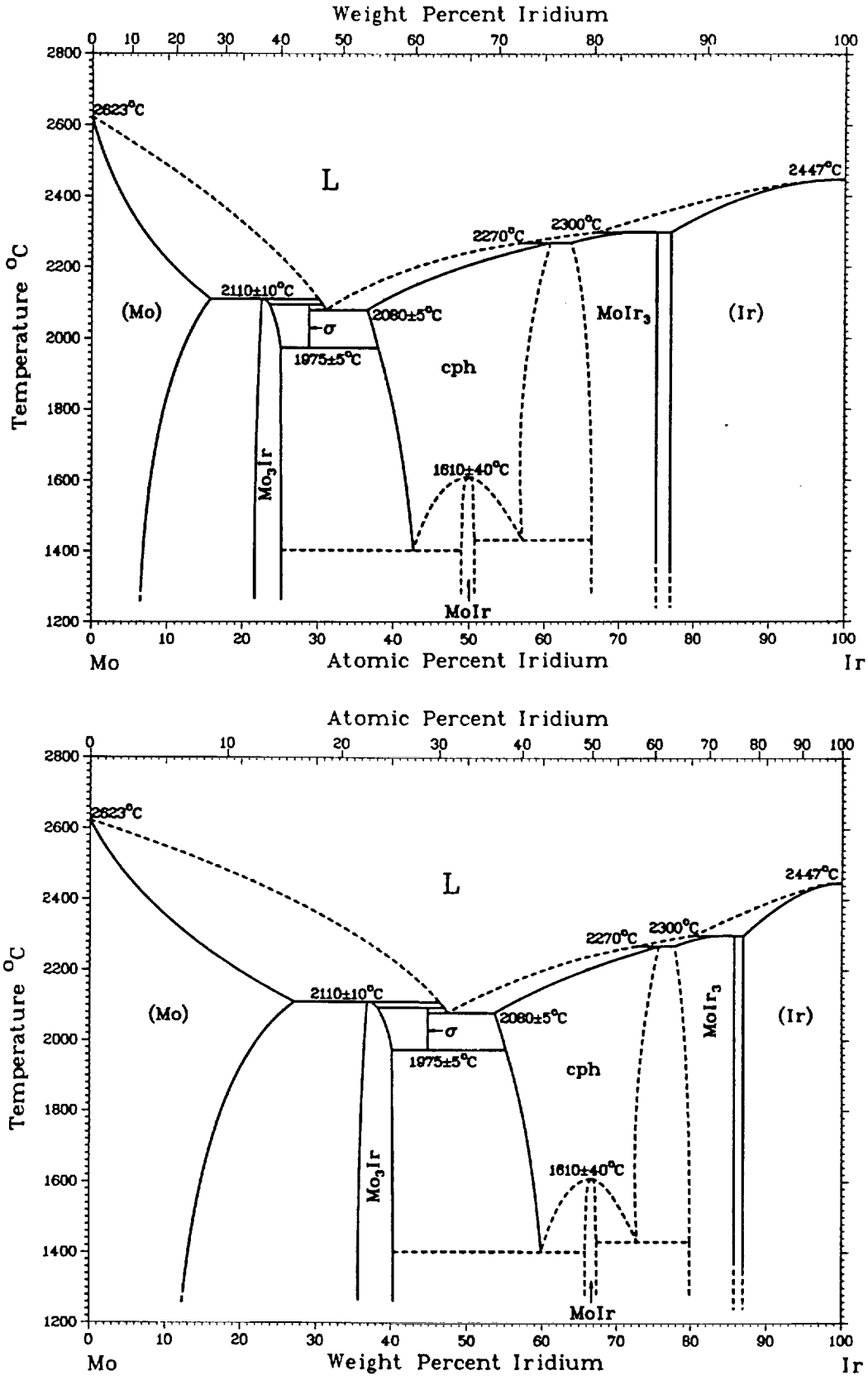

Figure 22. Mo-Ir phase diagram

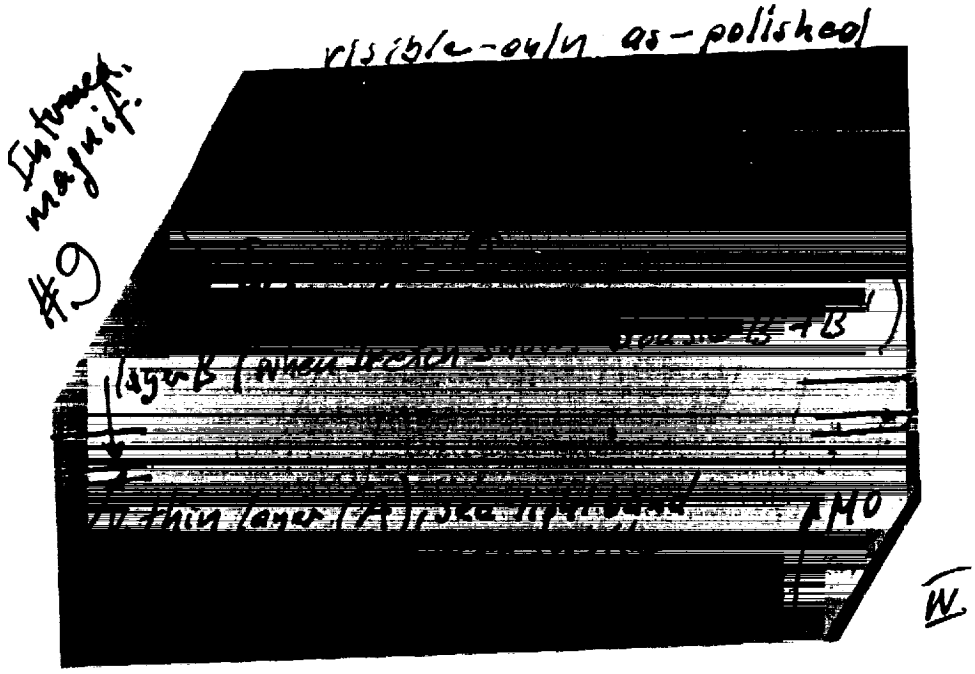

Figure 23. Optical micrograph (unetched cross-section) of Ir-Mo diffusion couple after heat treatment at 1200°C for nine hours, showing two diffusion layers; layer bordering iridium is actually two layers, resolved following etching (1000x)

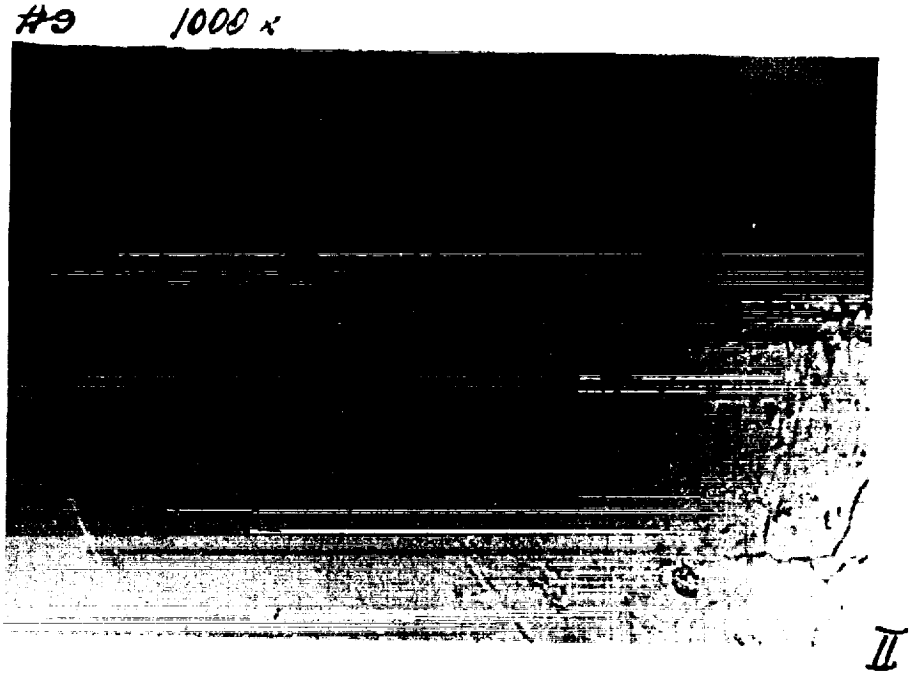

Figure 24. Optical micrograph (etched cross-section) of same Ir-Mo diffusion couple, resolving layers α and β; γ layer is very susceptible to iridium etchant, remaining only in masked regions at right (1000x)

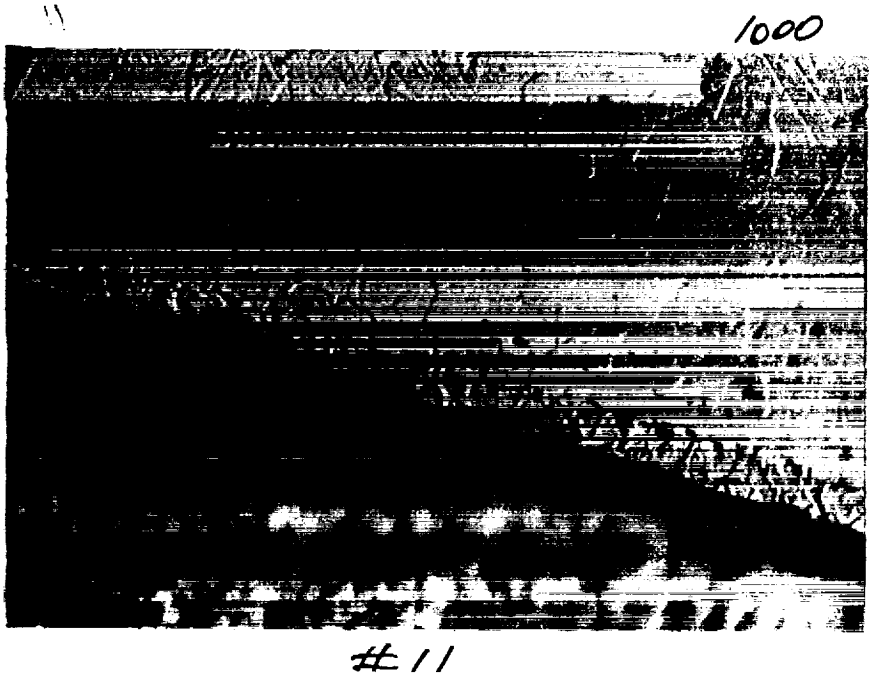

Figure 25. Optical micrograph (etched cross-section) of Ir-Mo diffusion couple after heat treatment at 1200°C for 16.5 hours, showing layers α and β; γ layer has been completely dissolved by etching (1000x)

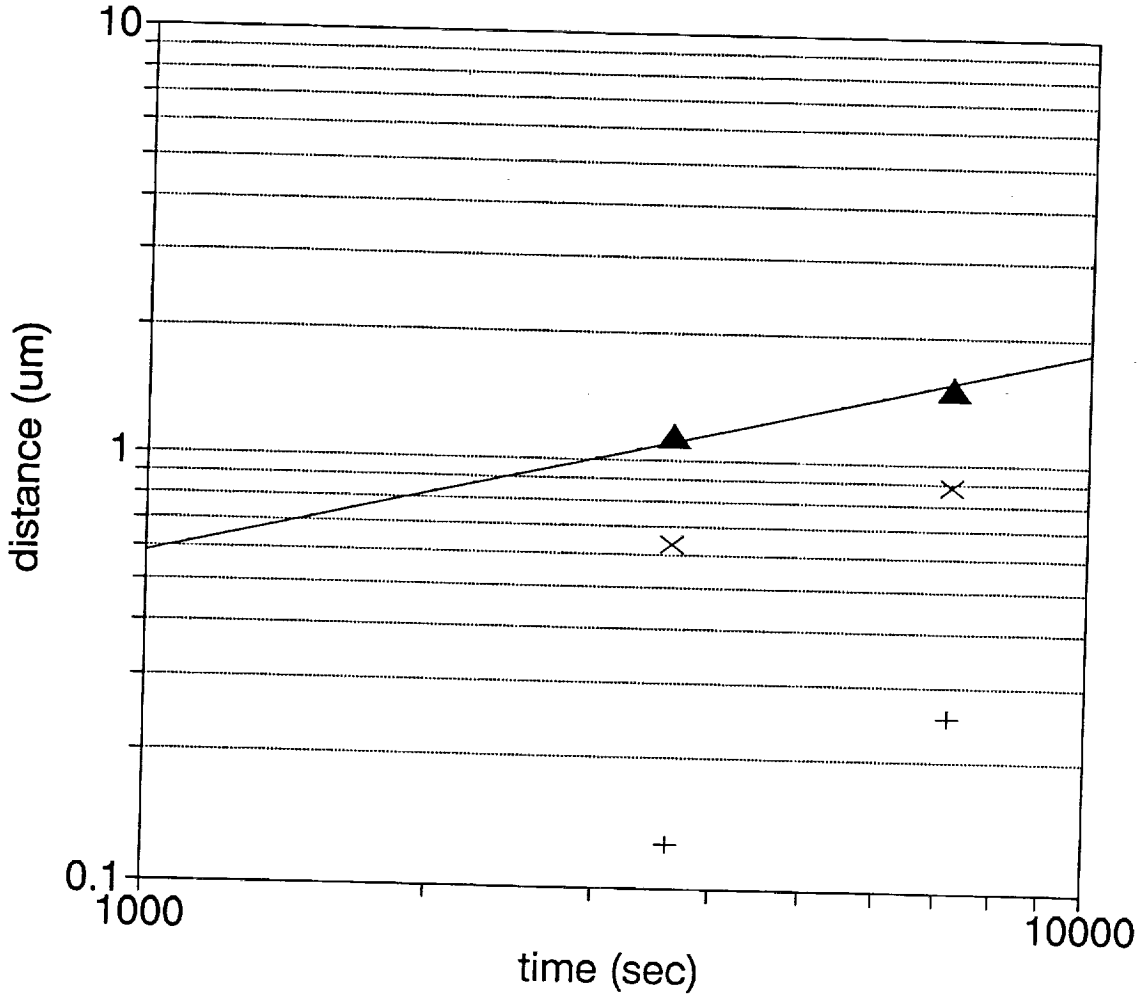

Figure 26. Ir-Mo diffusion vs. time at 1000°C
▲: total diffusion layer thickness ($\alpha+\beta+\gamma$)
×: combined thickness of γ and β layers
+: thickness of γ layer

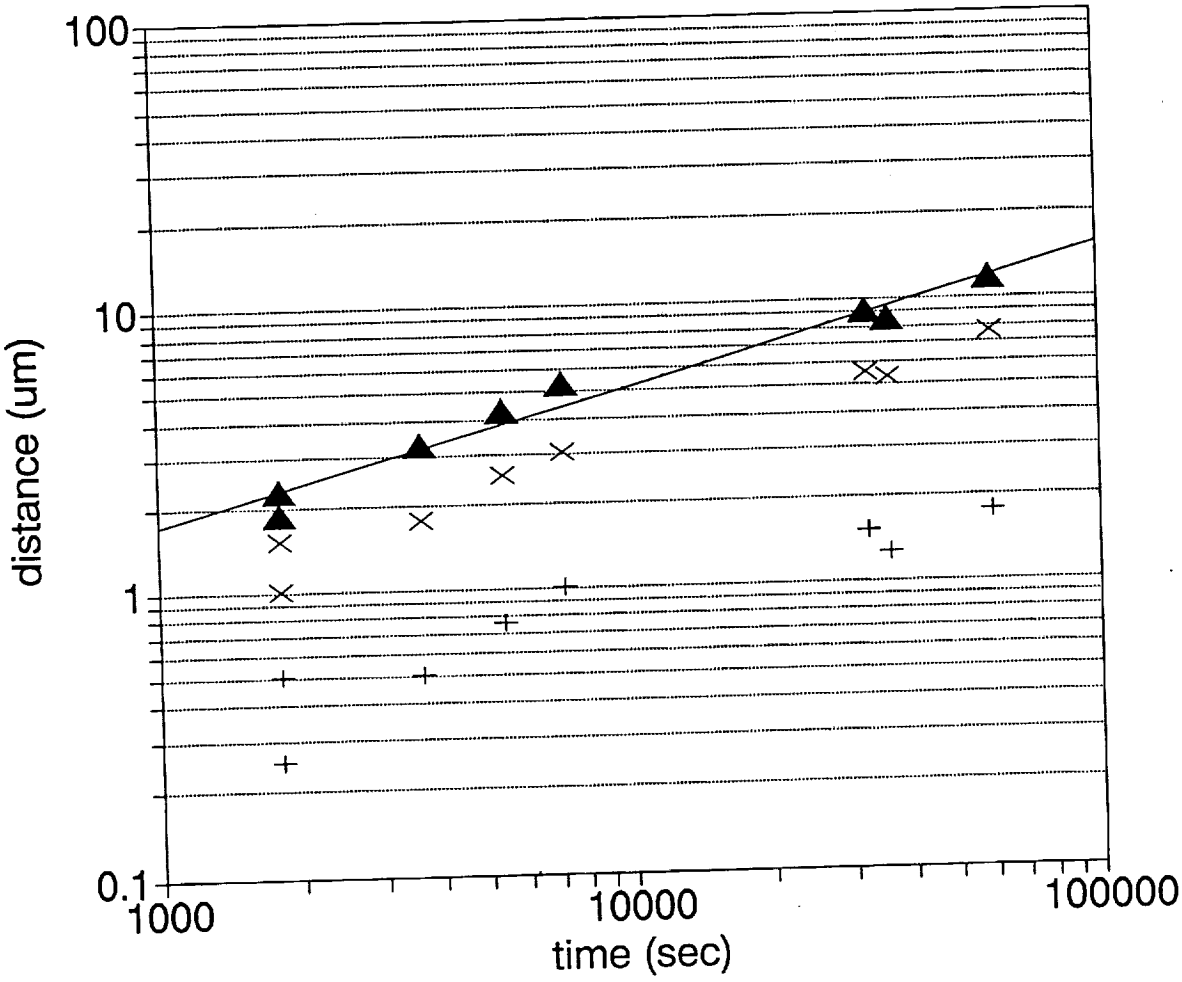

Figure 27. Ir-Mo diffusion vs. time at 1200°C
▲: total diffusion layer thickness ($\alpha+\beta+\gamma$)
×: combined thickness of γ and β layers
+: thickness of γ layer

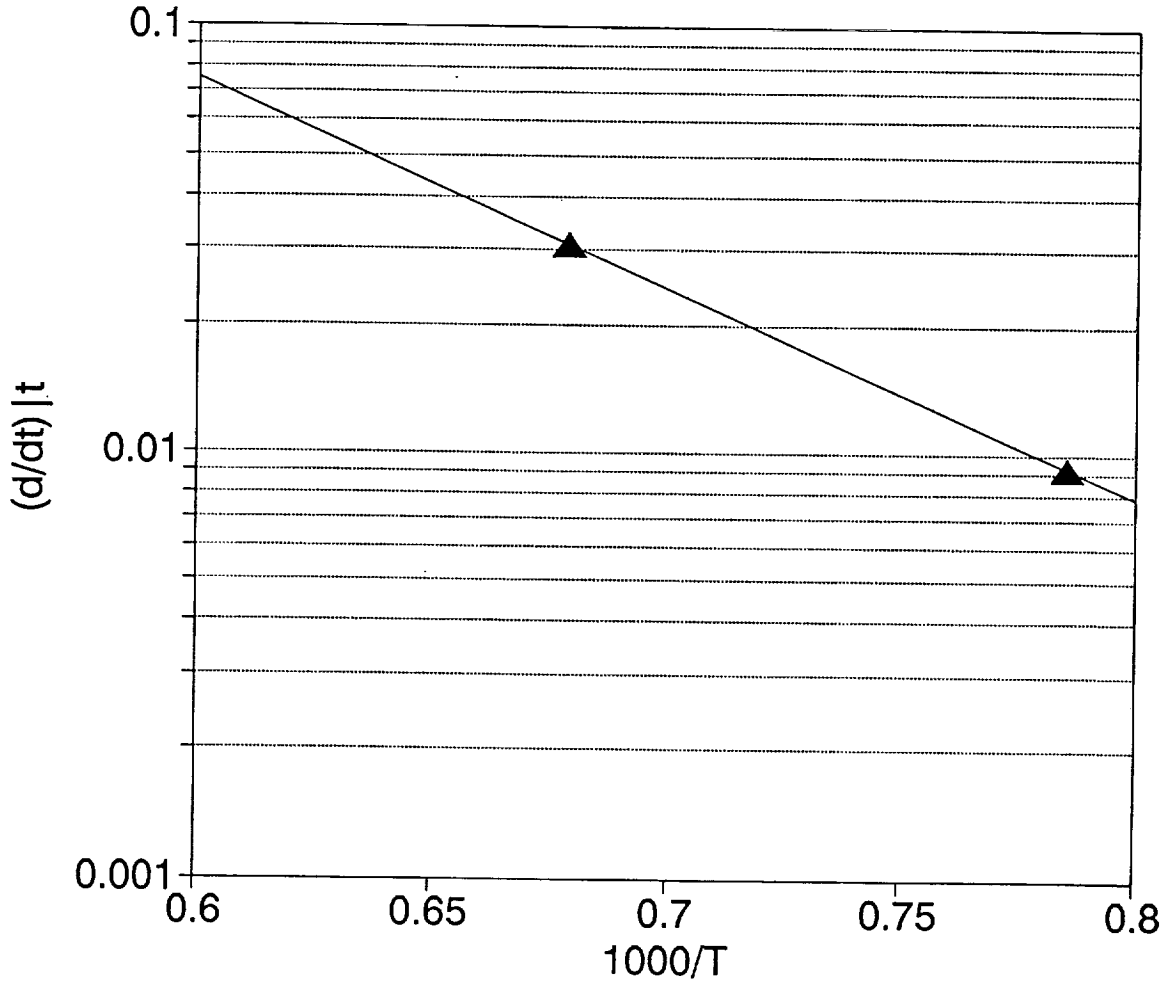

Figure 28. Arrhenius plot of Ir-Mo diffusion kinetics, fixed time

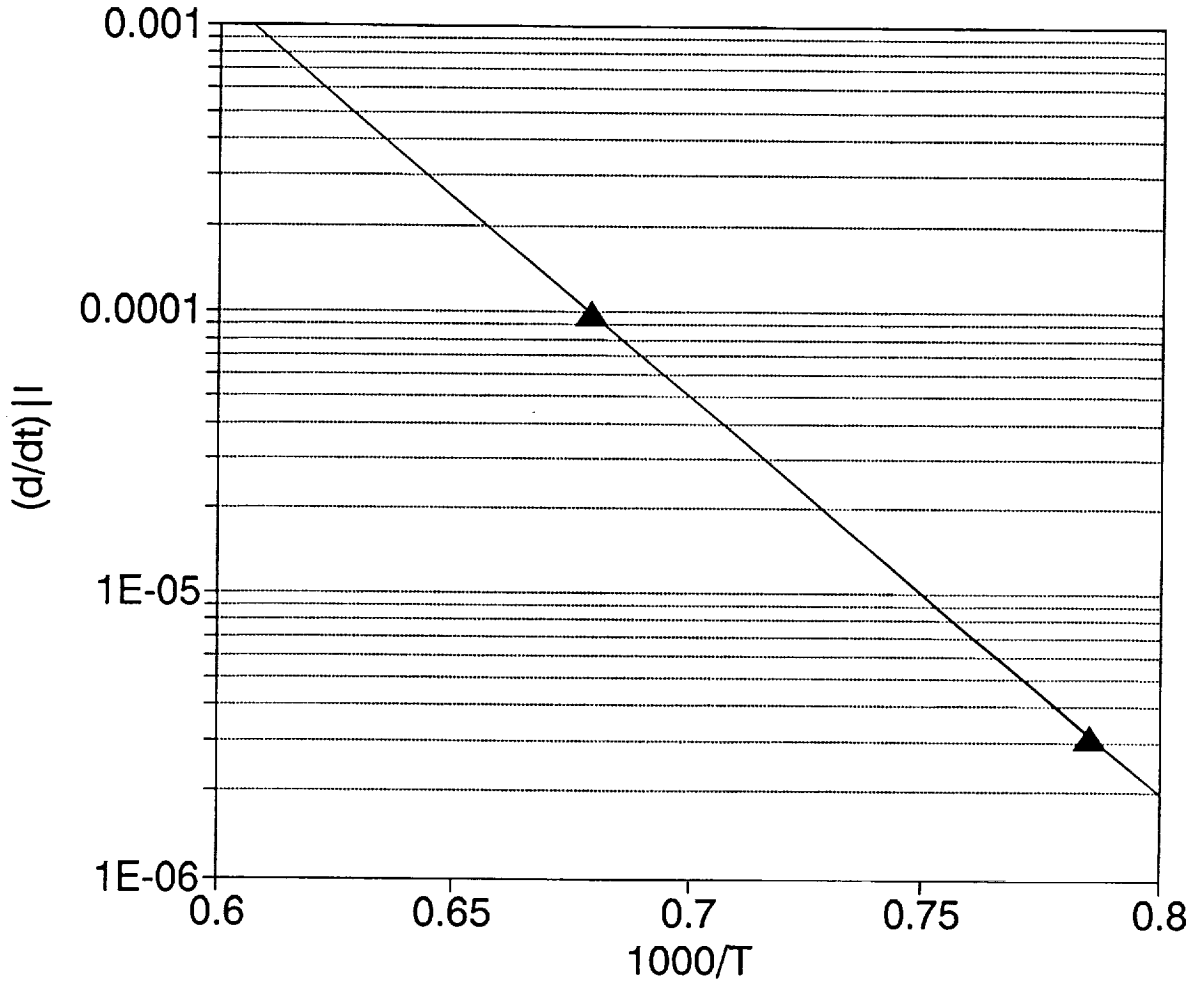

Figure 29. Arrhenius plot of Ir-Mo diffusion kinetics, fixed thickness

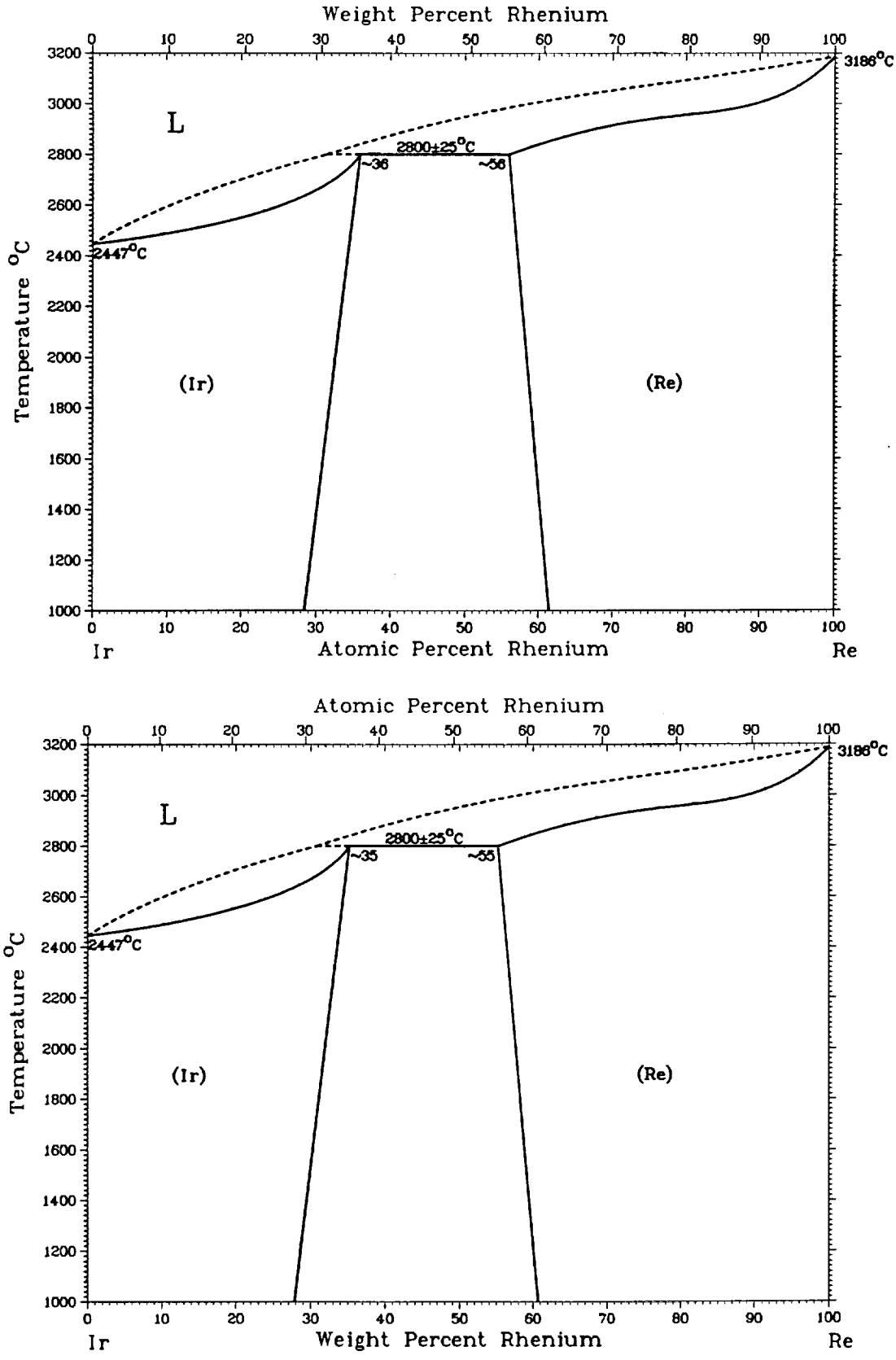

Figure 30. Re-Ir phase diagram

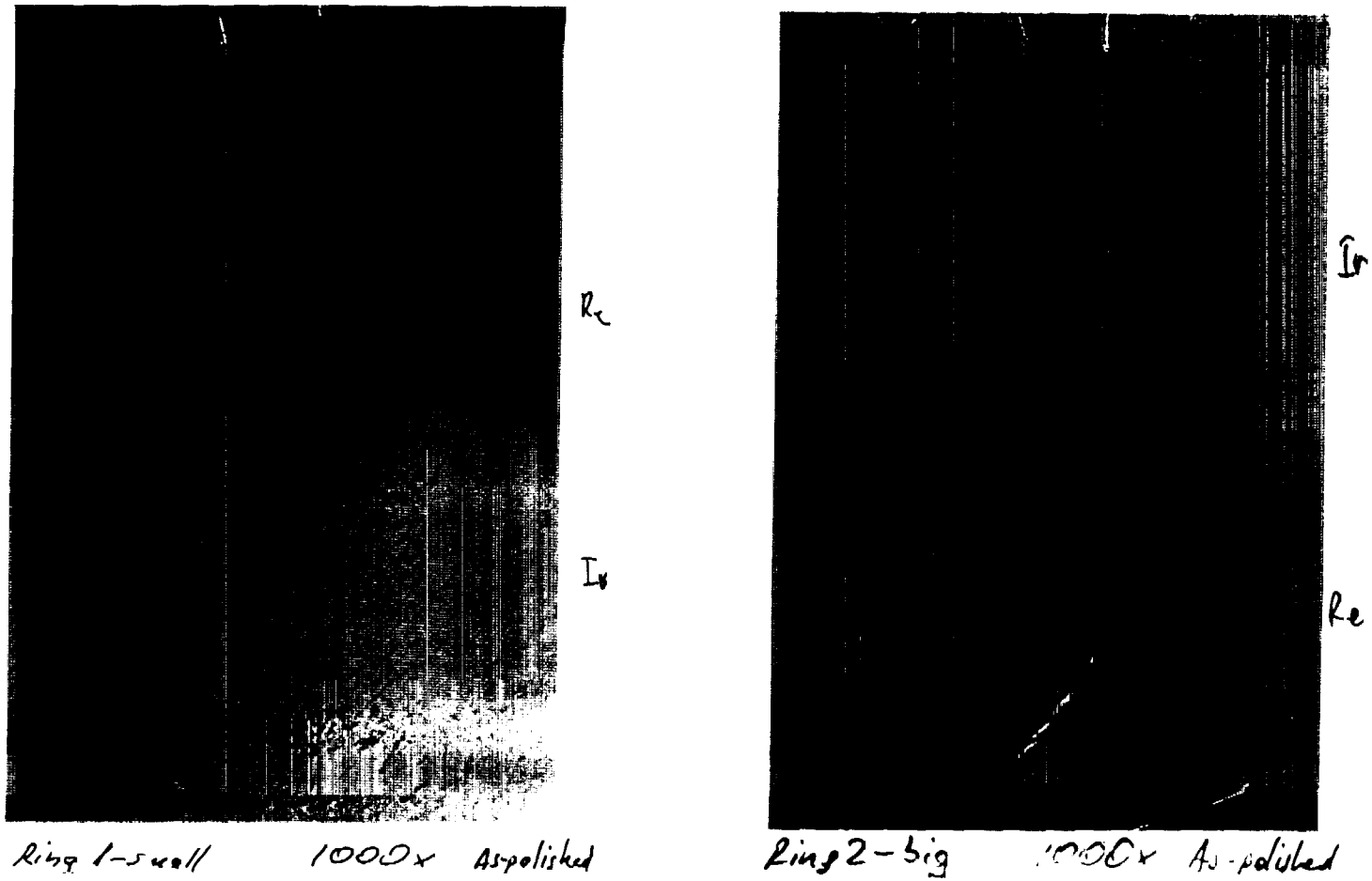

Figure 31. Optical micrographs (unetched cross-section) of Ir-Re diffusion couples after heat treatment at 1225°C for four hours, showing iridium-rhenium interface (1000x)

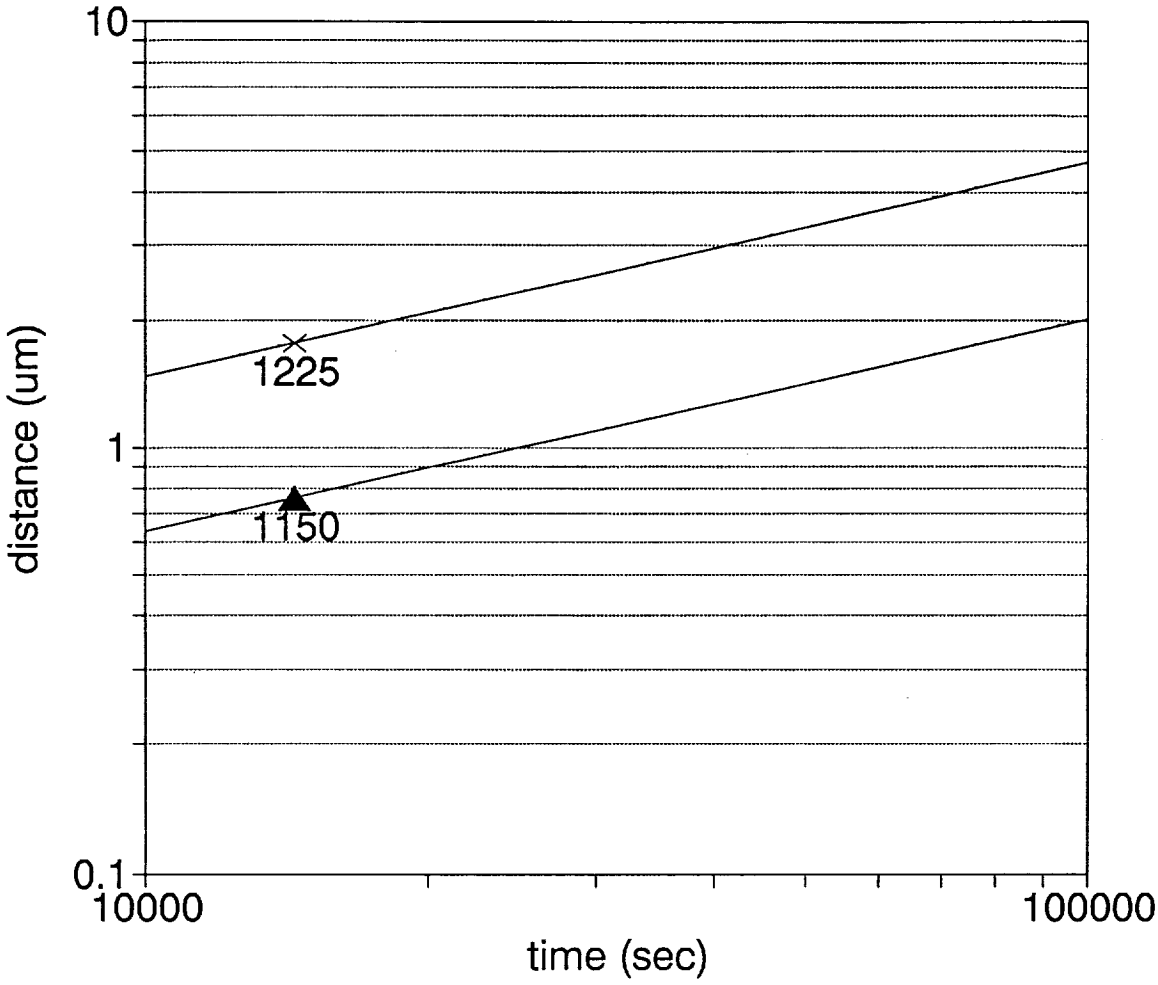

Figure 32. Ir-Re diffusion vs. time at 1150°C and 1225°C

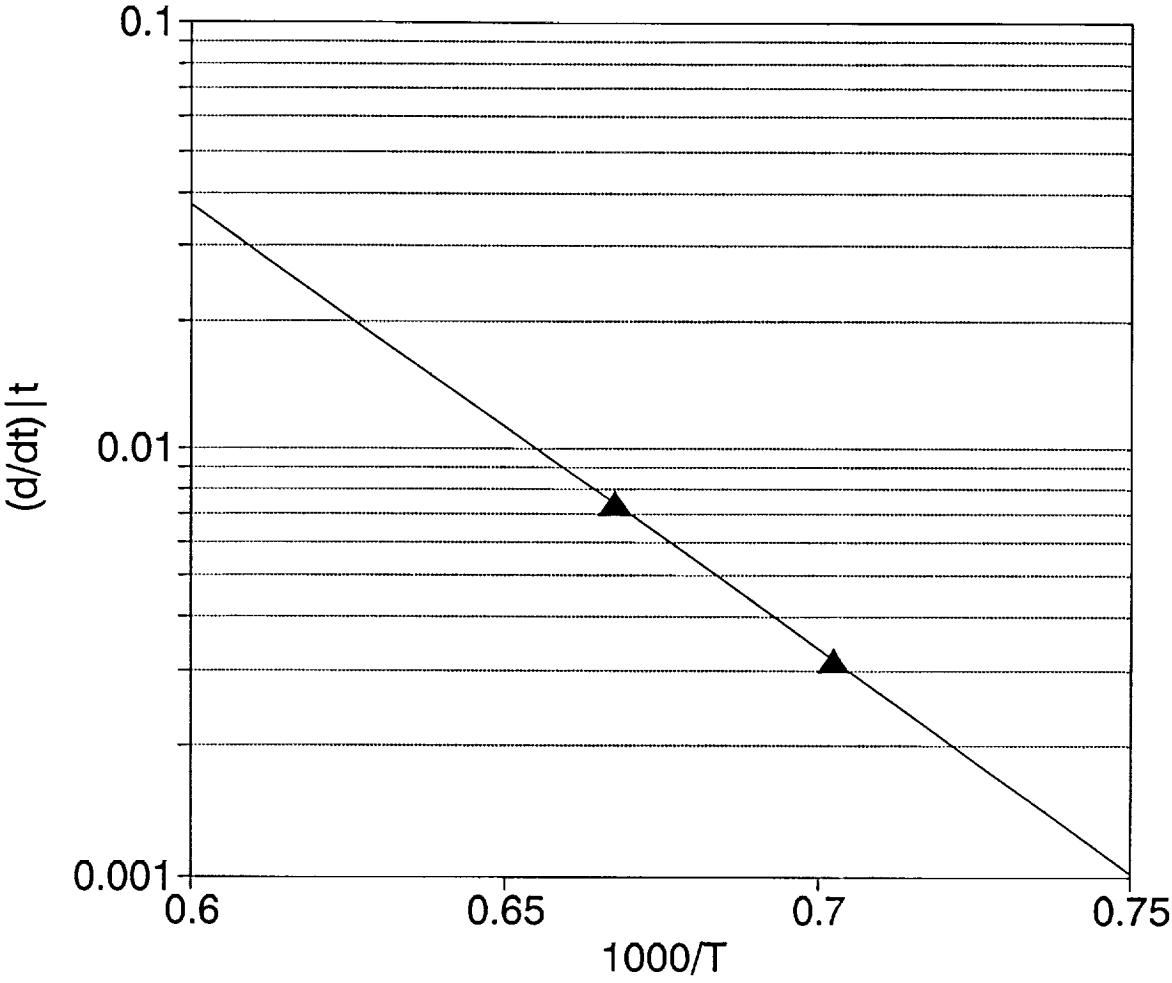

Figure 33. Arrhenius plot of Ir-Re diffusion kinetics, fixed time

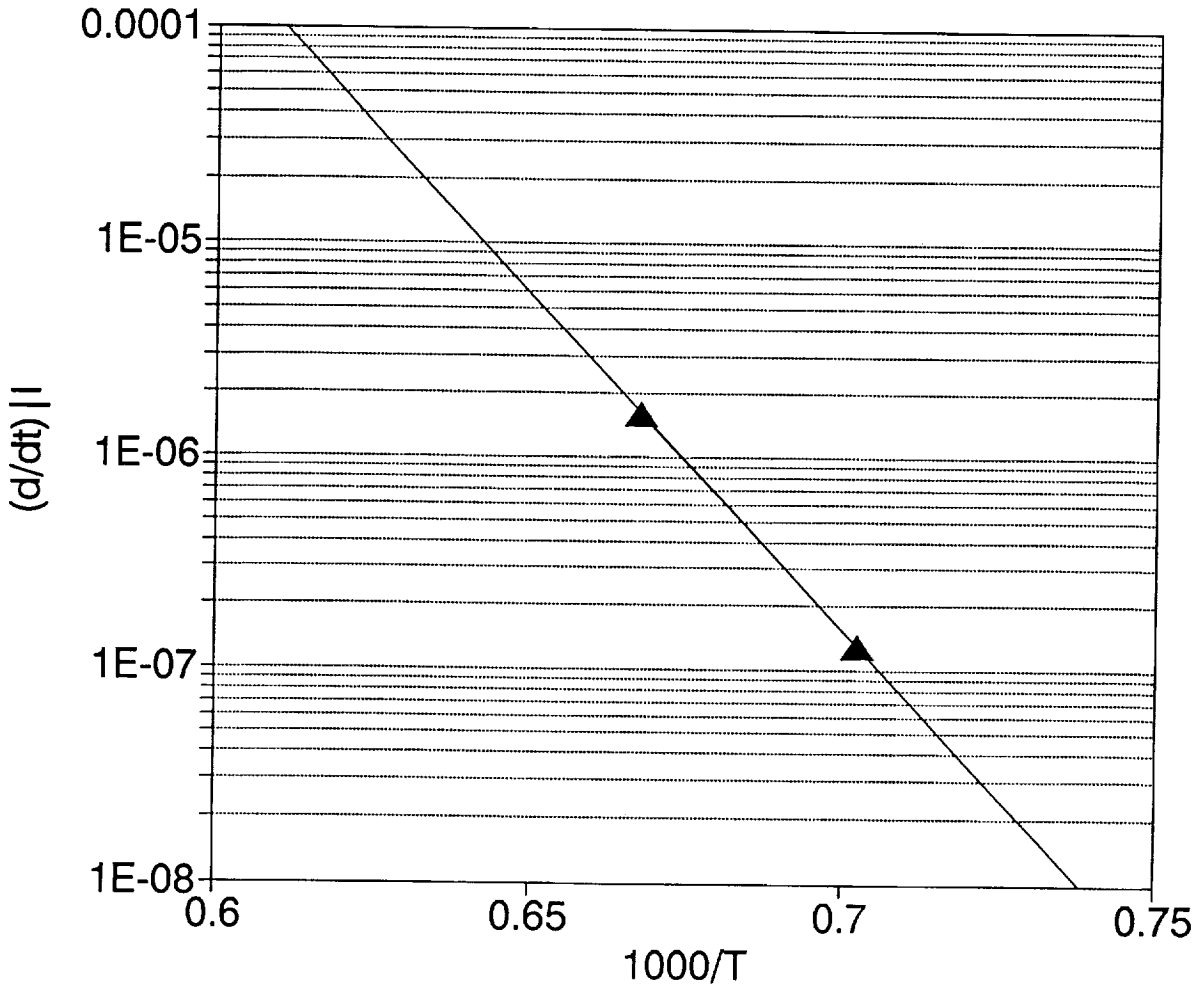

Figure 34. Arrhenius plot of Ir-Re diffusion kinetics, fixed thickness

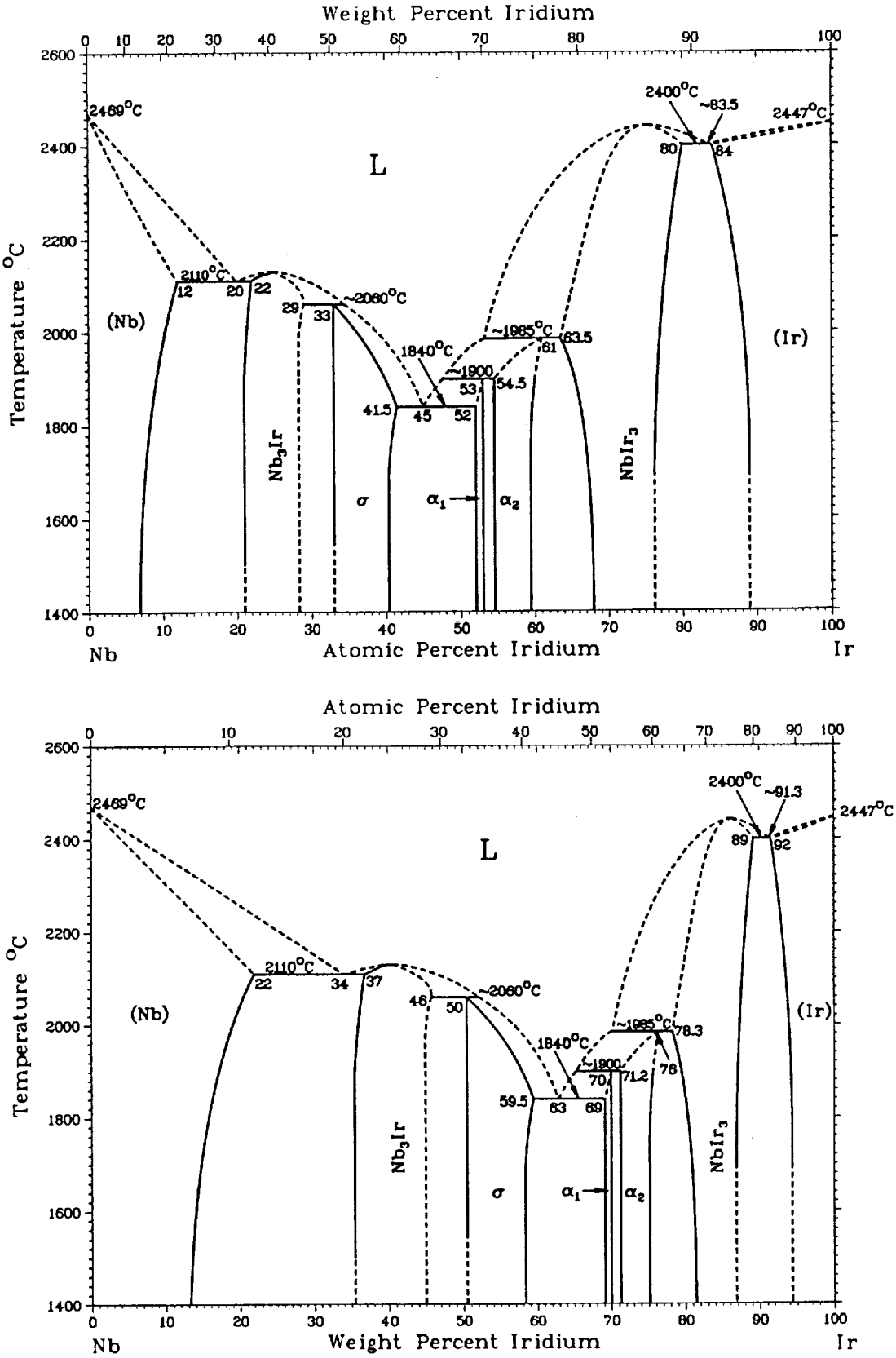

Figure 35. Nb-Ir phase diagram

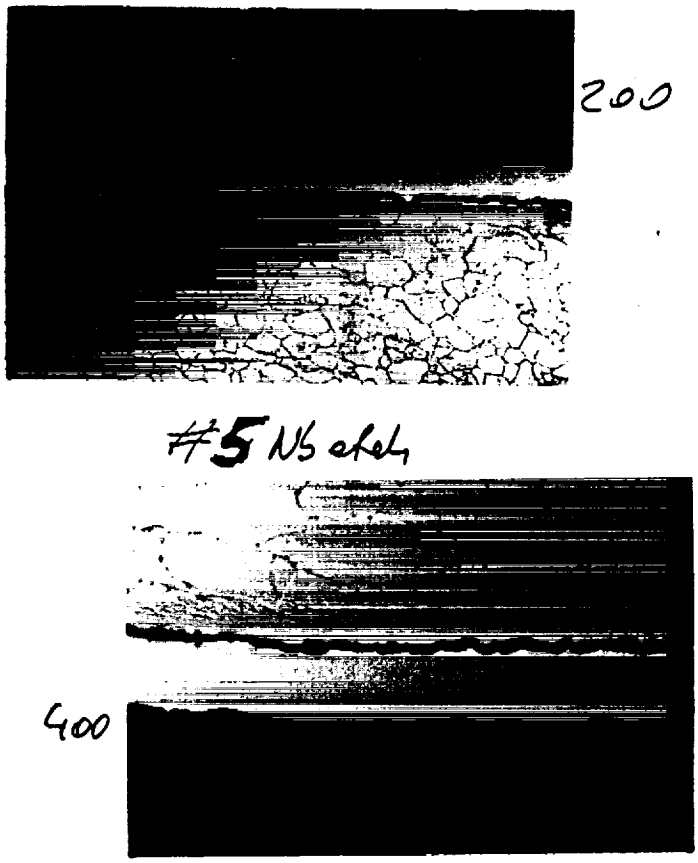

Figure 36. Optical micrograph (etched cross-section) of Ir-Nb diffusion couple before heat treatment, showing poor adhesion (top: 200x; bottom: 400x)

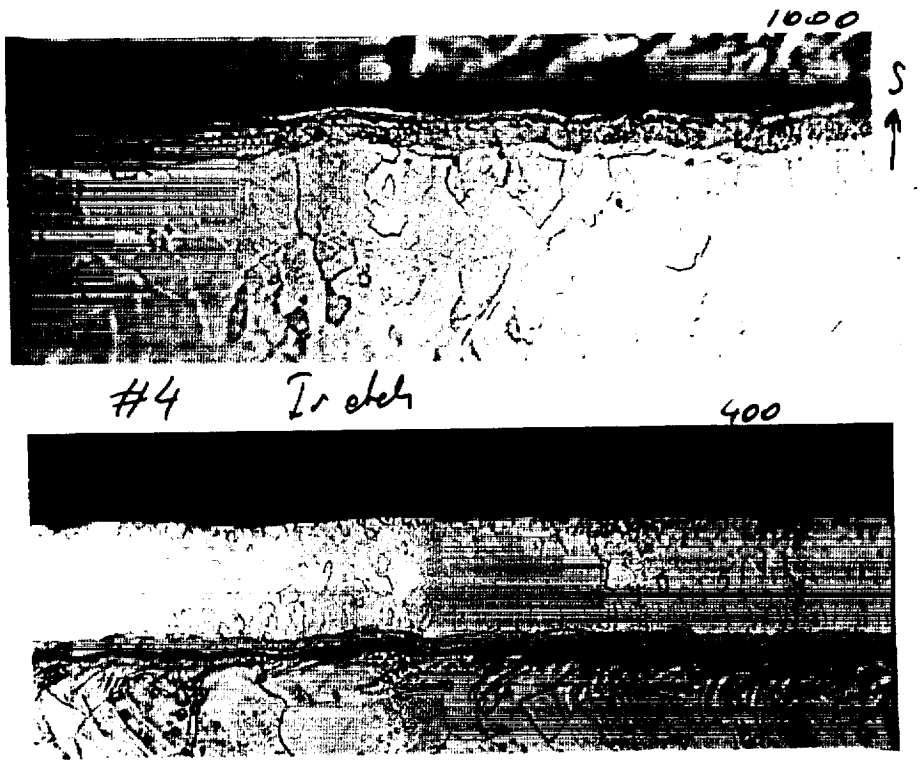

Figure 37A. Optical micrograph (etched cross-section) of Ir-Nb diffusion couple after heat treatment at 1320°C for 30 minutes, showing good adhesion; etching has caused interface to recede (top: 1000x; bottom: 400x)

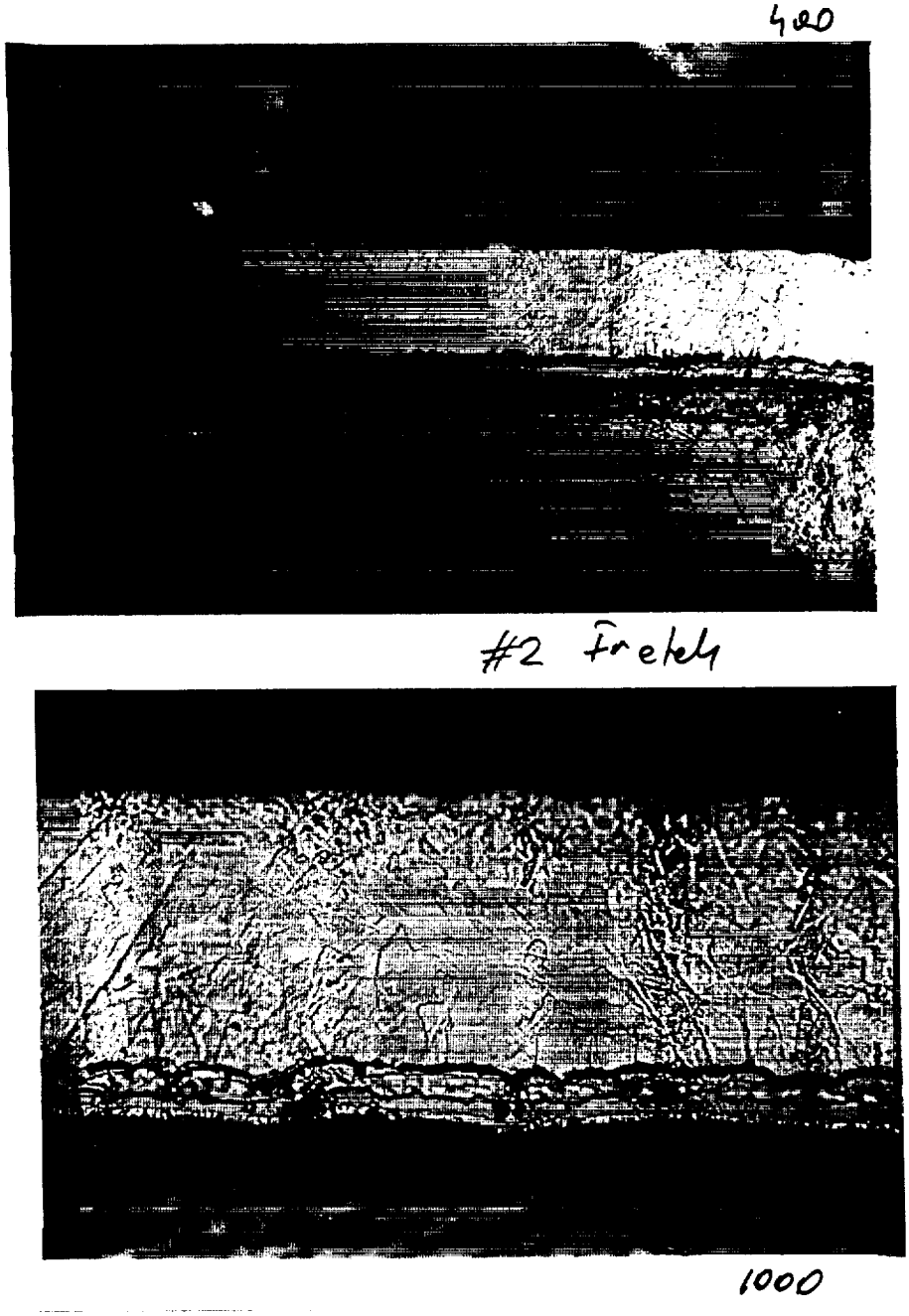

Figure 37B. Optical micrograph (etched cross-section) of Ir-Nb diffusion couple after heat treatment at 1320°C for 60 minutes, showing onset of void formation within diffusion layers (top: 400x; bottom: 1000x)

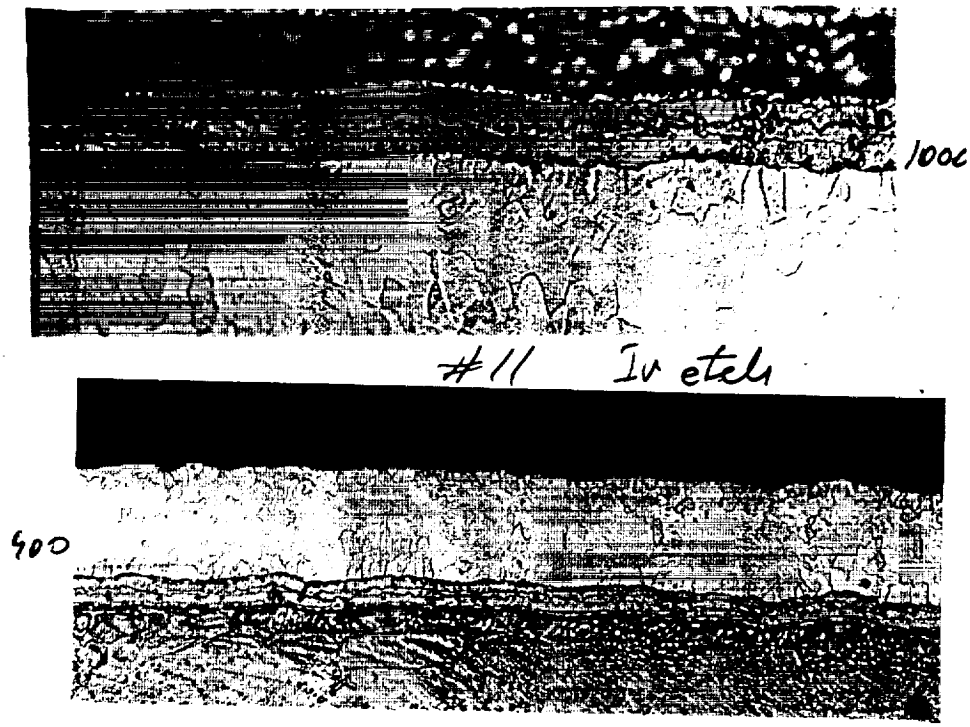

Figure 37C. Optical micrograph (etched cross-section) of Ir-Nb diffusion couple after heat treatment at 1320°C for 120 minutes (top: 1000x; bottom: 400x)

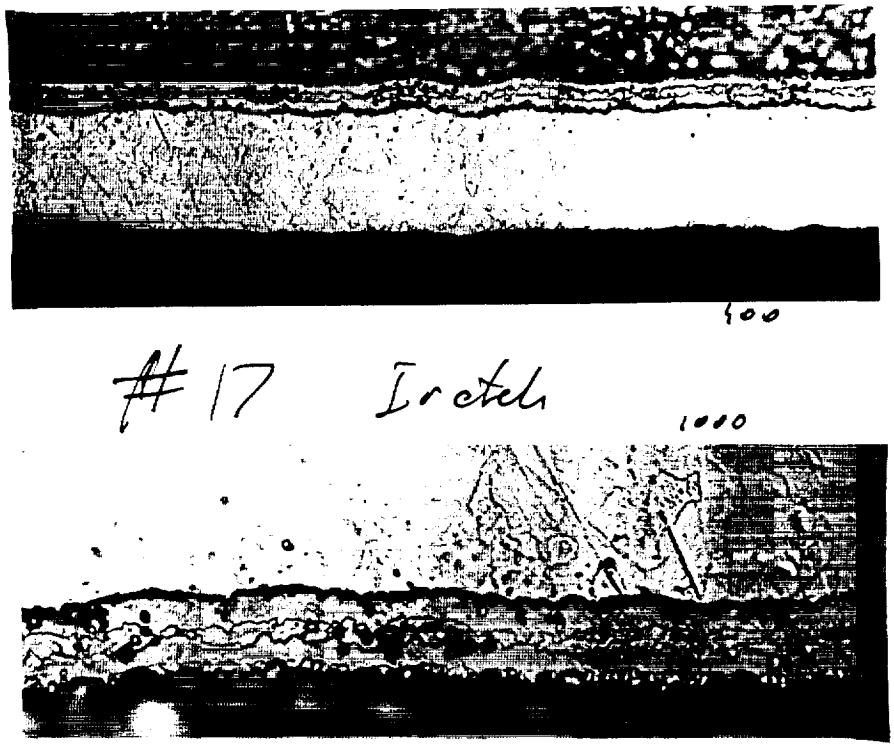

Figure 37D. Optical micrograph (etched cross-section) of Ir-Nb diffusion couple after heat treatment at 1320°C for 240 minutes (top: 400x; bottom: 1000x)

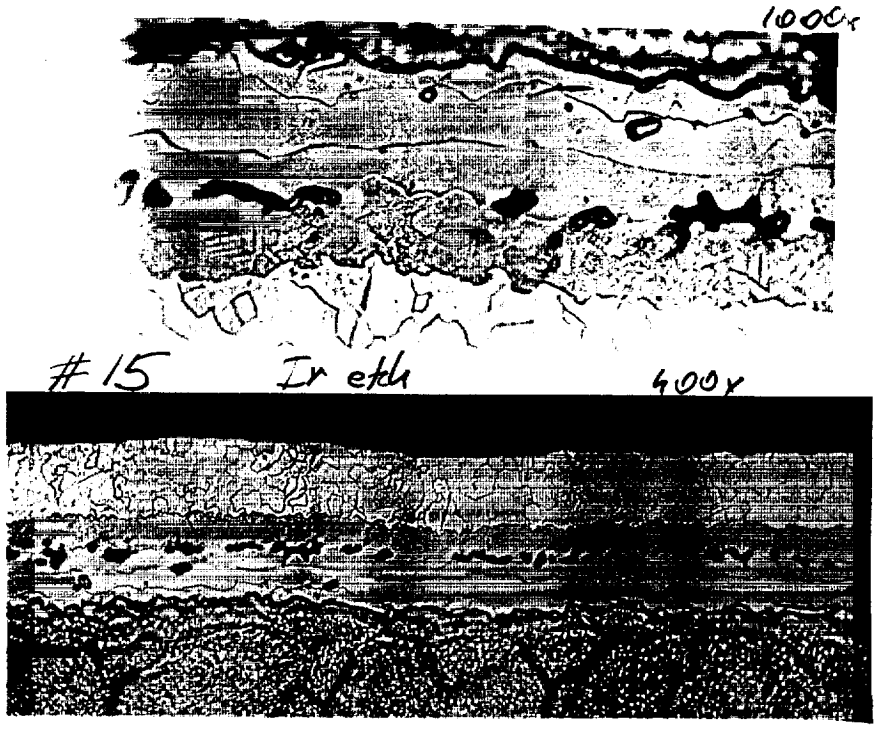

Figure 38. Optical micrograph (etched cross-section) of Ir-Nb diffusion couple after heat treatment at 1650°C for 240 minutes, showing accumulation of voids, particularly at α-β interface (top: 1000x; bottom: 400x)

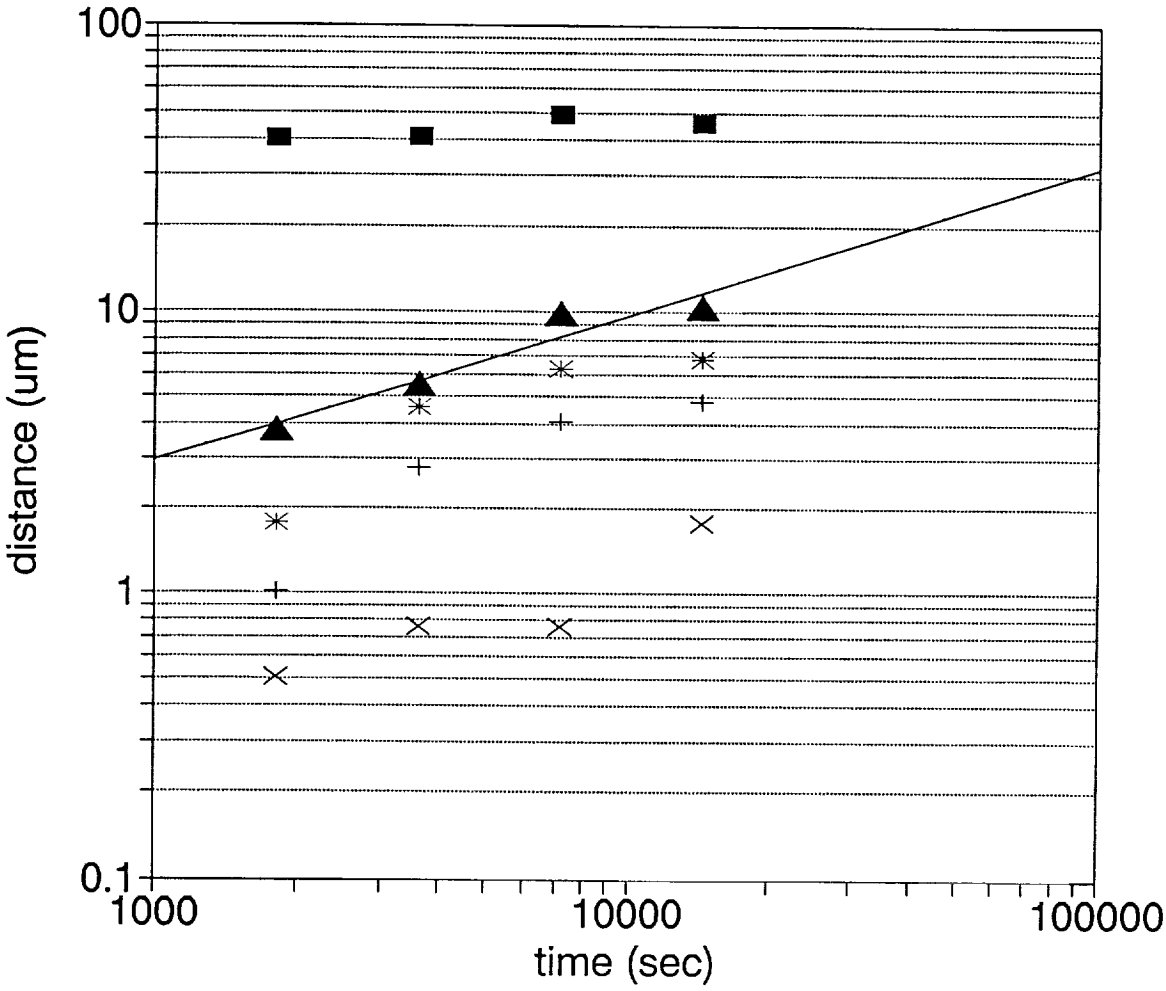

Figure 39. Ir-Nb diffusion vs. time at 1320°C (λ = 0.518)
□: total thickness, Ir + diffusion layers
▲: total diffusion layer thickness, $\delta+\gamma+\beta+\alpha$
*: combined thickness, $\delta+\gamma+\beta$
+: combined thickness, $\delta+\gamma$
×: thickness of δ layer

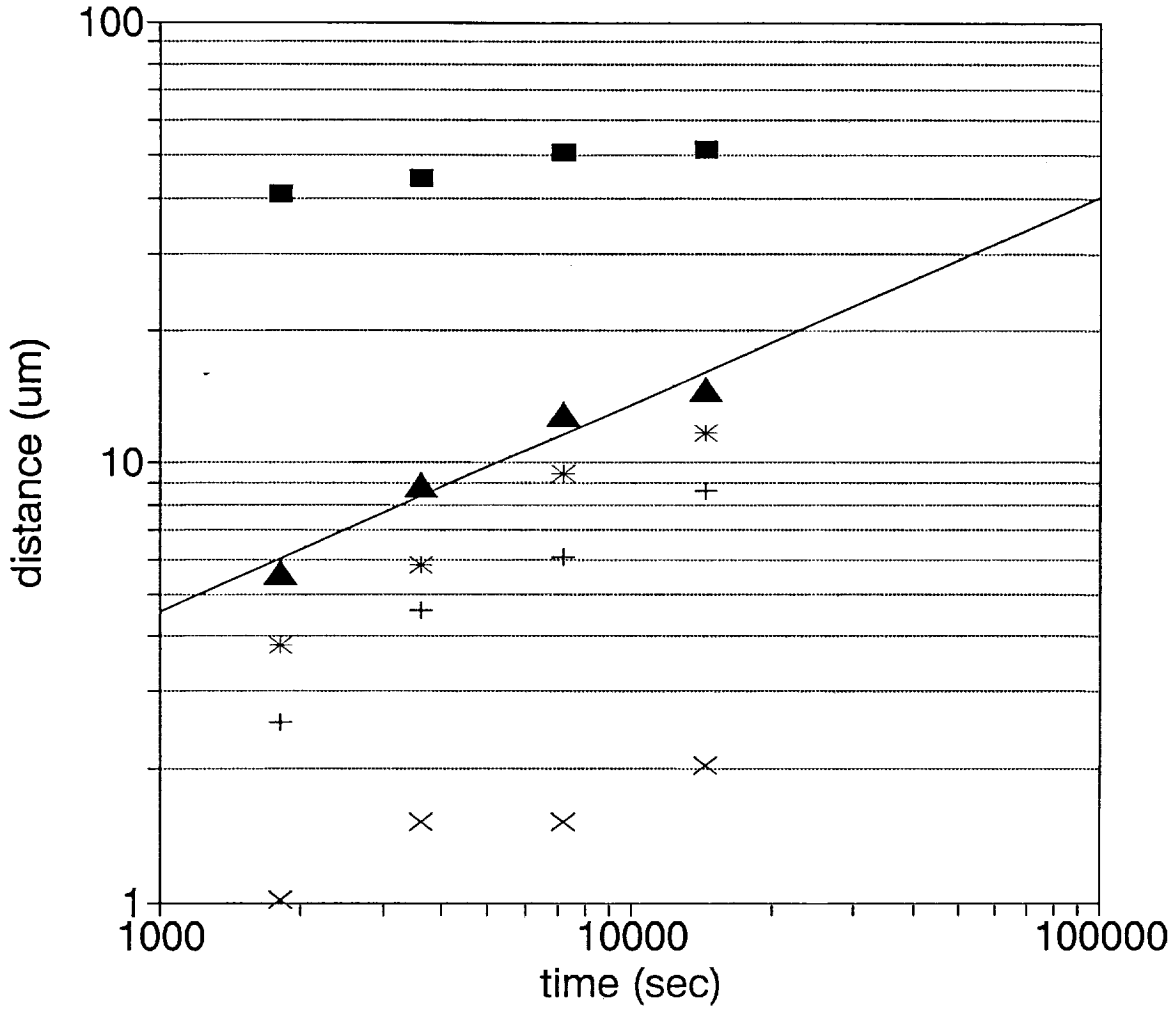

Figure 40. Ir-Nb diffusion vs. time at 1430°C (λ = 0.474)
□: total thickness, Ir + diffusion layers
▲: total diffusion layer thickness, $\delta+\gamma+\beta+\alpha$
*: combined thickness, $\delta+\gamma+\beta$
+: combined thickness, $\delta+\gamma$
×: thickness of δ layer

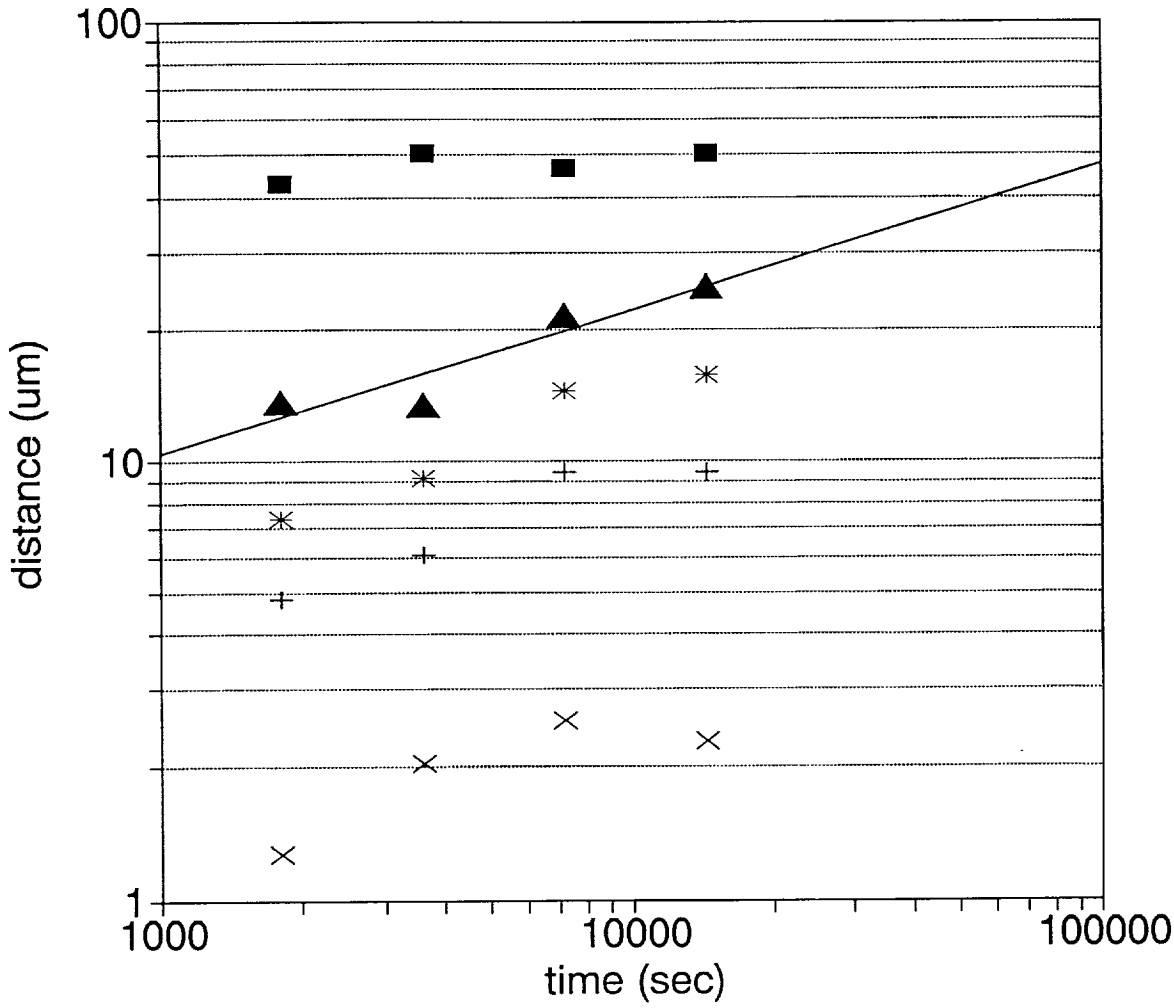

Figure 41. Ir-Nb diffusion vs. time at 1540°C (λ = 0.330)
□: total thickness, Ir + diffusion layers
▲: total diffusion layer thickness, $\delta+\gamma+\beta+\alpha$
*: combined thickness, $\delta+\gamma+\beta$
+: combined thickness, $\delta+\gamma$
×: thickness of δ layer

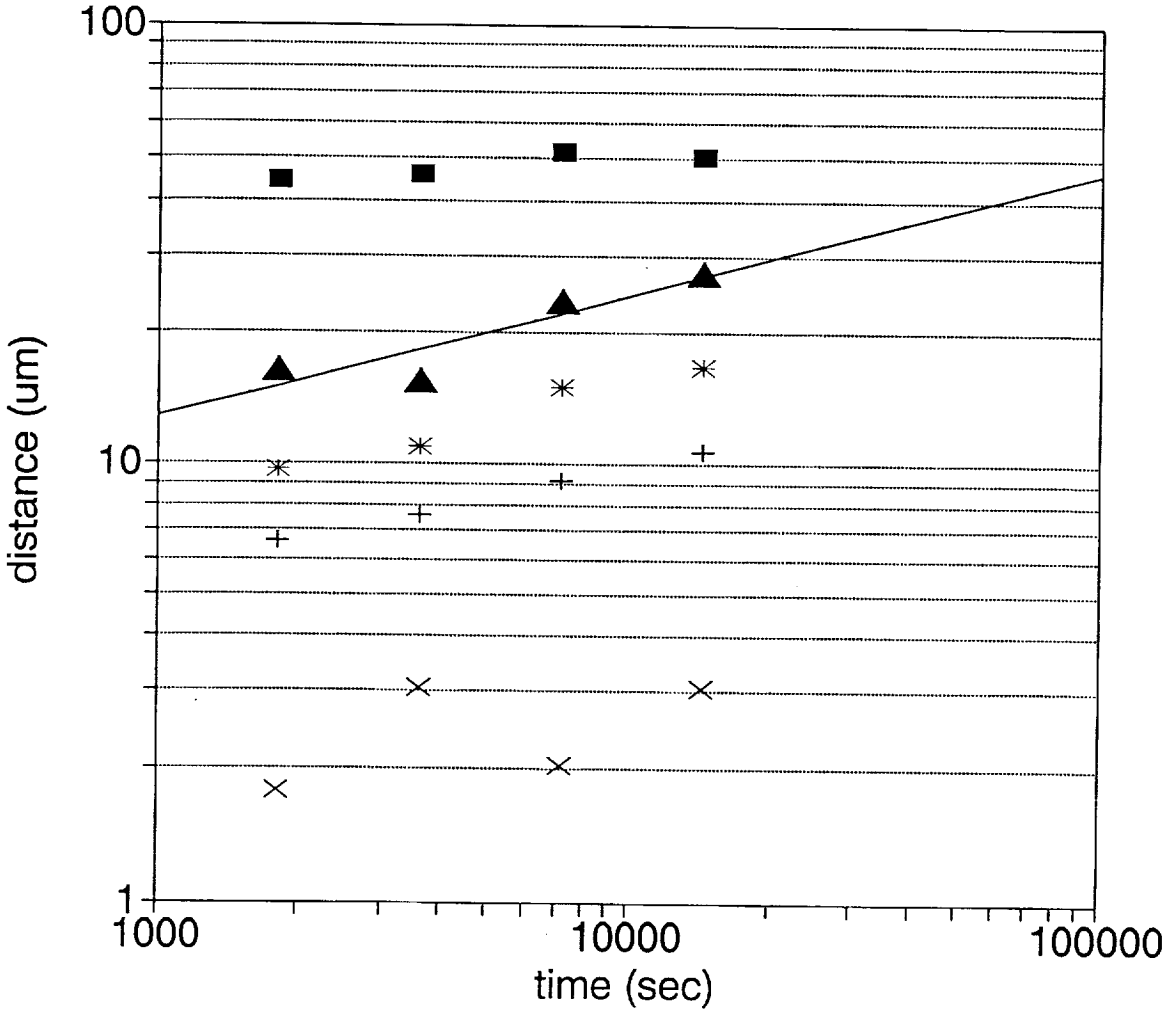

Figure 42. Ir-Nb diffusion vs. time at 1650°C (λ = 0.281)
□: total thickness, Ir + diffusion layers
▲: total diffusion layer thickness, $\delta+\gamma+\beta+\alpha$
*: combined thickness, $\delta+\gamma+\beta$
+: combined thickness, $\delta+\gamma$
×: thickness of δ layer

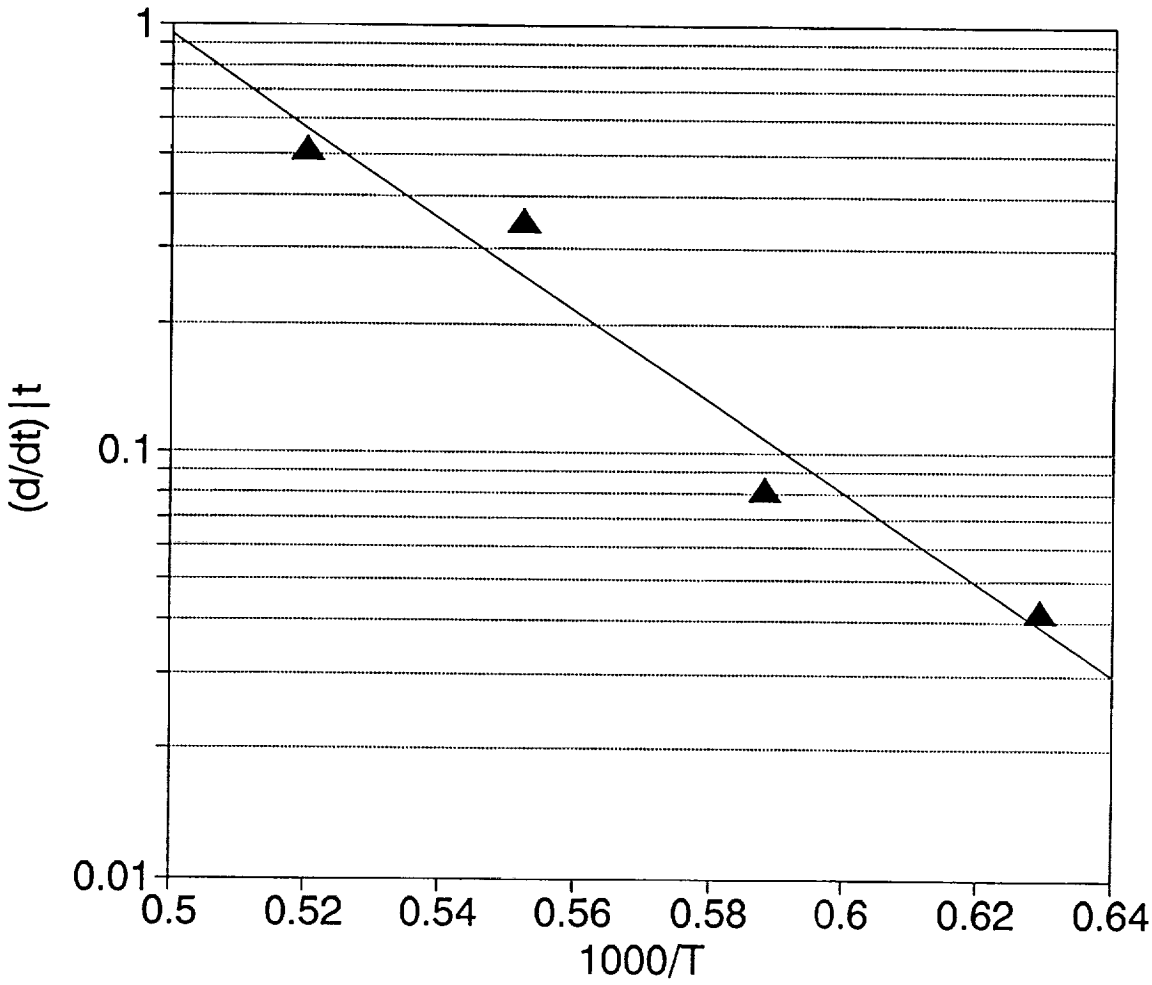

Figure 43. Arrhenius plot of Ir-Nb diffusion kinetics, fixed time

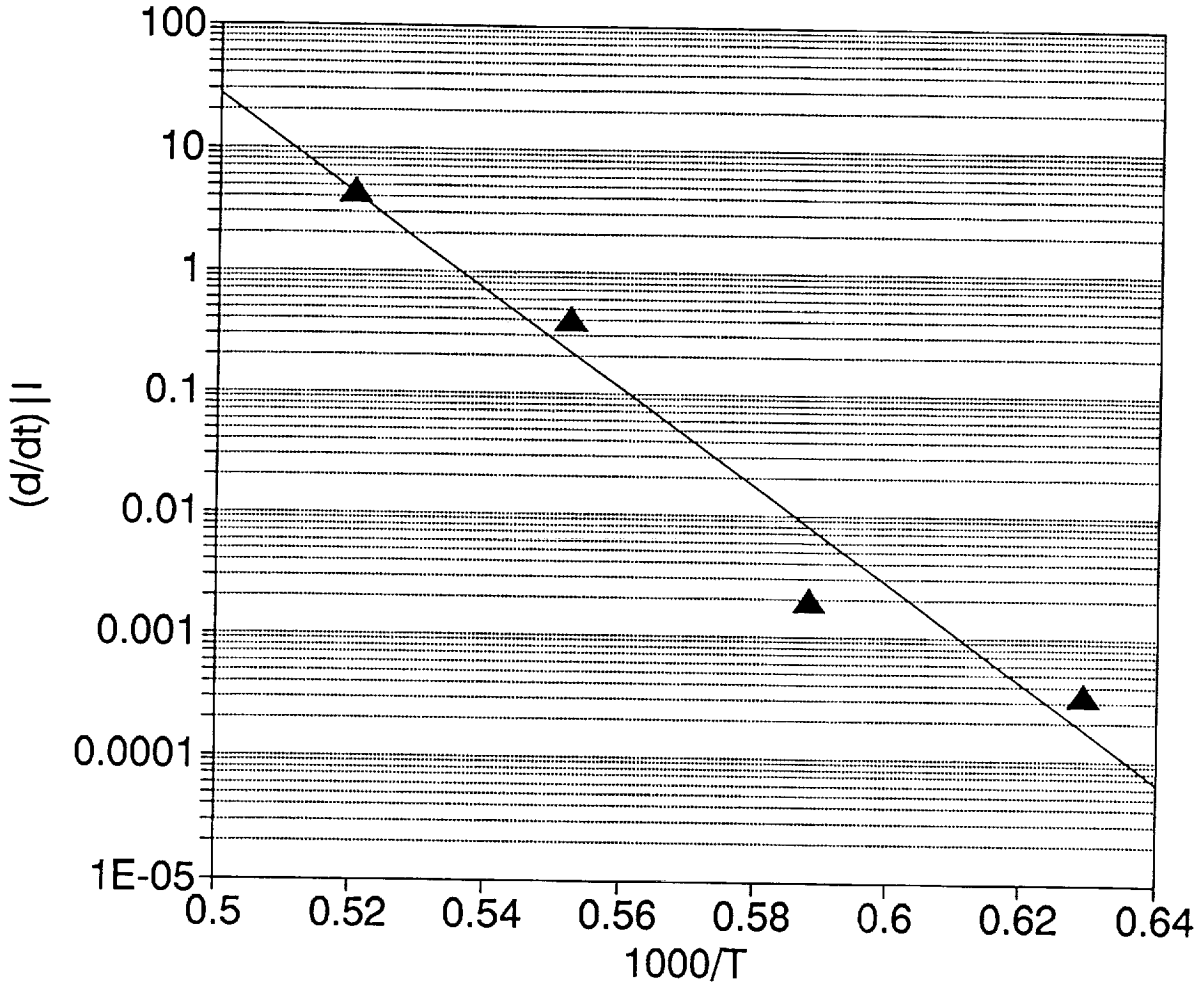

Figure 44. Arrhenius plot of Ir-Nb diffusion kinetics, fixed thickness

Table I. Hot-Fire Test Results for 5-lb_f Ir/Re Extended Skirt Chamber

Steady State Test

Test #160 at 280 sec

Pc	MR	Isp	Duration	Temperatures °F Valve Body	Inj	Trip	Throat
118 psig	1.60	311 sec	319 sec	220	280	920	3560

Pulse Test

Duty Cycle (%)	On Time (sec), Off (sec)	No. of Pulses				
10	.050, .450	1000	175	187	360	2580
20	.050, .200	86,800	200	240	575	2600
40	.050, .075	1800	>220	275	725	2970
50	.050, .050	1400	>220	300	775	3090
60	.050, .033	2855	>230	310	830	3370
70	.050, .021	1706	>230	320	860	3310
80	.050, .012	2240	>230	310	830	3370
90	.050, .005	2500	>230	305	825	3415

Cumulative Test Time On This Chamber

6,374 seconds

Table II. Oxidation Test Results for Ir/Re Alloys

A. Oxidation of iridium-rhenium alloys at 2300°C in 0.09 atm air-balance argon for 30 min.

Mol Fraction of Re	0.1	0.2	0.3
Weight Loss (mg/cm^2)	3.17	9.62	28.8
Recession (μm)	1.43	4.36	13.18

B. Oxidation of iridium-rhenium alloys at 2300°C in 0.36 atm air-balance argon for 30 min.

Mol Fraction of Re	0.1	0.2	0.3
Weight Loss (mg/cm^2)	18.28	21	71.43
Recession (μm)	8.22	9.53	32.69

C. Oxidation of iridium-rhenium alloys at 2430°C in 0.36 atm air-balance argon for 30 min. (The result for iridium-30 rhenium alloy is extrapolated from the 3 min oxidation result assuming a linear oxidation)

Mol Fraction of Re	0.1	0.2	0.3
Weight Loss (mg/cm^2)	34.36	60.34	133
Recession (μm)	15.46	27.37	60.86

D. Oxidation of iridium-rhenium alloys at 2500°C in 0.36 atm air-balance argon for 30 min. (Estimated)

Mol Fraction of Re	0.1	0.2	0.3
Weight Loss (mg/cm^2)	47.09	102	182
Recession (μm)	21.18	46.27	83.28

Table III. Iridium-Molybdenum Diffusion Layer Thicknesses

Sample ID	Temp. (°C)	Time (sec)	Diffusion layer thickness (μm)		
			α	β	γ
SL1	1200	1800	0.8	1.0	0.5
SL2	1200	3600	1.5	1.3	0.5
SL3	1200	5400	1.8	1.8	0.8
SL4	1200	7200	2.3	2.0	1.0
SL9	1200	32400	3.6	4.1	1.5
SL10	1200	1800	0.9	0.8	0.3
SL11	1200	59400	4.2	5.8	1.8
SL12	1200	36000	3.3	4.1	1.3
SL6	1000	3600	0.5	0.5	0.1
SL8	1000	7200	0.6	0.6	0.3

Table IV. Diffusion Layer Growth Coefficients for Ir-Mo Couple

Temp. (°C)	C_1	C_2
1000	0.018	0.500
1200	0.065	0.476

Table V. Iridium-Niobium Diffusion Layer Thicknesses

Sample ID	Temp. (°C)	Time (sec)	Diffusion Layer Thickness (μm)				
			Ir	α	β	γ	δ
1A-1	1320	1800	36.8	2.0	0.8	0.5	0.5
1A-2	1320	3600	35.6	1.0	1.8	2.0	0.8
1A-3	1320	7200	39.4	3.6	2.3	3.3	0.8
1A-4	1320	14400	35.6	3.6	2.0	3.0	1.8
1B-1	1430	1800	35.6	1.8	1.3	1.5	1.0
1B-2	1430	3600	35.6	3.0	1.3	3.0	1.5
1B-3	1430	7200	38.1	3.6	3.3	4.6	1.5
1B-4	1430	14400	36.8	3.0	3.0	6.6	2.0
2A-1	1540	1800	29.2	6.4	2.5	3.6	1.3
2A-2	1540	3600	36.8	4.3	3.0	4.1	2.0
2A-3	1540	7200	25.4	7.1	5.1	6.9	2.5
2A-4	1540	14400	25.4	9.4	6.4	7.1	2.3
2B-1	1650	1800	27.9	6.9	3.0	4.8	1.8
2B-2	1650	3600	30.5	4.6	3.3	4.6	3.0
2B-3	1650	7200	27.9	8.6	5.8	7.1	2.0
2B-4	1650	14400	22.9	10.7	6.1	7.6	3.0

Table VI. Diffusion Layer Growth Coefficients for Ir-Nb Couple

Temp. (°C)	C_1	C_2
1320	0.082	0.518
1430	0.173	0.474
1540	1.060	0.330
1650	1.840	0.281

REPORT DOCUMENTATION PAGE

Form Approved
OMB No. 0704-0188

1. AGENCY USE ONLY (Leave blank)	2. REPORT DATE	3. REPORT TYPE AND DATES COVERED
	March 1991	Final (May 1987-August 1990)

4. TITLE AND SUBTITLE
High Temperature Oxidation-Resistant Thruster Materials, Phase II

5. FUNDING NUMBERS
NAS3-25203

6. AUTHOR(S)
Robert H. Tuffias, G.J. Melden, and John T. Harding

7. PERFORMING ORGANIZATION NAME(S) AND ADDRESS(ES)
Ultramet
12173 Montague Street
Pacoima, CA 91331

8. PERFORMING ORGANIZATION REPORT NUMBER
ULT/TR-90-6230

9. SPONSORING/MONITORING AGENCY NAME(S) AND ADDRESS(ES)
National Aeronautics and Space Administration
Lewis Research Center
Cleveland, OH 44135

10. SPONSORING/MONITORING AGENCY REPORT NUMBER
NASA CR-187205

11. SUPPLEMENTARY NOTES
Small Business Innovation Research (SBIR) Program, Phase II
NASA Lewis Project Manager: John M. Kazaroff

12a. DISTRIBUTION/AVAILABILITY STATEMENT
Unclassified/Unlimited

12b. DISTRIBUTION CODE

13. ABSTRACT *(Maximum 200 words)*

The objective of this project was to advance the state of the art in materials and processes for the fabrication of bipropellant chemical rocket thrust chambers. The results of the effort included the demonstration of materials and processes that permit thrust chamber operation at 2200°C (4000°F) for tens of hours, providing a 20-second increase in specific impulse; demonstration of process scaleup, from 5-lb_f (22-N) to 100-lb_f (445-N) chamber size; and development and characterization of the process to permit application of this technology to satellite and/or spacecraft propulsion systems.

14. SUBJECT TERMS
high temperature, oxidation resistance, iridium, rhenium, niobium, chemical vapor deposition (CVD), liquid propellant, rocket engine, thrust chamber

15. NUMBER OF PAGES
93

16. PRICE CODE

17. SECURITY CLASSIFICATION OF REPORT	18. SECURITY CLASSIFICATION OF THIS PAGE	19. SECURITY CLASSIFICATION OF ABSTRACT	20. LIMITATION OF ABSTRACT
Unclassified	Unclassified	Unclassified	SAR